arXiv:hep-ex/9712022v1 17 Dec 1997

February 7, 2008

The Search for Supersymmetry at the Tevatron Collider

M. Carena,[1] R.L. Culbertson,[2] S. Eno,[3] H.J. Frisch,[2] and S. Mrenna[4]
[1] *Fermi National Accelerator Laboratory*
[2] *University of Chicago*
[3] *University of Maryland*
[4] *Argonne National Laboratory*

Abstract

We review the status of searches for Supersymmetry at the Tevatron Collider. After discussing the theoretical aspects relevant to the production and decay of supersymmetric particles at the Tevatron, we present the current results for Runs Ia and Ib as of the summer of 1997.

1 Introduction

The Tevatron is a 1–kilometer radius superconducting accelerator ring, located at the Fermi National Accelerator Laboratory (Fermilab), in Batavia, Illinois, U.S.A. The ring is used in two modes: as a source of high energy beams for fixed target experiments, and, in conjunction with the Antiproton Source, as a proton–antiproton collider, operating with a $p\overline{p}$ center–of–mass energy of $\sqrt{s} = 1.8$ TeV. The Tevatron Collider has been the world's accelerator–based high energy frontier since it first began taking data in 1987, and has thus been a prime location to search for the final pieces of the Standard Model[1] (SM) and new phenomena beyond.

With the discovery of the top quark at the Tevatron,[2] the SM particle spectrum is almost complete, with only the Higgs boson (and, arguably, the tau neutrino) lacking direct experimental confirmation. If the interactions of the leptons, quarks and gauge bosons of the SM remain perturbative up to very high energies (as appears to be the case from the measured running of the gauge couplings), then the mechanism responsible for electroweak symmetry breaking (EWSB) is expected to contain one or more fundamental scalar Higgs bosons that are light, *i.e.* with masses of the order of the symmetry–breaking scale.

The Higgs mechanism[3] plays a crucial role in the SM. The neutral component of the Higgs boson acquires a vacuum expectation value to give mass to the W and Z gauge bosons as well as to the SM fermions. In addition, the couplings of the Higgs boson to the gauge bosons and fermions are such as to cancel the infinities in the electroweak radiative corrections and prevent unitarity violation in the longitudinal scattering of the gauge bosons. However, if the SM is valid up to an energy cutoff of $\Lambda_{\rm cutoff} \approx M_{\rm Planck}$ ($M_{\rm Planck} = 1.22 \times 10^{19}$ GeV), the model has a fundamental problem, the so–called *naturalness problem*.[4]

The radiative corrections to the Higgs boson mass–squared calculated in the SM are quadratically divergent (proportional to $\Lambda^2_{\rm cutoff}$). A physical Higgs mass of the order of the electroweak scale requires a cancellation of one part in 10^{16} between these radiative corrections, which come from the interactions of the Higgs bosons with all other particles in the theory, and the bare Higgs mass at the Planck scale:

$$m_H^2 \simeq m_H^2(\Lambda_{\rm cutoff}) - \alpha\Lambda^2_{\rm cutoff}. \qquad (1)$$

Either there is an extreme "fine tuning" necessary to have a cancellation of two independent effects (the naturalness problem), or there must be some new principle at work.

Supersymmetry (SUSY)[5,6,7] is a new symmetry which provides a well–

motivated extension of the SM with an elegant solution to the naturalness problem. Supersymmetric transformations relate fermionic and bosonic degrees of freedom. Each left–handed and right–handed fermion of the SM is postulated to have its own bosonic superpartner with equal mass and coupling strengths. Similarly each SM boson would have its own fermionic superpartner, again with equal mass and couplings. Because bosons and fermions induce radiative effects of opposite signs, SUSY naturally provides an exact cancellation of the otherwise quadratically–divergent radiative corrections to the Higgs boson mass.[8]

Given that no superparticles have been observed so far, it is assumed that SUSY is broken, and that in general the sparticles must be heavier than their partners. In order to break SUSY without spoiling the necessary cancellation of quadratic divergences, the splittings between the masses of the SM particles and their SUSY partners should not be much larger than a few TeV. If SUSY is a consistent description of Nature, then the lower range of sparticle masses can be within the reach of the Tevatron,[9] motivating a wide range of searches in a large number of channels.[10] The mass of the lightest neutral Higgs boson is strongly constrained within SUSY,[11] and could be within the reach of the upgraded Tevatron.[12,13] In addition, the decay of the heavy top quark, pair produced in strong interactions with a cross section of $\simeq 6$ pb at the Tevatron, gives a unique mechanism for producing lighter supersymmetric particles which might not otherwise be produced at a large rate in proton–antiproton collisions.

Two experimental collaborations, CDF and DØ, have large, general–purpose detectors at Fermilab. The Tevatron had initial running periods in 1985 and 1987 with low luminosity.[a] In 1988 – 1989 (the '89 Run'), the Tevatron operated at $\sqrt{s} = 1.8$ TeV with an average instantaneous luminosity of 1.6×10^{30} cm^{-2}s^{-1}, and the CDF detector collected approximately 4.4 pb^{-1} of data. In 1992 – 93 (Run Ia), CDF and DØ accumulated approximately 20 and 15 pb^{-1}, respectively, and in 1994 – 95 (Run Ib) 90 and 108 pb^{-1}, for a total Run I integrated luminosity of more than 100 pb^{-1} per detector.[b] The average instantaneous luminosity during Run I was approximately 1×10^{31} cm^{-2}s^{-1}. A new run (Run II) utilizing the new Main Injector and Recycler rings and other major accelerator improvements is scheduled to begin around the year 2000, reaching an average instantaneous luminosity of 1×10^{32} cm^{-2}s^{-1} and an expected integrated luminosity of 1000 pb^{-1} per year.[14] In addition, the energy of the machine will be increased to $\sqrt{s} = 2$ TeV, substantially increasing the cross section for producing heavy particles (the top quark pair production cross section, for example, increases by 40% from $\sqrt{s} = 1.8$ TeV to 2 TeV). Run II, with an upgraded Collider and detectors, holds a great deal of promise for Higgs boson and sparticle searches.

---

[a] The 1985 run produced the first detected luminosity, with 20 events recorded by CDF.

[b] The difference in integrated luminosities in Run Ib comes partly from the fact that DØ uses the 11.3 pb^{-1} from Run Ic while CDF ignores it, and the fact that the DØ experiment normalizes its luminosity (and hence all cross sections) to an inelastic cross section that is 2.4% smaller than that used by CDF. For the actual luminosities used in each analysis see Table 1.

2 The MSSM

In the past two decades, a detailed picture of the Minimal Supersymmetric extension of the Standard Model (MSSM), has emerged.[15,16,17] In the MSSM, the particle spectrum is doubled by SUSY. Moreover, to generate masses for up– and down–type fermions while preserving SUSY and gauge invariance, the Higgs sector must contain two doublets.[18] After EWSB, there is a quintet of physical Higgs boson states: two CP–even scalar (h, H), one CP–odd pseudoscalar (A), and a pair of charged $(H^{\pm})$ Higgs bosons.[19] All the Higgs bosons and other SM particles have superpartners with the same quantum numbers under the SM gauge groups $SU(3)_C \times SU(2)_L \times U(1)_Y$, but with different spin.[6] The spin–1/2 partners of the gauge bosons (gauginos) are denoted as winos $\widetilde{W}^{\pm}$, zinos $\widetilde{Z}$, photinos[a] $\widetilde{\gamma}$, and gluinos $\tilde{g}$. The spin–1/2 partners of the Higgs bosons (Higgsinos) are $\widetilde{H}_1, \widetilde{H}_2$ and $\widetilde{H}^{\pm}$. Because of EWSB, the Higgsinos and $SU(2)_L \times U(1)_Y$ gauginos mix to give physical mass eigenstates consisting of two Dirac fermions of electric charge one, the charginos $\widetilde{\chi}^{\pm}_{1,2}$, and four neutral Majorana fermions, the neutralinos $\widetilde{\chi}^0_{1-4}$. The spin–0 partners of the fermions (sfermions)[b] are squarks $\widetilde{Q}$,[c] sleptons $\tilde{\ell}$ and sneutrinos $\tilde{\nu}$. Each charged lepton or quark has two scalar partners, one associated with each chirality. These are named left–handed squarks and sleptons, which belong to $SU(2)_L$ doublets, and right–handed squarks and sleptons, which are $SU(2)_L$ singlets. The neutrinos have only left–handed superpartners $\tilde{\nu}$, which belong to $SU(2)_L$ doublets. The gluino $\tilde{g}$ and squarks $\widetilde{Q}$ carry color indices and are $SU(3)_C$ octets and triplets, respectively.

The MSSM Lagrangian contains interactions between particles and sparticles, fixed by SUSY. There are also a number of soft SUSY–breaking mass parameters. "Soft" means that they break the mass degeneracy between SM particles and their SUSY partners without reintroducing quadratic divergences while respecting the gauge invariance of the theory. The soft SUSY–breaking parameters are extra mass terms for gauginos and scalar fermions, and trilinear scalar couplings. The exact number of extra parameters depends on the exact mechanism of SUSY breaking. In the remainder of this section, the MSSM particle spectrum and properties will be described in general, and also with reference to specific SUSY–breaking scenarios and variations.

---

[a] The superpartners of the $U(1)_Y$ and $SU(2)_L$ gauge bosons (before EWSB) are the Bino $\widetilde{B}$, the unmixed neutral Wino $\widetilde{W}_3$, and the unmixed charged Winos $\widetilde{W}_1$ and $\widetilde{W}_2$.

[b] Charge conjugate scalars are denoted by *, *e.g.* $\widetilde{Q}^*$.

[c] To allow easier reading, we use the non–standard symbol $\widetilde{Q}$ instead of $\tilde{q}$. This has no special significance.

2.1 Sparticle Spectrum

The chargino and neutralino masses and their mixing angles (that is, their gaugino and Higgsino composition) are determined by the SM gauge boson masses (M_W and M_Z), $\tan\beta$,[d] two soft SUSY–breaking parameters (the $SU(2)_L$ gaugino mass M_2 and the $U(1)_Y$ gaugino mass M_1), and the SUSY Higgsino mass parameter μ, all evaluated at the electroweak scale M_{EW}.[e] Explicit solutions are found by considering the 2×2 chargino $\mathbf{M_C}$ and 4×4 neutralino $\mathbf{M_N}$ mass matrices: [f]

$$\mathbf{M_C} = \begin{pmatrix} M_2 & \sqrt{2}M_W s\beta \\ \sqrt{2}M_W c\beta & \mu \end{pmatrix} ; \mathbf{M_N} = \begin{pmatrix} \mathbf{M_i} & \mathbf{Z} \\ \mathbf{Z^T} & \mathbf{M}_\mu \end{pmatrix} \tag{2}$$

$$\mathbf{M_i} = \begin{pmatrix} M_1 & 0 \\ 0 & M_2 \end{pmatrix} ; \mathbf{M}_\mu = \begin{pmatrix} 0 & -\mu \\ -\mu & 0 \end{pmatrix} ; \mathbf{Z} = \begin{pmatrix} -M_Z c\beta s_W & M_Z s\beta s_W \\ M_Z c\beta c_W & -M_Z s\beta c_W \end{pmatrix}$$

$\mathbf{M_C}$ is written in the $\widetilde{W}^+ - \widetilde{H}^+$ basis, $\mathbf{M_N}$ in the $\widetilde{B} - \widetilde{W}^3 - \widetilde{H}_1 - \widetilde{H}_2$ basis, with the notation $s\beta = \sin\beta, c\beta = \cos\beta, s_W = \sin\theta_W$ and $c_W = \cos\theta_W$. In general, the mass eigenstates are admixtures of the interaction states, but, for large values of $|\mu|$ or M_1 and M_2, the limit is reached where the mass eigenstates are mostly pure gaugino or Higgsino states (independent of $\tan\beta$). In particular, if $|\mu| \gg M_Z$ and $M_1, M_2 \simeq M_Z$, with $M_1 < M_2$, the lightest eigenstates are gaugino–like and the heaviest are Higgsino–like, leading to the spectrum:

$$\begin{gathered} M_{\widetilde{\chi}^\pm_1} \simeq M_2; \quad M_{\widetilde{\chi}^\pm_2} \simeq |\mu| \\ M_{\widetilde{\chi}^0_1} \simeq M_1; \quad M_{\widetilde{\chi}^0_2} \simeq M_2; \quad M_{\widetilde{\chi}^0_3} \simeq M_{\widetilde{\chi}^0_4} \simeq |\mu|. \end{gathered} \tag{3}$$

---

[d] One Higgs doublet, H_2, couples to u, c, and t, while the other, H_1, couples to d, s, b, e, μ, and τ. The parameter $\tan\beta$ is the ratio of vacuum expectation values $\langle H_2\rangle/\langle H_1\rangle \equiv v_2/v_1$, and $v^2 = v_1^2 + v_2^2$, where v is the order parameter of EWSB.

[e] The electroweak scale M_{EW} is roughly the scale of the sparticle masses themselves. Usually, in the literature, for simplicity, $M_{EW} \simeq M_Z$.

[f] Beware of different sign conventions for μ in the literature. Both `PYTHIA` and `ISAJET` use the convention used here.

Similarly, if $M_1, M_2 \gg M_Z$ and $|\mu| \simeq M_Z$, the lightest eigenstates are Higgsino–like and the heaviest are gaugino–like:

$$\begin{aligned} M_{\widetilde{\chi}_1^\pm} \simeq |\mu|; \quad M_{\widetilde{\chi}_2^\pm} \simeq M_2 \\ M_{\widetilde{\chi}_1^0} \simeq M_{\widetilde{\chi}_2^0} \simeq |\mu|; \quad M_{\widetilde{\chi}_3^0} \simeq M_1; \quad M_{\widetilde{\chi}_4^0} \simeq M_2. \end{aligned} \tag{4}$$

Another interesting example where $\widetilde{\chi}_1^0$ is Higgsino–like, $\widetilde{\chi}_2^0$ is photino–like, and all other charginos and neutralinos are mixtures, occurs for $M_1 = M_2 \simeq |\mu| \simeq M_Z$ and $\tan\beta \simeq 1$:

$$\begin{aligned} M_{\widetilde{\chi}_{1,2}^\pm} = \frac{1}{2}|M_2 + \mu \mp \sqrt{(M_2-\mu)^2 + 4M_W^2}| \\ M_{\widetilde{\chi}_1^0} = |\mu|; \quad M_{\widetilde{\chi}_2^0} = M_1; \quad M_{\widetilde{\chi}_{3,4}^0} = \frac{1}{2}|M_2 + \mu \mp \sqrt{(M_2-\mu)^2 + 4M_Z^2}|. \end{aligned} \tag{5}$$

Since the $SU(3)_C$ symmetry of the SM is not broken, the gluinos have masses determined by the $SU(3)_C$ gaugino mass parameter M_3.[g] The neutralinos and the gluinos are Majorana particles, and do not distinguish between states and their charged conjugate. Depending on their Higgsino or gaugino composition, the $\widetilde{\chi}$ couplings to gauge bosons, and left– and right–handed sfermions will differ substantially, and the production and decay processes will strongly depend on that composition (see the discussion below).

The mass eigenstates of squarks and sleptons are, in principle, mixtures of their left– and right–handed components, given for the first generation by:

$$\begin{aligned} m_{\tilde{u}_L}^2 \simeq m_{Q_1}^2 + m_u^2 + D_{\tilde{u}_L} \quad & m_{\tilde{u}_R}^2 \simeq m_{U_1}^2 + m_u^2 + D_{\tilde{u}_R} \\ m_{\tilde{d}_L}^2 \simeq m_{Q_1}^2 + m_d^2 + D_{\tilde{d}_L} \quad & m_{\tilde{d}_R}^2 \simeq m_{D_1}^2 + m_d^2 + D_{\tilde{d}_R} \\ m_{\tilde{e}_L}^2 \simeq m_{L_1}^2 + m_e^2 + D_{\tilde{e}_L} \quad & m_{\tilde{e}_R}^2 \simeq m_{E_1}^2 + m_e^2 + D_{\tilde{e}_R} \\ m_{\tilde{\nu}_e}^2 \simeq m_{L_1}^2 + D_{\tilde{\nu}_e}, & \end{aligned} \tag{6}$$

where $m_{Q_1}^2$, $m_{L_1}^2$, $m_{U_1}^2$, $m_{D_1}^2$, and $m_{E_1}^2$ are soft SUSY–breaking parameters and $D_{\tilde{f}_L} = M_Z^2 \cos(2\beta)(T_{3_f} - Q_f \sin^2\theta_W)$, $D_{\tilde{f}_R} = M_Z^2 \cos(2\beta) Q_f \sin^2\theta_W$ are D–terms [h] associated with EWSB (T_{3_f} is the weak isospin eigenvalue of the fermion, Q_f the electric charge). A similar expression holds for the second (third) generation with the substitutions $u \to c(t), d \to s(b), e \to \mu(\tau), 1 \to$

---

[g] The physical gluino mass is shifted from the value of the gluino mass parameter M_3 because of radiative corrections. As a result, there is an indirect dependence on the squark masses.

[h] D–terms are terms in the scalar potential which are quartic in the fields and are proportional to the gauge couplings squared.

2(3). In most high–energy models, the soft SUSY–breaking sfermion mass parameters are taken to be equal at the high–energy scale, but, in principle, they can be different for each generation or even within a generation. However, the sfermion flavor dependence can have important effects on low–energy observables, and it is often strongly constrained. The suppression of flavor changing neutral currents (FCNC's), such as $K_L \to \pi^\circ \nu\bar{\nu}$, requires that either (*i*) the squark soft–SUSY breaking mass matrix is diagonal and degenerate, or (*ii*) the masses of the first– and second–generation sfermions are very large.[66]

The magnitude of left–right sfermion mixing is always proportional to the mass of the corresponding fermion. The left–right mixing of squarks and sleptons of the first and second generation is thus negligible, and $\widetilde{Q}_{L,R}$, with $\widetilde{Q} = \tilde{u}, \tilde{d}, \tilde{c}, \tilde{s}$, and $\tilde{\ell}_{L,R}, \tilde{\nu}_\ell$, with $\ell = e, \mu$, are the real mass eigenstates with masses $m_{\widetilde{Q}_{L,R}}$ and $m_{\tilde{\ell}_{L,R}}, m_{\tilde{\nu}_\ell}$, respectively. For the third generation sfermions, the left–right mixing can be nontrivial. The mass matrix for the top squarks (stops) in the $(\tilde{t}_L, \tilde{t}_R)$ basis is given by

$$M_{\tilde{t}}^2 = \begin{pmatrix} m_{Q_3}^2 + m_t^2 + D_{\tilde{t}_L} & m_t(A_t - \mu/\tan\beta) \\ m_t(A_t - \mu/\tan\beta) & m_{U_3}^2 + m_t^2 + D_{\tilde{t}_R} \end{pmatrix}, \tag{7}$$

where A_t is a soft SUSY–breaking parameter.[i] Unless there is a cancellation between A_t and $\mu/\tan\beta$, left–right mixing occurs for the stop squarks because of the large top quark mass. The stop mass eigenstates are then given by

$$\begin{aligned} \tilde{t}_1 &= \cos\theta_{\tilde{t}}\ \tilde{t}_L + \sin\theta_{\tilde{t}}\ \tilde{t}_R \\ \tilde{t}_2 &= -\sin\theta_{\tilde{t}}\ \tilde{t}_L + \cos\theta_{\tilde{t}}\ \tilde{t}_R, \end{aligned} \tag{8}$$

where the masses and mixing angle $\theta_{\tilde{t}}$ are fixed by diagonalizing the squared–mass matrix Eq. (7). Because of the large mixing, the lightest stop $\tilde{t}_1$ can be one of the lightest sparticles. For the sbottom, an analogous formula for the mass matrix holds with $m_{U_3} \to m_{D_3}$, $A_t \to A_b$, $D_{\tilde{t}_{L,R}} \to D_{\tilde{b}_{L,R}}$, $m_t \to m_b$, and $\tan\beta \to 1/\tan\beta$. For the stau, substitute $m_{Q_3} \to m_{L_3}$, $m_{U_3} \to m_{E_3}$, $A_t \to A_\tau$, $D_{\tilde{t}_{L,R}} \to D_{\tilde{\tau}_{L,R}}$, $m_t \to m_\tau$ and $\tan\beta \to 1/\tan\beta$. The parameters A_t, A_b, and A_τ can be independent soft SUSY–breaking parameters, or they might be related by some underlying principle. When $m_b \tan\beta$ or $m_\tau \tan\beta$ is large ($\mathcal{O}(m_t)$), left–right mixing can also become relevant for the sbottom and stau. It will become clear below that A_b and A_τ do not contribute in a major way to left–right mixing, since they do not have a $\tan\beta$ enhancement.

---

[i] Beware also of different sign conventions for A_t. Both `PYTHIA` and `ISAJET` use the convention used here.

The Higgs boson spectrum at tree level can be expressed in terms of the weak gauge boson masses, the CP–odd Higgs boson mass M_A and $\tan\beta$: [j]

$$\begin{aligned} M^2_{h,H} &= 1/2\left[M^2_A + M^2_Z \mp \sqrt{(M^2_A+M^2_Z)^2 - 4M^2_Z M^2_A \cos^2 2\beta}\right] \\ M^2_{H^\pm} &= M^2_A + M^2_W. \end{aligned} \tag{9}$$

These relations yield $M_h \lesssim M_Z$, but this result is strongly modified by radiative corrections that depend on other MSSM parameters.[20] The dominant radiative corrections to M_h grow as m_t^4 and are logarithmically dependent on the third–generation squark masses. The heavy CP–even and charged Higgs boson masses, M_H and $M_{H^\pm}$, respectively, are directly controlled by M_A. If all SUSY particles were heavy, but M_A were small, then the low–energy theory would look like a two–Higgs–doublet model. For sufficiently large M_A, the heavy Higgs doublet decouples, and the effective low–energy theory has only one light Higgs doublet with SM–like couplings to gauge bosons and fermions.

Within the MSSM, a *general* **upper** bound on M_h can be determined by a careful evaluation of the one–loop and dominant two–loop radiative corrections.[11] For $m_t = 175$ GeV and an extremely conservative set of assumptions,[k] the upper bound on the lightest Higgs mass is maximized, yielding $M_h \lesssim 130$ GeV. For more moderate values of the MSSM parameters, the upper bound on M_h becomes smaller. Most importantly, given the general upper bound on M_h of about 130 GeV, the upgraded Tevatron has the potential to provide a crucial test of the minimal supersymmetric extension of the SM.[12,13]

R–parity, defined as [21] R$=(-1)^{2S+3B+L}$, is a discrete multiplicative symmetry where S is the particle spin, B is the baryon number, and L is the lepton number. All SM particles have R=1, while all superpartners have R=−1, so a single SUSY particle cannot decay into just SM particles if R–parity is conserved. In this case, the lightest superpartner (LSP) is absolutely stable. Astrophysical considerations imply that a stable LSP should be color– and charge–neutral. The best candidates, then, are the lightest neutralino $\widetilde{\chi}^0_1$ and the sneutrino $\tilde{\nu}$, or alternatively (see below) the gravitino $\widetilde{G}$. Since the LSP can carry away energy without interacting in a detector, the apparent violation of momentum conservation is an important part of SUSY phenomenology.[21] Also, when R–parity is conserved, superpartners must be produced in pairs from a SM initial state. The breaking of the R–parity symmetry would result in lepton and/or baryon number violating processes. While there are strong experimental constraints on some classes of R–parity violating interactions, others are hardly constrained at all. Unless it is explicitly stated otherwise, R–parity conservation is assumed below.

---

[j] In the MSSM, M_A is related to the values of the Higgs soft SUSY–breaking parameters m_{H_1} and m_{H_2} and the Higgsino mass parameter μ through $M^2_A = m^2_{H_1} + m^2_{H_2} + 2\mu^2$.

[k] To produce this bound, the masses of all SUSY particles and M_A are chosen to be around a TeV, $\tan\beta > 20$, and the stop mixing parameters are varied to give the largest possible effect.

Quite generally, the dependence of the SUSY spectrum on $\tan\beta$ can be very strong, and it is necessary to determine the possible range of values for this essential parameter of the theory. The fermion masses, which are not fixed by SUSY, are a function of $\tan\beta$ and the SM Yukawa couplings. For the up– and down–quark and lepton masses, it follows that $m_u = h_u v \sin\beta$, $m_d = h_d v \cos\beta$, and $m_\ell = h_\ell v \cos\beta$, where $h_{f=u,d,\ell}$ is the corresponding Yukawa coupling and $v=$ 174 GeV is the order parameter of EWSB. Equivalently, $m_u = h_u v_2, m_d = h_d v_1$ and $m_\ell = h_\ell v_1$, where $v_2 = v\sin\beta$ and $v_1 = v\cos\beta$. The value of $\tan\beta$ and the Yukawa couplings can vary in a range consistent with the experimental values of the fermion masses. However, for the theory to remain perturbatively well defined up to a given cutoff scale, the Yukawa couplings should remain finite up to this cutoff scale. Whether this is the case can be determined by studying the renormalization group evolution of each Yukawa coupling from low to high energy scales. In particular, the large value of the top quark mass is associated with a large value of the top Yukawa coupling at low energies, which, depending on $\tan\beta$, may become too large to be compatible with a perturbative description of the theory.[22,23,17,24] The measured value of the top quark mass, $m_t \simeq 175$ GeV, defines a lower bound on $\tan\beta$ of about 1.2, provided that the top Yukawa coupling remains finite up to a scale of the order of 10^{16} GeV. If, instead, the top Yukawa coupling should remain finite only up to scales of order of a TeV, values of $\tan\beta$ as low as .5 are still possible.[l] A similar situation occurs when $\tan\beta$ is large, but now the crucial role is played by the bottom Yukawa coupling. If $\tan\beta$ becomes too large, large values of the bottom Yukawa coupling are necessary to obtain values of the bottom mass compatible with experiment. The exact bound on $\tan\beta$ depends on the SUSY spectrum, since there are radiative corrections to the bottom mass coming from sparticle exchange loops.[25,26] Generically, it can be shown that values of $\tan\beta \geq 60$ are difficult to obtain if the MSSM is expected to remain a valid theory up to scales of order 10^{16} GeV.

2.2 Supergravity

At present, the exact mechanism of SUSY breaking is unknown. Supergravity (SUGRA) models assume the existence of extra superfields (the so–called "hidden sector") which couple to the MSSM particles only through gravitational–like interactions. When SUSY is spontaneously or dynamically broken in the hidden sector, some of the components of the hidden sector acquire vacuum expectation values. Interaction terms between those components of the hidden sector and the MSSM superfields give rise to the effective soft SUSY–breaking terms of the MSSM, which are proportional vacuum expectation values of the hidden sector divided by powers of $M_{\rm Planck}$. The low–energy Lagrangian then looks like a SUSY–conserving MSSM with a number of extra terms that break SUSY. Although low–energy gravitational interactions depend only on mass and spin, the general supergravity Lagrangian may contain higher–dimensional interactions between the hidden sector and MSSM superfields that are flavor dependent.

---

[l] This implies that a perturbative description of the MSSM would only be valid up to the weak scale, which is, of course, not a very interesting possibility.

The number of SUSY breaking terms is over one hundred. In the minimal SUGRA scenario, however, the MSSM sparticles couple universally to the hidden sector, and the number of terms is greatly reduced. Using this guiding principle, at a scale of order $M_{\rm Planck}$ (or, approximately, M_{GUT}, the scale where the gauge couplings unify), all scalars (Higgs bosons, sleptons, and squarks) are assumed to have a common squared–mass m_0^2, all gauginos (Bino, Wino, and gluino) have a common mass $m_{1/2}$, and all trilinear couplings have the value A_0. After specifying $\tan\beta$, all that remains is to relate the values of the soft SUSY–breaking parameters specified at M_{GUT} to their values at M_{EW}. This is accomplished using renormalization group equations (RGE's). The physical sparticle masses are then determined using relations like Eq. (6), or by diagonalizing mass matrices like those in Eqs. (2) and (7). Finally, the Higgsino mass parameter is determined (up to a sign) by demanding the correct radiative EWSB. At the tree level, this requires

$$\tan^2\beta = \frac{\mu^2 + m_{H_1}^2 + M_Z^2/2}{\mu^2 + m_{H_2}^2 + M_Z^2/2}, \tag{10}$$

where m_{H_1} and m_{H_2} are soft SUSY–breaking mass parameters for the two Higgs doublets evaluated at M_{EW}.

Not surprisingly, the masses of the gluinos, charginos and neutralinos are strongly correlated. The gaugino mass parameters M_i at the electroweak scale depend mainly on the running of the gauge couplings between M_{GUT} and M_{EW}:

$$M_3 = \frac{\alpha_3(M_3)}{\alpha_{GUT}} m_{1/2} \simeq 2.6 m_{1/2}$$

$$M_2 = \frac{\alpha_2(M_2)}{\alpha_{GUT}} m_{1/2} \simeq 0.8 m_{1/2}$$

$$M_1 = \frac{\alpha_1(M_1)}{\alpha_{GUT}} m_{1/2} \simeq 0.4 m_{1/2}, \tag{11}$$

(where we consider $m_{1/2} \sim M_{EW}$). As will be shown below, once the RGE evolution of the Higgs mass parameters is included in Eq. (10), it follows that the Higgsino mass term μ tends to be larger than the Bino and Wino masses M_1, M_2, becoming the largest for values of $\tan\beta$ closest to 1. As a result, the lightest two neutralinos and the lightest chargino tend to be gaugino–like. This is similar to the example presented in Eq. (3) with the approximate mass hierarchy:

$$M_{\widetilde{\chi}_2^0} \simeq 2M_{\widetilde{\chi}_1^0} \simeq M_{\widetilde{\chi}_1^\pm} \simeq 1/3 M_{\tilde{g}}. \tag{12}$$

The lightest neutralino $\widetilde{\chi}_1^0$ can be the LSP.

Because sleptons have only EW quantum numbers and the lepton Yukawa couplings are small, the slepton mass parameters do not evolve much from M_{GUT} to M_{EW}. The left– and right–handed soft SUSY–breaking parameters at the scale M_{EW} which determine the mass eigenstates through Eq. (6) are given by

$$m^2_{L_{1,2}} \simeq m^2_{L_3} \simeq m_0^2 + 0.5 m^2_{1/2}; \qquad m^2_{E_{1,2}} \simeq m^2_{E_3} \simeq m_0^2 + 0.15 m^2_{1/2}. \tag{13}$$

For $\tan\beta \geq 40$, the third generation mass parameters also receive non–negligible contributions from the τ Yukawa coupling in their running which can modify these expressions. The different coefficients of $m_{1/2}$ in Eq. (13) arise from the different EW quantum numbers for sleptons in $SU(2)_L$ doublets and singlets. If m_0 and $m_{1/2}$ are of the same order of magnitude, physical slepton masses are dominated by m_0. When m_0 is small, the sneutrino can be the LSP instead of the $\widetilde{\chi}_1^0$. The $\tilde{\nu}$ mass is fixed by a sum rule $m^2_{\tilde{\nu}_\ell} = m^2_{\tilde{\ell}_L} + M_W^2 \cos 2\beta$.

The squark mass parameters evolve mainly through the strong coupling to the gluino, so their dependence on the common gaugino mass is stronger than for sleptons. For the first and second generation, the left– and right–handed soft SUSY–breaking parameters at M_{EW} are given approximately by

$$m^2_{Q_{1,2}} \simeq m_0^2 + 6.3 m^2_{1/2}; \qquad m^2_{U_{1,2}} \simeq m^2_{D_{1,2}} \simeq m_0^2 + 5.8 m^2_{1/2}. \tag{14}$$

In general, the squarks are heavier than the sleptons or the lightest neutralino and chargino. Since first and second generation squark soft SUSY–breaking parameters are the same for squarks with the same quantum numbers, FCNC's are suppressed.

For the third–generation squarks, the large top and bottom Yukawa couplings play a crucial role in the RGE evolution. As mentioned generically in section 2.1, the top Yukawa coupling h_t is related to the top quark mass by

$m_t = (246/\sqrt{2})h_t \sin\beta$ GeV and the bottom Yukawa coupling h_b is given by $m_b = (246/\sqrt{2})h_b \cos\beta$ GeV, so that h_b is large (of order h_t) when $\tan\beta$ is about 40 or larger. When h_t at M_{GUT} is sufficiently large, it turns out that its low–energy value is independent of its exact value at M_{GUT}. This behavior is known as the *infrared fixed point* solution of the top quark mass.[22,23,24,27] With the definition $Y_t \equiv h_t^2/(4\pi)$, the infrared fixed point value of Y_t at the scale m_t is $Y_t^{ir} \simeq 8\alpha_3/9$. Within the one–loop approximation, the effects of the top Yukawa coupling on the RGE evolution can be parameterized in terms of the ratio Y_t/Y_t^{ir}. For small and moderate values of $\tan\beta$, the left– and right–handed soft SUSY–breaking parameters which determine the stop and sbottom masses are then given by[28,29,30]

$$\begin{aligned} m_{Q_3}^2 &\simeq m_0^2\left(1-\frac{1}{2}\frac{Y_t}{Y_t^{ir}}\right)+m_{1/2}^2\left(6.3+\frac{Y_t}{Y_t^{ir}}\left(-\frac{7}{3}+\frac{Y_t}{Y_t^{ir}}\right)\right) \\ m_{U_3}^2 &\simeq m_0^2\left(1-\frac{Y_t}{Y_t^{ir}}\right)+m_{1/2}^2\left(5.8+\frac{Y_t}{Y_t^{ir}}\left(-\frac{14}{3}+2\frac{Y_t}{Y_t^{ir}}\right)\right), \end{aligned} \tag{15}$$

and $m_{D_3} \simeq m_{D_{1,2}}$. For large $\tan\beta$, assuming $t-b$ Yukawa coupling unification at high energies ($Y_b = Y_t$ at M_{GUT}, which is a generic prediction of $SO(10)$ GUT models), the expressions for the third generation soft SUSY–breaking parameters are:[26]

$$\begin{aligned} m_{Q_3}^2 &\simeq m_0^2\left(1-\frac{6}{7}\frac{Y_t}{Y_t^{ir}}\right)+m_{1/2}^2\left(6.3+\frac{Y_t}{Y_t^{ir}}\left(-4+\frac{12}{7}\frac{Y_t}{Y_t^{ir}}\right)\right) \\ m_{U_3}^2 \simeq m_{D_3}^2 &\simeq m_0^2\left(1-\frac{6}{7}\frac{Y_t}{Y_t^{ir}}\right)+m_{1/2}^2\left(5.8-\frac{Y_t}{Y_t^{ir}}\left(-4+\frac{12}{7}\frac{Y_t}{Y_t^{ir}}\right)\right). \end{aligned} \tag{16}$$

Contributions proportional to A_0^2 and $A_0 m_{1/2}$ with a prefactor proportional to $(1 - Y_t/Y_t^{ir})$ are also present in Eqs. (15) and (16). For $m_t \simeq 175$ GeV, the value of the ratio Y_t/Y_t^{ir} varies from 3/4 to 1 depending on $\tan\beta$, with $Y_t/Y_t^{ir} \to 1$ as $\tan\beta \to 1$, and $Y_t/Y_t^{ir} \simeq 0.85$ for $\tan\beta = 40$. The value of A_t is governed by $m_{1/2}$, and, for large values of the top Yukawa coupling, depends weakly on its initial value and $\tan\beta$,[28]

$$A_t \simeq \left(1-\frac{Y_t}{Y_t^{ir}}\right)A_0 - 2m_{1/2}. \tag{17}$$

The exact values of A_b and A_τ are not important, since the mixing in the stau and sbottom sectors is governed by the terms $m_b\mu\tan\beta$ and $m_\tau\mu\tan\beta$, respectively. In SUGRA models, the above relations between the mass parameters leads to the general prediction, $m_{\widetilde{Q}} \geq 0.85 M_{\tilde{g}}$ (for the five lightest squarks and small or moderate $\tan\beta$).

The soft–SUSY breaking parameters in the Higgs sector also have simple expressions. For small and moderate $\tan\beta$, [28,29,30]

$$\begin{aligned} m^2_{H_1} &\simeq m^2_0 + 0.5 m^2_{1/2} \\ m^2_{H_2} &\simeq m^2_0\left(1-\frac{3}{2}\frac{Y_t}{Y_t^{ir}}\right)+m^2_{1/2}\left(0.5+\frac{Y_t}{Y_t^{ir}}\left(-7+3\frac{Y_t}{Y_t^{ir}}\right)\right). \end{aligned} \tag{18}$$

Substituting these relations back into Eq. (10) yields the result:

$$\begin{aligned} \mu^2 + M_Z^2/2 = m_0^2\left(1+\left(\frac{3}{2}\frac{Y_t}{Y_t^{ir}}-1\right)\tan^2\beta\right)\frac{1}{\tan^2\beta-1}+ \\ m^2_{1/2}\left(0.5-\left(0.5+\frac{Y_t}{Y_t^{ir}}\left(-7+3\frac{Y_t}{Y_t^{ir}}\right)\right)\tan^2\beta\right)\frac{1}{\tan^2\beta-1}. \end{aligned} \tag{19}$$

Note in Eq. (18) that $m^2_{H_2} < 0$, which is usually a sufficient condition to induce EWSB. For large $\tan\beta$, the Higgs mass parameters are more complicated. In the limit of $t-b$ Yukawa unification, they simplify to[26]

$$m^2_{H_1} \simeq m^2_{H_2} \simeq m^2_0\left(1-\frac{9}{7}\frac{Y_t}{Y_t^{ir}}\right)+m^2_{1/2}\left(0.5+\frac{Y_t}{Y_t^{ir}}\left(-6+\frac{18}{7}\frac{Y_t}{Y_t^{ir}}\right)\right), \tag{20}$$

and Eq. (19) must be modified accordingly. All of these relations are only approximate: the coefficients of $m_{1/2}$ depend on the exact values of α_s and the scale of the sparticle masses; the coefficients of m_0 and A_0 depend mainly on $\tan\beta$.

The SUGRA model presented here is minimal (mSUGRA) in the sense that it is defined in terms of only five parameters at a high scale: m_0, $m_{1/2}$, A_0, $\tan\beta$, and the sign of μ. It is natural to question exact universality of the soft SUSY–breaking parameters.[31] For example, in a $SU(5)$ SUSY GUT model, the left–handed sleptons and right–handed down–type squarks reside in the same 5–multiplet of $SU(5)$, and naturally have the common mass parameter $m_0^{(5)}$ at the GUT scale. Similarly, $\tilde{u}_L, \tilde{d}_L$, $\tilde{u}_R$, and $\tilde{e}_R$, which reside in the same 10–multiplet, have a common mass $m_0^{(10)}$. The two Higgs bosons doublets reside in different 5– and $\bar{5}$–multiplets, with masses $m_0^{(5')}$ and $m_0^{(\bar{5}')}$. There is no symmetry principle that demands that all these mass parameters should be the same. The most naive breakdown of exact universality is to consider different values for $m_0^{(5')}$ and $m_0^{(\bar{5}')}$, taking m_0 as the common mass for sleptons and squarks.

Depending on the exact mechanism of SUSY breaking, it may occur that $m_{1/2} \simeq 0$. Low–energy gaugino masses are then dominated by contributions of stop–top and Higgs–Higgsino loops.[32] In this case the gluino could be the LSP with a mass of $M_{\tilde{g}} \lesssim$ a few GeV and the lightest neutralino may be somewhat heavier due to contributions from electroweak loops.[33] Light gluino scenarios are being explored by many experiments.[34]

2.3 Gauge–Mediated Supersymmetry Breaking

In SUGRA, gravitational interactions generate the soft SUSY–breaking terms in the MSSM Lagrangian. Alternatively, soft SUSY–breaking terms can be generated through gauge interactions. This has the feature that mass degeneracies between sfermions with the same quantum numbers (and, hence, the same gauge couplings) occur naturally, which suppresses FCNC's. Also, in gauge–mediated models, the scale of the SUSY breaking is much smaller than the scale where gravity becomes relevant, so there is no possibility of Planck–scale corrections to these degeneracies (as there can be between the GUT and Planck scales in SUGRA).[35] In simple models,[36] the existence of heavy messenger superfields ψ with SM quantum numbers is postulated. SUSY is broken in a hidden sector which also couples to the messengers, so that the ψ fermion components have mass M, while the scalar components have masses $M\sqrt{1 \pm x}$, where x is a dimensionless parameter that controls the size of SUSY breaking. The MSSM gauginos and sfermions acquire masses different from their SM partners because of the radiative effects generated by the messenger fields. It is more convenient to define $\Lambda \equiv xM$, which fixes Λ as the overall mass scale of the MSSM sparticles. The gaugino masses at a low energy scale μ are

$$M_i(\mu) = \frac{\alpha_i(\mu)}{4\pi}\, g(x)(b_i - b_i')\Lambda, \tag{21}$$

where i specifies the gauge group, b_i is the MSSM coefficient of the beta function for the running of α_i, b_i' includes the additional effect of the messenger fields in the running, and $g(x) \simeq 1 + x^2/6$. The mass–squared of the MSSM scalars acquire values

$$\begin{aligned} m_i^2(\mu) = 2\Lambda^2 \sum_i \left(\frac{\alpha_i(M)}{4\pi}\right)^2 C_i \,[f(x)(b_i - b_i') + \\ g(x)^2 \left((b_i - b_i')^2/b_i\right)\left(\alpha_i^2(\mu)/\alpha_i^2(M) - 1\right)], \end{aligned} \tag{22}$$

where $C_1 = 5/3Y^2, C_2 = 3/4$, and $C_3 = 4/3$ (Y is the weak hypercharge) and $f(x) \simeq 1 + x^2/36$. The mass formula in Eq. (22) ignores Yukawa couplings, and will be modified for the stop and possibly sbottom and stau. By comparing the previous two equations, it is clear that the gaugino and scalar masses are roughly of the same order of magnitude. Even after evolving these mass parameters to M_{EW} (ignoring the effects of Yukawa couplings), sfermions with the same quantum numbers acquire the same masses, yielding a natural mass hierarchy between weakly and strongly interacting sfermions; the mass hierarchy of the gauginos is fixed by the gauge couplings (as in SUGRA models). If the superfields ψ reside in a complete representation of $SU(5)$ or $SO(10)$, then unification of the gauge couplings at a high scale is not compromised, though the unification will occur at stronger values of the couplings and at a slightly different scale from the naive GUT scale. One distinctive feature of these models is that the spin–3/2 superpartner of the graviton, the gravitino $\widetilde{G}$, can play a crucial role in the phenomenology. Since the gravitino mass is given by the relation $M_{\widetilde{G}} = M\Lambda/M_{\rm Planck}$, the gravitino can be very light depending on the value of M, unlike SUGRA, where the gravitino has a mass on the order of M_W. As a result, in gauge–mediated Supersymmetry breaking, the gravitino can be the LSP.

In the above discussion, it is assumed that the messengers ψ form a complete GUT multiplet. However, if the messengers were neutral under some gauge group, then the associated gauginos would be massless at one–loop because of gauge invariance. In particular, it is possible to construct a model where the gluino is a stable LSP with a mass of a few tens of GeV.[37] In this case, the missing energy signal for SUSY disappears, since a stable LSP gluino will form stable hadrons.

2.4 R–Parity Violation

One simple extension of the MSSM is to break the multiplicative R–parity symmetry. Presently, neither experiment nor any theoretical argument demand R–parity conservation, so it is natural to consider the most general case of R–parity breaking. It is convenient to introduce a function of superfields called the superpotential, from which the Feynman rules for R–parity violating processes can be derived. The R–parity violating (RPV) terms which can contribute to the superpotential are[m]

$$W_{RPV} = \lambda_{ijk} L^i L^j \bar{E}^k + \lambda^{'}_{ijk} L^i Q^j \bar{D}^k + \lambda^{''}_{ijk} \bar{U}^i \bar{D}^j \bar{D}^k \tag{23}$$

where i, j, k are generation indices (1,2,3), $L_1^i \equiv \nu_L^i$, $L_2^i = \ell_L^i$ and $Q_1^i = u_L^i$, $Q_2^i = d_L^i$ are lepton and quark components of $SU(2)_L$ doublet superfields, and $E^i = e_R^i$, $D^i = d_R^i$ and $U^i = u_R^i$ are lepton, down and up– quark $SU(2)_L$ singlet superfields, respectively. The unwritten $\mathrm{SU}(2)_L$ and $\mathrm{SU}(3)_C$ indices imply that the first term is antisymmetric under $i \leftrightarrow j$, and the third term is antisymmetric under $j \leftrightarrow k$. Therefore, $i \neq j$ in $L^i L^j \bar{E}^k$ and $j \neq k$ in $\bar{U}^i \bar{D}^j \bar{D}^k$. The coefficients λ_{ijk}, $\lambda^{'}_{ijk}$ and $\lambda^{''}_{ijk}$ are Yukawa couplings, and there is no *a priori* generic prediction for their values. In principle, W_{RPV} contains 45 extra parameters over the R–parity–conserving MSSM case.

---

[m] In Eq. (23) bilinear terms are ignored. A discussion of the phenomenological implications of such terms can be found in the literature.[38]

Expanding Eq. (23) as a function of the superfield components, the interaction Lagrangian derived from the first term is

$$\mathcal{L}_{LLE} = \lambda_{ijk} \left\{ \tilde{\nu}^i_L e^j_L \bar{e}^k_R + \tilde{e}^i_L \nu^j_L \bar{e}^k_R + (\tilde{e}^k_R)^* \nu^i_L e^j_L + h.c. \right\} \tag{24}$$

and from the second term,

$$\begin{aligned}\mathcal{L}_{LQD} = \lambda^{'}_{ijk} \Big\{ & \tilde{\nu}^i_L d^j_L \bar{d}^k_R - \tilde{e}^i_L u^j_L \bar{d}^k_R + \tilde{d}^j_L \nu^i_L \bar{d}^k_R - \tilde{u}^j_L e^i_L \bar{d}^k_R + \\ & (\tilde{d}^k_R)^* \nu^i_L d^j_L - (\tilde{d}^k_R)^* e^i_L u^j_L + h.c. \Big\}\end{aligned} \tag{25}$$

Both of these sets of interactions violate lepton number. The $\bar{U}\bar{D}\bar{D}$ term, instead, violates baryon number. In principle, all types of R–parity violating terms may co–exist, but this can lead to a proton with a lifetime shorter than the present experimental limits. The simplest way to avoid this is to allow only operators which conserve baryon–number but violate lepton–number or vice versa.

There are several effects on the SUSY phenomenology due to these new couplings: (1) lepton or baryon number violating processes are allowed, including the production of single sparticles (instead of pair production), (2) the LSP is no longer stable, but can decay to SM particles within a collider detector, and (3) because it is unstable, the LSP need not be the neutralino or sneutrino, but can be charged or colored.

Present data are in remarkable agreement with the SM predictions, and very strong bounds on the R–parity–breaking operators can be derived from the following processes: (a) charged–current universality, (b) $\Gamma(\tau \rightarrow e\nu\bar{\nu})/\Gamma(\tau \rightarrow \mu\nu\bar{\nu})$, ($c$) the bound on the mass of ν_e, (d) neutrino–less double–beta decay, (e) atomic parity violation, (f) $D^0 - \bar{D}^0$ mixing, (g) $R_\ell = \Gamma_{had}(Z^0)/\Gamma_\ell(Z^0)$, ($h$) $\Gamma(\pi \rightarrow e\bar{\nu})/\Gamma(\pi \rightarrow \mu\bar{\nu})$, ($i$) $BR(D^+ \rightarrow \bar{K}^{0*}\mu^+\nu_\mu)/BR(D^+ \rightarrow \bar{K}^{0*}e^+\nu_\mu)$, ($j$) ν_μ deep–inelastic scattering, (k) $BR(\tau \rightarrow \pi\nu_\tau)$, ($l$) heavy nucleon decay, and (m) $n - \bar{n}$ oscillations. Additional limits can be derived from deep inelastic experiments at HERA.[39] On the other hand, within the allowed values of the R–parity–violating couplings, $\lambda_{ijk}, \lambda'_{ijk}$, a whole new world opens up for SUSY searches.

2.5 Run Ia Parameter Sets (RIPS)

Some CDF and DØ SUSY searches are analyzed in the framework of so–called "SUGRA–inspired models." To understand the limits that appear in many published analyses, it is necessary to state explicitly the framework behind RIPS.

First, there are five main input parameters: $M_{\tilde{g}}, m_{\widetilde{Q}}, M_A, \tan\beta$ and the magnitude and sign of μ. The gluino mass $M_{\tilde{g}}$ is defined to be M_3, which is equivalent to specifying $m_{1/2}$ and, hence, M_1 and M_2 using the unification relations Eq. (11). The chargino and neutralino properties are then fixed by $M_1, M_2, \tan\beta$ and μ. In practice, the value of μ is set much larger than M_1 and M_2, so the properties of the neutralinos, charginos, and gluino are similar to those in a pure SUGRA model.

Next, all squark soft SUSY–breaking mass parameters are set to $m_{\widetilde{Q}}$, and the D–terms are neglected. The result is that the first 5 squarks are degenerate in mass. This may be unrealistic if $\tan\beta$ is large, since the sbottom mass can be naturally lighter because of non–negligible off–diagonal elements in the sbottom mass matrix. The stop squarks are made heavier than the other squarks by fixing $A_t = \mu/\tan\beta$ (see Eq. (7)), which tunes away the mixing between $\tilde{t}_L$ and $\tilde{t}_R$. The resulting stop masses are $m_{\tilde{t}_1} = m_{\tilde{t}_2} = \sqrt{m^2_{\widetilde{Q}} + m^2_t}$. Therefore, experimental limits placed on RIPS show no sensitivity to the stop squarks. Note that, in SUGRA models, the stop squared–mass soft SUSY–breaking parameters $m^2_{Q_3}$ and $m^2_{U_3}$ are generally not equal and are smaller than the other squark parameters at M_{EW}, so that one stop squark is lighter than the other squarks.

Giving the other five squarks a common value at the weak scale ignores the details of running from the GUT scale (see Eq. (14)) and the different D–terms. However, using an average of the two formulae in Eq. (14), a specific $m_{1/2}$ and $m_{\widetilde{Q}}$ roughly determine a value of m^2_0. Whenever there is a solution with $m^2_0 > 0$ (which implies $m_{\widetilde{Q}} > 0.85 M_{\tilde{g}}$), RIPS has many features of a SUGRA model. Indeed, when $m_{\widetilde{Q}} > M_{\tilde{g}}$, the approximate SUGRA relations $m^2_{\tilde{\ell}_L} = m^2_{\widetilde{Q}} - 0.73 M^2_{\tilde{g}} - 0.27 M^2_Z \cos 2\beta$, $m^2_{\tilde{\ell}_R} = m^2_{\widetilde{Q}} - 0.78 M^2_{\tilde{g}} + 0.23 M^2_Z \cos 2\beta$, and $m^2_{\tilde{\nu}} = m^2_{\widetilde{Q}} - 0.73 M^2_{\tilde{g}} + 0.5 M^2_Z \cos 2\beta$ are used to fix the slepton masses.[n] The region $m_{\widetilde{Q}} < M_{\tilde{g}}$ is very hard to realize in SUGRA models, but is also worth investigating. In this case, for some analyses, a constant value of 350

---

[n] Observe that the D–terms for the sleptons, although correct, are negligible in comparison with the approximation made in defining a common $m_{\widetilde{Q}}$. However, D–terms are included to assure the correct splittings between the $\tilde{\ell}_L$ and $\tilde{\nu}$ masses.

GeV is set by hand for $m_{\tilde{\ell}_L}$, $m_{\tilde{\ell}_R}$, and $m_{\tilde{\nu}}$. Accordingly, experimental limits placed on RIPS when $m_{\widetilde{Q}} < M_{\tilde{g}}$ show little sensitivity to the sleptons.

Finally, the Higgs mass M_A is used to determine the Higgs boson sector. This is equivalent to considering partial non–universality for the scalar sfermion and Higgs boson soft SUSY–breaking mass parameters at high energies, *i.e.* $m_0 \neq m_0^{(5')} \neq m_0^{(5')}$ (see the discussion near the end of Sec. 2.2). In practice, the CP–odd Higgs boson mass M_A is set to a large value, so that the lightest neutral Higgs boson h has SM–like couplings to gauge bosons and fermions, and all other Higgs bosons are so heavy they are not kinematically accessible at the Tevatron.

3 The CDF and DØ Detectors

The CDF [41] and DØ [42] detectors are located at the interaction regions B0 and D0 in the accelerator ring.[a] Both detectors feature particle tracking detectors close to the interaction region, surrounded by quasi–hermetic calorimetry covering the region of pseudorapidity[b] of approximately $|\eta| < 4$. Muon detection systems are located outside the calorimeters for both detectors.

3.1 The CDF Detector

The CDF detector is distinguished by its magnetic spectrometer: a 3–m diameter, 5–m long superconducting solenoidal magnet, which creates a 1.4 T field uniform at the 0.1% level and contains the particle tracking detectors. A four–layer silicon microstrip vertex detector (SVX),[43] located directly outside the beampipe, tracks charged particles in the $r - \phi$ plane. The SVX measures the impact parameter of tracks coming from secondary vertices of bottom and charm decays with a typical resolution of 30 μm, providing heavy–flavor tagging for jets. A set of vertex time projection chambers (VTX) surrounding the SVX provides tracking in the radial and z directions and is used to find the z position of the $\overline{p}p$ interaction. Outside the VTX, between from a radius of 30 to 150 cm, the 3.2–m long central tracking chamber (CTC) is used to measure the momentum of charged particles, with up to 84 measurements per track.

The calorimeter is divided into a central barrel ($|\eta| < 1.1$), end–plugs [c] ($1.1 < |\eta| < 2.4$) and forward/backward modules ($2.4 < |\eta| < 4.2$). Each of

---

[a] The Tevatron ring has six–fold symmetry, with the centers of the straight sections labelled as A0, B0, C0, D0, E0, and F0.

[b] The pseudorapidity η is defined as $-\ln(\tan\frac{\theta}{2})$. In the CDF and DØ coordinate systems, θ and ϕ are the polar and azimuthal angles, respectively, with respect to the proton beam direction z.

[c] "End–plugs" because they plug into the ends of the solenoid and central calorimeter.

these is segmented into projective[d] electromagnetic and hadronic towers subtending 0.1 in η by 15° in ϕ in the central calorimeter and 5° elsewhere. Wire chambers with cathode strip readout give information on electromagnetic shower profiles in the central and plug calorimeters (CES and PES systems, respectively). A system of drift chambers (CPR) outside the magnet coil and in front of the electromagnetic calorimeters serves as a "preradiator," allowing additional photon/π^0 discrimination on a statistical basis. Muons are identified with the central muon chambers, situated outside the calorimeters in the region $|\eta| < 1.1$.

The magnetic spectrometer measures muon and other charged particle transverse momenta with a resolution $\sigma_{p_T}/p_T < 0.001 p_T$ (p_T in GeV) and allows a precision calibration of the electromagnetic calorimeters by comparing the measured calorimeter response to the measured momentum from high–energy electrons from W decays.[45] Electron energies are measured with a resolution $\sigma_E/E = .135/\sqrt{E_T} \oplus .01$ (E_T in GeV).[e] Jets are reconstructed as energy clusters in the calorimeter, using a cone algorithm [44] with a cone radius of either $R = 0.7$ [46] or $R = 0.4$ [47] in $\Delta\eta \times \Delta\phi$ space. The jet energy resolution in the central region is approximately $\sigma_E/E = .80/\sqrt{E} \oplus .04$ (E in GeV).

Missing transverse energy,[f] ($\not\!\!E_T$), a key quantity in SUSY searches, is calculated as $\sum E^{\mathrm{tower}}\,(\hat{\mathbf{n}} \cdot \hat{\mathbf{r}})\,\hat{\mathbf{r}}$, where the sum is over both electromagnetic and hadronic calorimeter towers[g] in $|\eta| < 3.6$, E^{tower} is the energy measured in the tower, $\hat{\mathbf{n}}$ is the unit vector pointing in the direction of the center of the tower from the event vertex, and $\hat{\mathbf{r}}$ is the unit vector in the radial direction. The $\not\!\!E_T$ is always corrected for the momentum of muons; for many SUSY analyses, it is also corrected for the calorimeter response to jets. The typical resolution on a component of $\not\!\!E_T$ is 5.7 GeV in $Z^0 \rightarrow e^+e^-$ events.

3.2 The DØ Detector

The DØ detector consists of three major components: a non–magnetic central tracking system, central and forward Liquid Argon sampling calorimeters, and a toroidal muon spectrometer. The central tracking system consists of four detector subsystems: a vertex drift chamber, a transition radiation detector, a central drift chamber, and two forward drift chambers. Its outer radius is

---

[d] Projective means pointing approximately at the interaction region.

[e] The symbol $\oplus$ denotes addition in quadrature, *e.g.* $a \oplus b = \sqrt{a^2 + b^2}$. The total resolution can be parameterized this way when there are two or more independent components of resolution.

[f] The transverse momentum of a particle with momentum p is $p_T = p \sin\theta$. The analogous quantity using energy, defined as $E_T = E \sin\theta$, is called transverse energy.

[g] A tower is a cell in $\eta - \phi$ space.

76 cm. The system provides identification of charged tracks in the pseudorapidity range $|\eta| \leq 3.5$. It measures the trajectories of charged particles with a resolution of 2.5 mrad in ϕ and 28 mrad in θ. Using the reconstructed charged tracks, the position of the primary interaction along the beamline direction is reconstructed with a resolution of 8 mm. The central tracking system also measures the ionization of tracks to allow single charged particles to be distinguished from e^+e^- pairs from photon conversion. The transition radiation detector aids in distinguishing electrons from charged pions.

The calorimeter is transversely segmented into pseudoprojective towers with $\Delta\eta \times \Delta\phi = 0.1 \times 0.1$ and provides full coverage to $|\eta| \leq 4.2$. The calorimeter is divided into three parts, a central calorimeter and two end calorimeters. These are further segmented into an inner electromagnetic section, followed by a fine hadronic section, and then a coarse hadronic section. Between the central and end–cap calorimeters, a set of scintillator tiles provides improved energy resolution for jets that straddle the two detectors. The electromagnetic (EM) calorimeter is divided into 32 modules in ϕ, each of which has 22 layers, each approximately 1 radiation length[h] thick, with Liquid Argon as the active element and ^{238}U plates as the passive element. These layers are arranged into four longitudinal segments per tower, called cells. The first cell contains 2 layers, the second cell contains 2 more layers, the third cell is finely segmented, with $\Delta\eta \times \Delta\phi = 0.05$ x 0.05 and contains 7 layers, and the last cell contains 10 layers. The fine hadronic calorimeter uses a Uranium–Niobium alloy as its passive element, and the coarse hadronic uses copper. The electron energy resolutions, as measured in the EM calorimeter, are $\sigma_E/E = 0.130/\sqrt{E_T} \oplus 0.0115 \oplus 0.4/E$ for $|\eta| < 1.1$, and $\sigma_E/E = 0.157/\sqrt{E} \oplus 0.010 \oplus 0.4/E$ for $1.4 \leq |\eta| \leq 3.0$.[48] The azimuthal position resolution for electrons above 50 GeV as measured by the calorimeter is 2.5 mm. The muon spectrometer provides muon detection in the range $|\eta| \leq 3.3$. The total thickness of the calorimeter plus the toroid varies from 13 to 19 interaction lengths, making hadronic punch–through backgrounds negligible. The muon momentum resolution is $\sigma_p/p = 0.18(p - p_0)/p \oplus 0.008p$ (p in GeV/c, $p_0 = 2$ GeV/c). The DØ detector has a compact tracking volume which helps control backgrounds to prompt muons from in–flight decays of π and K mesons. Jets are reconstructed as energy clusters in the calorimeter, using a cone algorithm with a cone radius of $R = 0.5$ or $R = 0.7$ in $\Delta\eta \times \Delta\phi$.[49] The jet energy resolution is approximately $\sigma_E/E = 0.8/\sqrt{E}$ (E in GeV).[50]

$\not\!\!E_T$ is calculated using the vector sum of energy deposited in all calorimeter cells, over the full calorimeter coverage for $|\eta| \leq 4.2$, with corrections applied to clustered cells to take account of the jet energy scale, and to unclustered cells as determined from studies of E_T balance in $Z^0 \rightarrow e^+e^-$ events that do not contain hadronic calorimeter clusters. The resolution on a component of $\not\!\!E_T$ in "minimum–bias" events[i] is 1.1 GeV+ 0.02 $\sum E_T$, where $\sum E_T$ is the scalar sum of transverse energies in all calorimeter cells. For some analyses, the $\not\!\!E_T$ is corrected for the presence of muons, which only leave a small fraction of their energy in the calorimeter.

---

[h] The radiation length is the mean distance traversed by an electron in a given material during which it radiates a fraction $1 - e^{-1}$ of its energy via bremsstrahlung.

3.3 Experimental Realities

There are potentially two types of backgrounds to any experimental signature, physics and instrumental. Physics backgrounds mimic the event signature even in an ideal detector, while instrumental backgrounds arise because of detector flaws. Experimental signatures – SUSY or otherwise – are identified from "objects" – the building blocks of the event. Examples of objects that CDF and/or DØ use are electrons, muons, tau's, $\not\!\!E_T$, so–called "generic jets" (presumably from quarks and/or gluons, but without flavor identification), c's, b's, photons, and, using another level of kinematic reconstruction, W's, Z's, and t's. The selection of each of these objects carries with it an efficiency and also a "fake rate," a probability that the object is actually a different object which has been misidentified. The description of an object as an "electron," for example, more precisely means an "electron candidate that passes the electron cuts," and no more and no less.

For the majority of searches, the signal and its physics backgrounds can be estimated using Monte Carlo simulation. The output of an event generator such as `ISAJET`[51] or `PYTHIA`[52] can be folded with relatively simple parameterizations of the detector response to give a good description of the data. A typical simple simulation transforms the final state partons from a Monte Carlo into jets, using a clustering algorithm similar to the one used for the data. It then convolutes the momenta of the electrons, photons, muons, and jets with the appropriate experimental resolutions, generating "smeared" momenta. $\not\!\!E_T$ is calculated by first summing the smeared visible momenta, and then adding the effects of additional minimum–bias events in the same beam crossing. When calculating the geometric acceptance of the detector, it is necessary to include the distribution for the interaction vertex position in z, which is Gaussian with an RMS of approximately 30 cm. Finally, the detection efficiencies for electrons, photons, b–quarks, τ's, and muons (jets above 20 GeV are usually found with good efficiency) are applied. Initial and final state gluon radiation need to be included, since they can affect the efficiency by adding extra jets which can modify the event signature or "promote" backgrounds into the signature.

---

[i] These events are defined by the requirement that a beam–beam collision took place as measured by arrays of scintillation counters forward and backward near the beampipe, and therefore have a smaller selection bias than events selected with more selective triggers.

In order to make even rough predictions of instrumental backgrounds, imperfections in the detectors must be taken into account. Two effects make these difficult to estimate: fakes, and tails on jet energy resolution distributions. Because of the very large multi–jet production rate at the Tevatron, there can be significant fake backgrounds, even if the fake probability is very small. Fakes are very complicated, and the fake rate must be evaluated for each analysis using the appropriate data. In general, the efficiency for properly identifying an object and the probability that another object fakes it are complementary. For signatures dominated by instrumental backgrounds, tighter selection criteria ("cuts") make for a purer sample, but reduce the efficiency. For signatures dominated by physics backgrounds, looser cuts are preferred because they produce a higher efficiency for the same ratio of signal to background. Fakes are an especially serious problem for signatures involving photons, tau's, b– and c–quark tagging, and $\not{E}_T$ in events with jets. Although jet energy resolutions are roughly Gaussian, even small non–Gaussian tails, convoluted with the large jet cross section, can lead to significant numbers of events with large fake $\not{E}_T$. In addition, there are some other factors which contribute to fakes and which are unique to working at the Tevatron, such as the long interaction region, the existence of multiple collisions in a single event, the presence of the Main Ring in the same tunnel as the beam, and larger cosmic ray backgrounds than found at detectors that are deeper underground (such as the LEP experiments). Even a full detector simulation cannot correctly model all detector imperfections and these other effects.

4 The Present Status of Sparticle Searches

Most previous Tevatron searches have been made under very specific assumptions. Several of the classic signatures, such as "jets+$\not{E}_T$,"[53] "trileptons,"[54,56] and "same–sign dileptons"[55] are likely to be fruitful in many models; others may be specific to a certain model. We advocate a signature–based approach, in which a broad range of channels are studied for departures from SM expectations, without engineering the analysis for a specific class of models (see Appendices A and B). While this may sound obvious, it is a large task with no well–defined beginning. With the experience of several years of data taking, however, experimentalists now have an idea of what they can do well. Signatures involving high–p_T isolated electrons, muons, and photons, b–quarks, c–quarks, τ leptons, and/or $\not{E}_T$ can be measured accurately and have understandable backgrounds. Such signatures then are a practical starting point for the new generation of searches. In addition, there are motivations that are more general than the predictions of specific models for studying samples of (*i*) high–mass, high–$\not\!\!E_T$ events to probe gluino and squark production, (*ii*) inclusive leptons, lepton pairs, and gauge bosons (γ, W, and Z) to probe both direct and cascade production of charginos and neutralinos, and (*iii*) third–generation fermions (t, b, and τ) to probe decays of light squarks and sleptons, as well as decays of Higgs bosons and Higgsinos. When setting limits, it is convenient to use specific models which reduce the number of free parameters (such as SUGRA or RIPS), but the quoted limits are valid only in that context and are not general limits. New physics may appear where we do not expect it.

In the sections below we discuss the present status of searches at the Tevatron. We also discuss the phenomenology behind these searches and comment on possible improvements. Table 1 summarizes those CDF and DØ analyses that have been published or presented at conferences. The pace and scope of supersymmetry searches at the Tevatron, as well as the sophistication, have grown enormously in the last several years as the emphasis has shifted beyond the top quark and more data have become available; there are many analyses currently in progress. A much broader picture of the Tevatron's capabilities should emerge as these results become available.

4.1 Charginos and Neutralinos

In SUGRA models, the light neutralinos and charginos are much lighter than the gluino or squarks, and may be the only sparticles directly accessible at the Tevatron. In general, the lightest neutralino is a good LSP candidate, so, assuming all charginos and neutralinos are relatively light, a discussion of their phenomenology is a good starting point for an overview of Tevatron searches.

Chargino and neutralino pairs would be produced directly[a] at hadron colliders through their electroweak couplings to squarks and the vector bosons γ, W, and Z. The production cross sections are not a simple function of chargino and neutralino masses, but depend also on their (model–dependent) mixings and the squark masses. Quite generally, there are three contributions to $\widetilde{\chi}\widetilde{\chi}$ production: (*i*) s–channel gauge boson production, (*ii*) t–channel squark exchange, and (*iii*) interference. For type (*i*), the reactions $q\bar{q}^{'} \rightarrow W^* \rightarrow \widetilde{\chi}_i^{\pm}\widetilde{\chi}_j^0$ and $q\bar{q} \rightarrow \gamma^*/Z^* \rightarrow \widetilde{\chi}_i^+\widetilde{\chi}_j^-$ occur through Wino and Higgsino components, and $q\bar{q} \rightarrow Z^* \rightarrow \widetilde{\chi}_i^0\widetilde{\chi}_j^0$ through Higgsino components of the neutralinos and

---

[a] They may also be produced indirectly in the decays of heavier sparticles.

Table 1: A compilation of results from Run I Tevatron SUSY searches as of the summer of 1997. The symbol b denotes an additional b–tagged jet. Also listed are the references and the section of this chapter where each analysis is discussed. More information is available for DØ at $http://www-d0.fnal.gov/public/new/new\_public.html$, and for CDF at $http://www-cdf.fnal.gov/$

Sparticle	Signature	Expt.	Run	$\int \mathcal{L}dt(\mathrm{pb}^{-1})$	Ref.	Sec.
Charginos and Neutralinos	$\not\!\!E_T$+trilepton	CDF	Ia	19	[60]	4.1
	$\not\!\!E_T$+trilepton	CDF	Iab	107	[61]	”
	$\not\!\!E_T$+trilepton	DØ	Ia	12.5	[62]	”
	$\not\!\!E_T$+trilepton	DØ	Ib	95	[63]	”
	$\gamma\gamma$+$\not\!\!E_T$or jets	CDF	Ib	85	[119]	4.10
	$\gamma\gamma$+$\not\!\!E_T$	DØ	Iab	106	[120]	”
Squarks and Gluinos	$\not\!\!E_T$+ $\geq$3,4 jets	CDF	Ia	19	[68]	4.2
	$\not\!\!E_T$+ $\geq$3,4 jets	DØ	Ia	13.5	[67]	”
	$\not\!\!E_T$+ $\geq$3 jets	DØ	Ib	79.2	[69]	”
	dilepton+ $\geq$2 jets	CDF	Ia	19	[74]	”
	$\not\!\!E_T$+dilepton+ $\geq$2 jets	CDF	Ib	81	[75]	”
	$\not\!\!E_T$+dilepton	DØ	Ib	92.9	[73]	”
Stop	$\not\!\!E_T$+ℓ+ $\geq$2 jets+b	CDF	Ib	90	[80]	4.3
	$\not\!\!E_T$+ℓ+ $\geq$3 jets+b	CDF	Iab	110	[82]	”
	dilepton+jets	DØ	Ib	74.5	[81]	”
	$\not\!\!E_T$+2 jets	DØ	Ia	7.4	[79]	”
	$\not\!\!E_T$+γ+b	CDF	Ib	85	[119]	4.11
Sleptons	$\gamma\gamma$ $\not\!\!E_T$	DØ	Iab	106	[120]	4.10
Charged Higgs	dilepton + $\not\!\!E_T$	CDF	Ia	19	[100]	4.5
	τ+2 jets+$\not\!\!E_T$	CDF	Ia	19	[99]	”
	τ+b+$\not\!\!E_T$+(ℓ,τ,jet)	CDF	Iab	91	[87]	”
	τ+b+$\not\!\!E_T$+(ℓ,τ,jet)	DØ	Iab	125	[90]	”
Neutral Higgs	$WH \to \ell + \not\!\!E_T$+$b$+jet	CDF	Iab	109	[95]	4.6
	$WH \to \ell + \not\!\!E_T$+$b$+jet	DØ	Ib	100	[94]	”
	$WH, ZH \to \gamma\gamma$+2 jets	DØ	Ib	101.2	[97]	”
	$ZH \to b$+jet+$\not\!\!E_T$	DØ	Ib	20	[101]	”
	$WH, ZH \to$ 2 jets+2 b's	CDF	Ib	91	[96]	”
R violating	dilepton+$\geq$ 2 jets	CDF	Iab	105	[104]	4.8
Charged LSP	slow, long–lived particle	CDF	Ib	90	[102]	4.7

charginos, respectively.[b] In type (ii), the scattering quarks and antiquarks exchange squarks subject to the constraint that $\widetilde{Q}_R$ couples only to Bino component of neutralinos, and $\widetilde{Q}_L$ to Bino and Wino components of the neutralinos and to charginos. Any $\widetilde{Q}_R$ or $\widetilde{Q}_L$ coupling to Higgsino–components is proportional to the corresponding quark mass and can be ignored for chargino and neutralino pair production (even though $\tilde{b}$ and $\tilde{t}$ have large couplings, the contribution of b and t initial states from hadrons is small). Hence, in chargino pair production (*e.g.* $\widetilde{\chi}_1^+\widetilde{\chi}_1^-$), only $\widetilde{Q}_L$ exchange is important, since $\widetilde{Q}_R$ only couples to the charged Higgsino. In the case when all squarks are heavy, type (*i*) contributions dominate. When the squarks are sufficiently light, both type (*ii*) and (*iii*) can be important. For example, if $|\mu| \gg M_1, M_2$ (see Eq. (3)), then $\widetilde{\chi}_1^0$, $\widetilde{\chi}_2^0$, and $\widetilde{\chi}_1^\pm$ are mostly gaugino–like, and both $\widetilde{Q}_L$ and $\widetilde{Q}_R$ can have electroweak strength couplings to them. If, on the other hand, $|\mu| \ll M_1, M_2$ (see Eq. (4)), $\widetilde{Q}$ exchange is only important for the heavier states, which might not be kinematically accessible.

---

[b] An asterisk superscript * on a gauge boson refers to a resonance off the mass shell.

Figure 1 shows the production cross sections of various chargino and neutralino pairs at the Tevatron for the limiting cases considered earlier in Eq. (3) and Eq. (4). In this figure, $\tan\beta = 2$, $m_{\widetilde{Q}} = 500$ GeV, and the gauginos obey the unification relations (see Eq. (11)). The left figure is generated by fixing $\mu = -1$ TeV and varying $m_{1/2}$, the right figure by fixing $m_{1/2}$=1 TeV and varying μ. For reference, the SM $W^\pm h$ production cross section is shown as a function of M_h. The example of Eq. (3) is most like a pure SUGRA model, in which the couplings of $W\widetilde{\chi}_1^\pm\widetilde{\chi}_2^0$ and $Z\widetilde{\chi}_1^+\widetilde{\chi}_1^-$ are large, so the $\widetilde{\chi}_1^\pm\widetilde{\chi}_2^0$ and $\widetilde{\chi}_1^+\widetilde{\chi}_1^-$ production cross sections are the largest.

Charginos and neutralinos can also be produced in associated production: $\widetilde{Q}\widetilde{\chi}$ and $\tilde{g}\widetilde{\chi}$. This is discussed further in Section 4.2.

The decay patterns for the charginos and neutralinos are also very model dependent. When kinematically allowed, a tree–level 2–body decay dominates over a tree–level 3–body decay, because the latter has an extra factor of $g^2/(4\pi^2)$ in the decay rate. Possible 2–body decays of the chargino are to $W^\pm\widetilde{\chi}_1^0$, $H^\pm\widetilde{\chi}_1^0$, $\tilde{\ell}_{L,R}\nu$, $\tilde{\nu}\ell$ and $\widetilde{Q}q'$. The heavier chargino $\widetilde{\chi}_2^\pm$ can also decay to $Z\widetilde{\chi}_1^\pm$ and $h\widetilde{\chi}_1^\pm$ (when Higgs bosons are part of the event signature, the final states can contain heavy flavor quarks or tau leptons). When no 2–body final states are kinematically allowed, the chargino will decay to a 3–body final state with contributions similar to those for chargino production (described previously): (*i*) virtual gauge boson decays, (*ii*) virtual sfermion decays, and (*iii*) interference. A common decay is $\widetilde{\chi}^\pm \to \widetilde{\chi}^0 f\bar{f}'$. If sfermions are much heavier than a chargino, then type (*i*) dominates, and the decays proceed through W^* with branching ratios similar to those of the on–shell W boson. Virtual squarks and sleptons can significantly alter the branching ratios to a specific $f\bar{f}'$ final state depending on the squark and slepton masses, so that a 100% branching

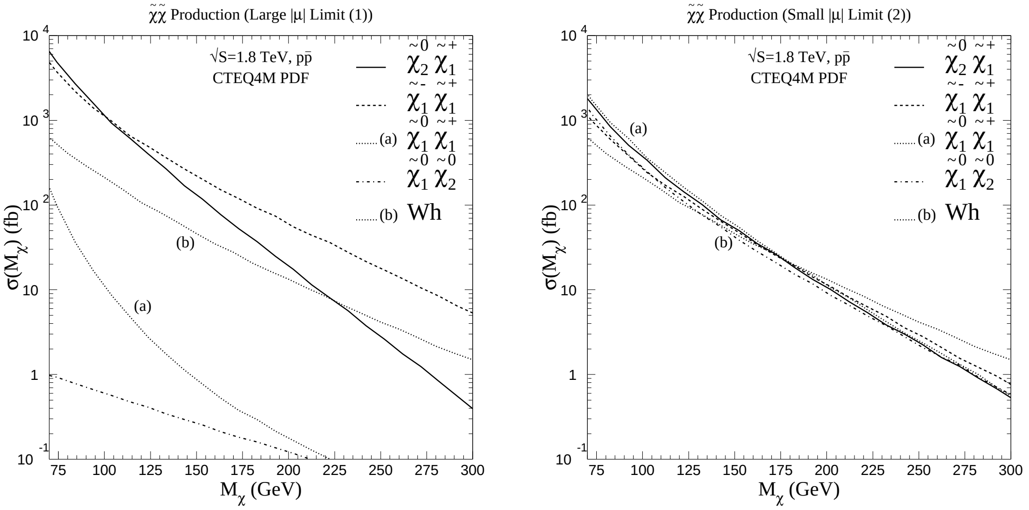

Figure 1: Production cross sections at the Tevatron for chargino and neutralino pair production versus the lightest chargino mass for two limiting models discussed in the text: large $|\mu|$ (Left) and small $|\mu|$ (Right). The Wh cross section (curve b) is shown for reference as a function of M_h.

ratio to $\ell\nu\widetilde{\chi}_1^0$ or $jj\widetilde{\chi}_1^0$ final states is possible. A 3–body decay $\widetilde{\chi}_j^\pm \to \tilde{g}q\bar{q}'$ can occur through virtual squark decays, provided the gluino is light enough (see Appendix A).

Similarly, for neutralinos, the 2–body decays to $Z\widetilde{\chi}^0$, $h\widetilde{\chi}^0$, $W^\mp\widetilde{\chi}^\pm$, $H^\mp\widetilde{\chi}^\pm$, $\tilde{\ell}_{L,R}\ell$, $\tilde{\nu}\nu$ or $\widetilde{Q}q$ will dominate when kinematically allowed. When this is not the case, the 3–body decay $\widetilde{\chi}_i^0 \to \widetilde{\chi}_j^0 f\bar{f}$ (or $\widetilde{\chi}^0 \to \tilde{g}q\bar{q}$) can occur through virtual Z bosons, squarks, or sleptons. Three–body decays can also be in competition with a loop decay, so that $\widetilde{\chi}_2^0 \to \widetilde{\chi}_1^0\gamma$, since the same factor of $g^2/(4\pi)^2$ coming from a loop integral for a 2–body decay also appears in the 3–body decay rate. Such a decay is important when the $\widetilde{\chi}_1^0$ is Higgsino–like and $\widetilde{\chi}_2^0$ is gaugino–like, or *vice versa*.

In general, for $\widetilde{\chi}_2^0\widetilde{\chi}_1^\pm$ production, the final states are (i) four leptons and $\not\!\!E_T$, or (ii) two leptons, two jets and $\not\!\!E_T$, or (iii) four jets and $\not\!\!E_T$. Some of the leptons can be neutrinos. For $\widetilde{\chi}_1^+\widetilde{\chi}_1^-$ production, the final states are (i) two acollinear charged leptons and $\not\!\!E_T$, (ii) one charged lepton, 2 jets, and $\not\!\!E_T$, or (iii) four jets and $\not\!\!E_T$. A wide variety of signatures is possible from the production of other chargino and neutralino combinations.

Trileptons

The production of $\widetilde{\chi}_1^{\pm}\widetilde{\chi}_2^0$, followed by the decays $\widetilde{\chi}_1^{\pm} \to \widetilde{\chi}_1^0 \ell\nu$ and $\widetilde{\chi}_2^0 \to \ell^+\ell^-\widetilde{\chi}_1^0$, is a source of three charged leptons (e or μ) and $\not\!\!E_T$, called trilepton events (the $\not\!\!E_T$ is silent). The trilepton signal has small SM backgrounds, and is consequently one of the "golden" SUSY signatures.[54,57,56,58]

The overall efficiency for $\widetilde{\chi}_1^{\pm}\widetilde{\chi}_2^0$ production with decays into three detected leptons is set mainly by the branching ratio for the trilepton final state, which is highly model–dependent. The efficiency depends on mass splittings between the $\widetilde{\chi}_1^{\pm}$ and $\widetilde{\chi}_2^0$ and the $\widetilde{\chi}_1^0$. For example, if the 2–body decay chain $\widetilde{\chi}_2^0 \to \tilde{\ell}\ell$ and $\tilde{\ell} \to \ell\widetilde{\chi}_1^0$ occurs, and the mass splitting between $\widetilde{\chi}_2^0$ and $\tilde{\ell}$ or between $\tilde{\ell}$ and $\widetilde{\chi}_1^0$ is small, one of the leptons can be too soft to detect. In addition, if the mass splitting between $\widetilde{\chi}_1^0$ and $\widetilde{\chi}_2^0$ is large, decays to real Z or h bosons are possible. Real Z bosons have a small branching ratio to e^+e^- and $\mu^+\mu^-$ and are a SM background, and h will decay mainly to $b\bar{b}$, decreasing the trilepton rate. A similar discussion holds for the decays of the $\widetilde{\chi}_1^{\pm}$, especially in SUGRA since $M_{\widetilde{\chi}_1^{\pm}} \simeq M_{\widetilde{\chi}_2^0}$. For example, in SUGRA models, the branching ratios can be $BR(\widetilde{\chi}_1^{\pm} \to \ell\nu\widetilde{\chi}_1^0) = 0.22, BR(\widetilde{\chi}_2^0 \to \ell^+\ell^-\widetilde{\chi}_1^0) = 0.32$ when the sleptons are off–shell but lighter than the squarks, or $BR(\widetilde{\chi}_1^{\pm} \to \ell\nu\widetilde{\chi}_1^0) = 0.66, BR(\widetilde{\chi}_2^0 \to \ell^+\ell^-\widetilde{\chi}_1^0) \simeq 0$ when the sneutrinos are light enough to allow $\widetilde{\chi}_2^0 \to \tilde{\nu}\nu$ on–shell. The branching fractions also depend on $\tan\beta$, and, for large $\tan\beta$, decays to b's and τ's are enhanced. The decays of $\widetilde{\chi}_2^0$ to e^+e^- and $\mu^+\mu^-$ are strongly suppressed for large $\tan\beta$, falling a factor of about 5 between $\tan\beta$=2 and $\tan\beta$=20 if the squarks are much heavier than the sleptons.[59]

The results of the CDF [60,61] and DØ searches [62,63] are shown in Fig. 2 analyzed using RIPS (see Sec. 2.5). The searches include four channels: $e^+e^-e^{\pm}$, $e^+e^-\mu^{\pm}$, $e^{\pm}\mu^+\mu^-$ and $\mu^{\pm}\mu^+\mu^-$. The CDF analysis is based on the cuts listed in Table 2, and requires one lepton with E_T >11 GeV, passing tight identification cuts, and two other leptons with E_T >5 GeV (electrons) or p_T >4 GeV (muons), passing loose identification cuts. All leptons must be isolated, meaning there is little excess E_T in a cone of size $R = 0.4$ in $\eta - \phi$ space centered on the lepton. The event must have two leptons with the same flavor and opposite sign. If two leptons of the same flavor and opposite charge have a mass consistent with the J/Ψ, Υ or Z boson, the event is rejected. After this selection, six events remain in the data set, while the expected background, dominated by Drell–Yan pair production plus a fake lepton, is 8 events. After demanding $\not\!\!E_T$> 15 GeV, no events remain, while 1.2 are expected from SM model sources.

The DØ analysis requires leptons with $E_T > 5$ GeV satisfying the selection criteria of Table 3. However, several different triggers are used, and some

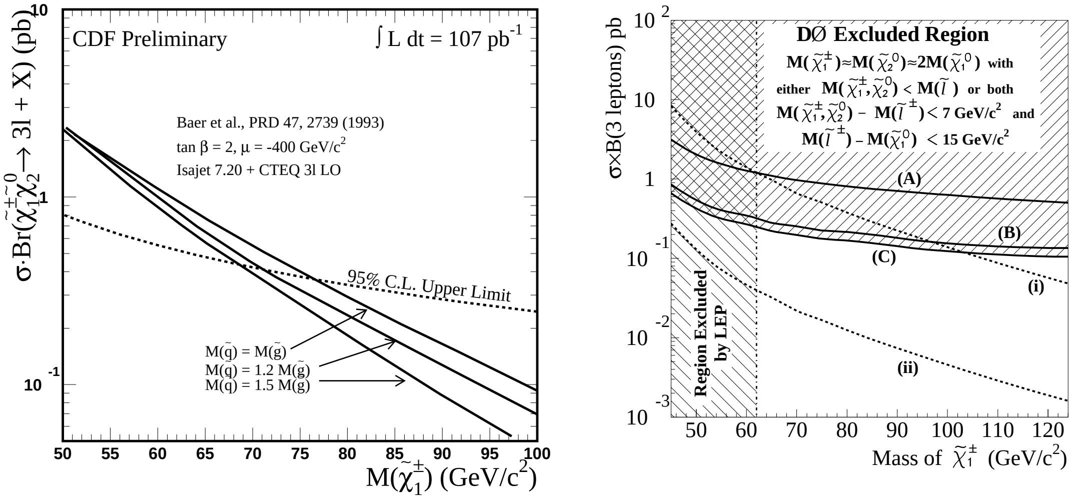

Figure 2: (Left) The CDF 95% C.L. limits on cross section × branching ratio for $\widetilde{\chi}_1^{\pm}\widetilde{\chi}_2^0$ production in 107 pb^{-1}of data. The limit is on the *sum* of the final states $eee, ee\mu, \mu\mu\mu$ and $\mu\mu e$ when $\widetilde{\chi}_1^{\pm} \to \ell\nu\widetilde{\chi}_1^0$ and $\widetilde{\chi}_2^0 \to \ell\ell\widetilde{\chi}_1^0$. The signals expected for three different RIPS scenarios are shown for comparison.[57] Typically, $M_{\widetilde{\chi}_2^0} \simeq M_{\widetilde{\chi}_1^{\pm}} \simeq 2M_{\widetilde{\chi}_1^0}$. (Right) Similar limits from DØ, but for the *average* of all four channels. The curves (A), (B), and (C) show the Run Ia, Run Ib, and combined limits. Curve (i) shows the predicted cross section × branching ratio assuming BR($\widetilde{\chi}_1^{\pm} \to \ell\nu\widetilde{\chi}_1^0$)= BR($\widetilde{\chi}_2^0 \to \ell^+\ell^-\widetilde{\chi}_1^0$)=1/3 ($\ell = e, \mu, \tau$). Curve (ii) assumes BR($\widetilde{\chi}_1^{\pm} \to \ell\nu\widetilde{\chi}_1^0$)=0.1 and BR($\widetilde{\chi}_2^0 \to \ell^+\ell^-\widetilde{\chi}_1^0$)=0.033. For both CDF and DØ, kinematic efficiencies are calculated using the production cross section from `ISAJET`.

lepton categories are required to have a larger E_T to pass the various trigger thresholds. All leptons are required to be isolated. To reduce events with mismeasured $\not\!\!E_T$, the $\not\!\!E_T$ must not be along or opposite a muon. Additional cuts are tuned for each topology. For example, the background from Drell–Yan pair production plus a fake lepton is highest in the *eee* channel, so these events are rejected if an electron pair is back–to–back. The $\not\!\!E_T$ cut is 15 GeV for *eee*, and 10 GeV for the other three topologies. No events are observed in any channel with a total of 1.26 events expected from (*i*) Drell-Yan production plus a fake lepton and (*ii*) heavy–flavor production.

To compare the DØ and CDF 95% C.L. results, note that the two experiments present different quantities: the DØ limit is on the "average" of the 4 modes ($eee, ee\mu, e\mu\mu$,and $\mu\mu\mu$), while the CDF limit is on the sum. After

Table 2: Selection criteria and results for the CDF trilepton gaugino search. The 'Very Loose' muon category refers to isolated stiff tracks that leave only small amounts of energy in the calorimeters, but do not have a corresponding track in a muon chamber (this substantially increases the acceptance).

Quantity	Criteria/Cut Value
Lepton ID Categories	1 Tight + 2 Loose, $\lvert\Sigma Q\rvert \neq 3$
Lepton Isolation	$\Sigma E_T < 2$ GeV in a cone $R = 0.4$
Tight E_T^e, η range	> 11 GeV, $\lvert\eta\rvert < 1.0$
Loose E_T^e, η range	> 5 GeV, $\lvert\eta\rvert < 2.4$
Tight p_T^μ, η range	> 11 GeV, $\lvert\eta\rvert < 0.6$
Loose p_T^μ, η range	> 4 GeV, $\lvert\eta\rvert < 1.0$
Very Loose Muon p_T^μ, η range	> 10 GeV, $\lvert\eta\rvert < 1.0$
Z,Υ,J/ψ mass window cuts	$75 - 105, 9 - 11, 2.9 - 3.1$ GeV
$\Delta\phi$ between highest 2 E_T leptons	$< 170°$
ΔR between any 2 leptons	> 0.4
$\not\!\!E_T$	> 15 GeV
$\int \mathcal{L} dt$	107 pb^{-1}
Expected Background	1.2 events
Observed Events	0 events

Table 3: Selection Criteria and Results for the DØ Run Ib Trilepton Search.

	Channel and Trigger							
	eee	Trigger	$ee\mu$	Trigger	$e\mu\mu$	Trigger	$\mu\mu\mu$	Trigger
Energy ordered E_T (GeV)	$> 22, 5, 5$ $> 14, 9, 5$	$e\not\!\!E_T$ $2e\not\!\!E_T$	$> 22(e), 5, 5$ $> 14, 9, 5(\mu)$ $> 9(e), 10(\mu), 5$	$e\not\!\!E_T$ $2e\not\!\!E_T$ $e\mu$	$> 9(e), 10, 5$ $> 17(\mu), 5, 5$ $> 5, 5, 5$	$e\mu$ μ $\mu\mu$	$> 17, 5, 5$ $> 5, 5, 5$	μ $\mu\mu$
Mass window cut	80–100 GeV		None		0–5 GeV		0–5 GeV	
$\not\!\!E_T$	> 15 GeV		> 10 GeV		> 10 GeV		> 10 GeV	
$\Delta\phi$ cuts	$\lvert\pi - \Delta\phi_{e,e}\rvert > 0.2$ 2 leading e's		None		$\lvert\pi - \Delta\phi_{\mu,\mu}\rvert > 0.1$		$\lvert\pi - \Delta\phi_{\mu,\mu}\rvert > 0.1$ all combinations	
$\int \mathcal{L} dt$	94.9 pb^{-1}		94.9 pb^{-1}		89.5 pb^{-1}		75.3 pb^{-1}	
Background	0.34 ±0.07		0.61±0.36		0.11 ± 0.04		0.20 ± 0.04	
Observed	0		0		0		0	

accounting for this difference, the CDF limit is twice as sensitive at a given $\widetilde{\chi}_1^{\pm}$ mass. The CDF limit shown is compared to three RIPS, which have different ratios of $m_{\widetilde{Q}}$ to $M_{\tilde{g}}$. The DØ limit is compared to a wide variation of possible branching ratios. Curve (*i*) assumes BR($\widetilde{\chi}_1^\pm \to \ell\nu\widetilde{\chi}_1^0$) = BR($\widetilde{\chi}_2^0 \to \ell\ell\widetilde{\chi}_1^0$) = 1/3 (no hadronic decays), while curve (*ii*) assumes BR($\widetilde{\chi}_1^\pm \to \ell\nu\widetilde{\chi}_1^0$) = 0.1 and BR($\widetilde{\chi}_2^0 \to \ell\ell\widetilde{\chi}_1^0$) = 0.033 (gauge boson–like decays). The DØ theory curve assumes heavy squarks, suppressing the squark exchange diagram but the CDF curves do not. The wide differences in the theory curves in Fig. 2 show the dangers of quoting a mass limit rather than a cross section × branching ratio limit.

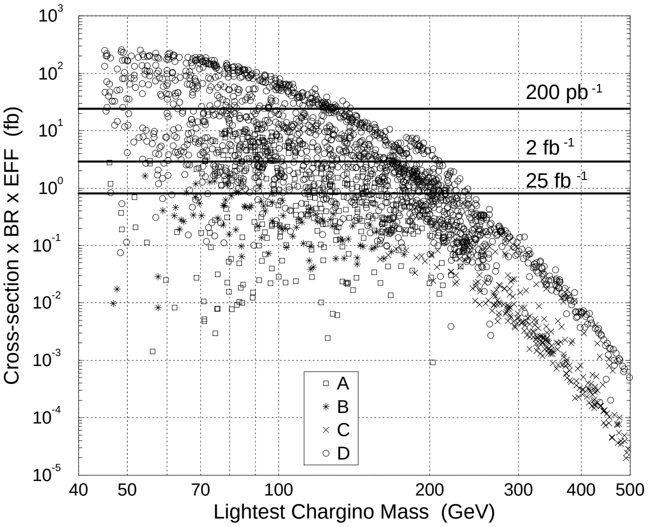

Figure 3: The overall trilepton signal rate[64] for an ensemble of SUGRA models as a function of the lightest chargino mass $M_{\widetilde{\chi}_1^\pm}$. The kinematics cuts are different than those used in the present experimental analyses. The different symbols refer to solutions showing interesting behavior where $\widetilde{\chi}_2^0$ has (A) a neutral "invisible" branching ratio (generally $\widetilde{\chi}_2^0 \to \tilde{\nu}\bar{\nu}$) > 90%, (B) a large destructive interference in 3–body leptonic decays, (C) a branching ratio to Higgs > 50% dominates, or (D) all other solutions. The horizontal lines represent the reach for various integrated luminosities.

The experimental limit on the cross section (times branching ratio) depends on the kinematics of the decays, mostly through the mass splitting between $\widetilde{\chi}_1^\pm, \widetilde{\chi}_2^0$ and the LSP. For $\mu > 0$, the mass splitting $M_{\widetilde{\chi}_1^\pm} - M_{\widetilde{\chi}_1^0}$ is smaller, and the lepton p_T cuts are less efficient. As long as the sleptons are heavier than $\widetilde{\chi}_1^\pm$ and $\widetilde{\chi}_2^0$, the leptonic decays of $\widetilde{\chi}_1^\pm$ and $\widetilde{\chi}_2^0$ through virtual W and Z

bosons and sleptons have similar kinematics since the decays are dominated by phase space. However, when the experimental result is presented as a limit on the mass of the lightest chargino rather than as a cross section limit, the result is highly model–dependent. The theoretical cross section and branching ratios are strongly affected by the SUSY parameters. If sleptons and squarks are both heavy, the decays of $\widetilde{\chi}_1^{\pm}$ and $\widetilde{\chi}_2^0$ to leptons follow the pattern of the SM gauge particles. If the sleptons are light and the squarks are heavy, decays to trileptons are enhanced.

Figure 3 shows the wide variation in total efficiency×cross section×branching ratio at a given chargino mass for the trilepton signature by sampling a large ensemble of SUGRA models.[64] The horizontal lines represent the reach for various integrated luminosities, showing that the Tevatron reach can be quite good for sufficiently high luminosities. However, even in the restrictive SUGRA framework, no absolute lower limit on the chargino mass is possible.

4.2 Squarks and Gluinos

Since the Tevatron is a hadron collider it can produce gluinos and squarks through their $SU(3)_C$ couplings to quarks and gluons. The dominant production mechanisms are $gg, q\bar{q} \to \tilde{g}\tilde{g}$ or $\widetilde{Q}\widetilde{Q}^*$, $qq \to \widetilde{Q}\widetilde{Q}$ and $qg \to \widetilde{Q}\tilde{g}, \bar{q}g \to \widetilde{Q}^*\tilde{g}$. Because QCD is unbroken,[a] the production cross sections of gluinos and squarks can be calculated as a function of only the squark and gluino masses (ignoring EW radiative corrections). Figure 4 shows the production cross sections for squarks and gluinos as a function of the sparticle masses at $\sqrt{s} = 1.8$ TeV (left) and 2 TeV (right), where NLO Supersymmetric QCD corrections have been included.[65] The total cross sections can be of the order of a few picobarns for squark and gluino masses up to 400 GeV. The NLO corrections are in general significant and positive (evaluated at the scale[b] $Q = \bar{m}$, the average mass of the two produced particles), and much less sensitive to the choice of scale than a

---

[a] The strong couplings of gluinos and squarks are the same as those of gluons and quarks, so that the production cross sections are the usual strong interaction cross sections.

[b] In the perturbative calculation of scattering probabilities in field theory, two scales appear: a factorization scale, where the parton distribution functions are evaluated, and a renormalization scale, where the running coupling is evaluated. In practice, these scales are chosen to be the same. This scale should be representative of the typical momentum flowing through a Feynman diagram. In Drell–Yan production, for example, the scale is the invariant mass of the Drell–Yan pair. The higher the order of a perturbative calculation, the lesser the dependence on this scale.

LO calculation.[c] In Fig. 4, five degenerate squark flavors are assumed,[d] which is one way to suppress FCNC's.

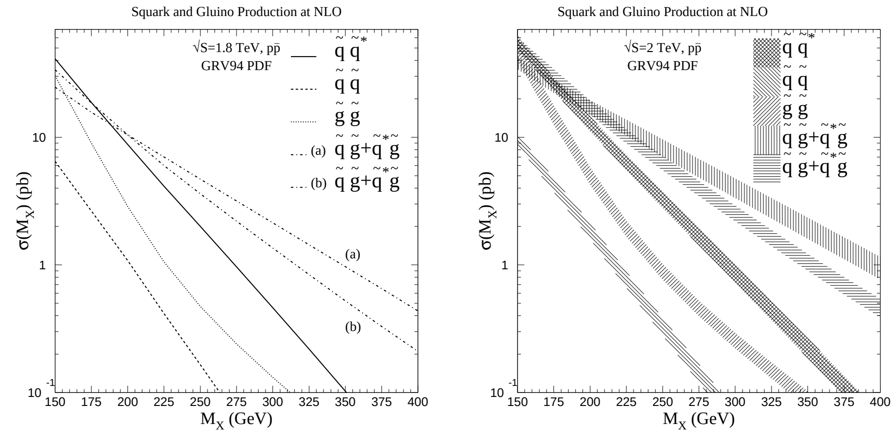

Figure 4: (Left) Production cross sections for gluinos and squarks versus sparticle mass M_X at the Tevatron, $\sqrt{s} = 1.8$ TeV, assuming degenerate masses for 5 flavors of squarks. For $\widetilde{Q}\widetilde{Q}^*$ and $\widetilde{Q}\widetilde{Q}$ production, M_X is the squark mass and $M_{\tilde{g}} = 200$ GeV. For $\tilde{g}\tilde{g}$ production, M_X is the gluino mass and $M_{\widetilde{Q}} = 200$ GeV. For $\widetilde{Q}\tilde{g}$ production (a), M_X is the squark mass and $M_{\tilde{g}} = 200$ GeV; for (b), M_X is the gluino mass and $M_{\widetilde{Q}} = 200$ GeV. The scale is the average mass of the two produced sparticles. (Right) The same curves with $\sqrt{s} = 2$ TeV. The bands show the change in rate from varying the scale from 1/2 to 2 times the average mass of the produced particles.

The ultimate detectability of squarks and gluinos depends upon their decays, which, in turn, depends on the electroweak couplings of the squarks and the mixings in the neutralino and chargino sector. Since squarks and gluinos decay into charginos and neutralinos, their signatures can be similar to $\widetilde{\chi}\widetilde{\chi}$ production, but with accompanying jets. If $m_{\widetilde{Q}} > M_{\tilde{g}}$, then the squark has the 2–body decay $\widetilde{Q} \rightarrow \tilde{g}q$. The gluino has then the possible decays $\tilde{g} \rightarrow q\bar{q}\widetilde{\chi}_i^0$ or $\tilde{g} \rightarrow q\bar{q}'\widetilde{\chi}_i^{\pm}$, where q can stand for t or b as well, or even $\tilde{g} \rightarrow t\tilde{t}^*$ or $\overline{t}\tilde{t}$ if kinematically allowed. The gluino can also decay via one–loop diagrams as $\tilde{g} \rightarrow g\widetilde{\chi}_i^0$. If, instead, $m_{\widetilde{Q}} < M_{\tilde{g}}$, then the gluino has the 2–body decay $\tilde{g} \rightarrow \widetilde{Q}q$. The squarks can then decay as $\widetilde{Q}_{L,R} \to q\widetilde{\chi}_i^0$, $\widetilde{u}_L \to d\widetilde{\chi}_i^+$, and $\widetilde{d}_L \to u\widetilde{\chi}_i^-$. The final event signatures depend on the decay channels of the charginos and neutralinos, but, typically involve $\not\!\!E_T$ and a multiplicity of jets and/or leptons. The 3–body or top–stop decay modes of the gluino can produce a higher multiplicity of SM particles in their decays than the squark 2–body decays to neutralinos or charginos, particularly if $\widetilde{Q} \to q\widetilde{\chi}_1^0$ is the dominant squark decay. On the other hand, the LSP in gluino decays must share energy with more particles, producing less $\not\!\!E_T$ on the average (see Fig. 5).

---

[c] The inclusion of NLO effects in the cross sections will typically raise the lower bounds for squark and gluino masses by 10 to 30 GeV with respect to the LO cross sections evaluated at a scale equal to the invariant mass of the produced particles.

[d] Assuming the same mass for the bottom squark is a simplification that becomes questionable in the large $\tan\beta$ region.

Gluinos and squarks may also be produced at the Tevatron in association with charginos or neutralinos (analogous to W and Z + jet production). These processes can be more important than pair production of gluinos and squarks if the latter are kinematically limited. Event signatures are similar to $\widetilde{Q}$ and $\tilde{g}$ production, but possibly with fewer jets, though the events may still pass the selection criteria for the squark and gluino searches. For example, $\widetilde{Q}\widetilde{\chi}_1^\pm$ production will have one less jet than $\widetilde{Q}\widetilde{Q}$ production, assuming the decay $\widetilde{Q} \to q'\widetilde{\chi}_1^\pm$ or $\widetilde{Q} \to q\widetilde{\chi}_1^0$

Promising signatures for squark and gluino production are (*i*) multiple jets and $\not\!\!E_T$[53] and (*ii*) isolated leptons and jets and $\not\!\!E_T$.[55]

Jets + $\not\!\!E_T$

Both CDF and DØ have performed searches for events with jets and $\not\!\!E_T$. This signature has significant physics and instrumental backgrounds. The three dominant physics backgrounds are (*i*) $Z \to \nu\bar{\nu}$ plus jets, (*ii*) $W \to \tau\nu$ plus jets, where the τ decays hadronically, and (*iii*) $t\bar{t} \to \tau$ plus jets, where the τ decays hadronically. The $\not\!\!E_T$ in leptonic W decays peaks at $M_W/2 \simeq 40$ GeV, with a long tail at high $\not\!\!E_T$ due to off–shell or high–p_T W's and energy mismeasurements, so a large $\not\!\!E_T$ cut is needed to remove these events. Instrumental backgrounds come from mismeasured vector boson, top, and QCD multijet events. Backgrounds from vector boson production occur for $W \to e\nu, \mu\nu$ plus jets events when the lepton is lost in a crack or is misidentified as a jet. The same problem can occur when the W is produced in a $t\bar{t}$ event. QCD multijet production is a background when jet energy mismeasurements cause false $\not\!\!E_T$.

The DØ Run Ia analysis[67] searches for events with 3 or more jets and $\not\!\!E_T$ and with 4 or more jets and $\not\!\!E_T$. The analysis is described in Table 4. The resulting mass limits on squarks and gluinos are shown in Fig. 6 (right, the plot containing the CDF results also shows the DØ Ia results) and were set using a RIPS model with the following parameters: $M_{H^\pm} = 500$ GeV, $\tan\beta = 2$, $\mu = -250$ GeV, and $M_{\tilde{\ell}} = m_{\widetilde{Q}}$. The efficiency and theoretical cross sections were calculated using `ISAJET`[51] assuming 5 flavors of mass degenerate squarks without top squark production and a detector simulation.

DØ also has a 3–jet analysis [69] based on 79.2 pb^{-1} of Run Ib data. The basic requirements are three jets with $E_T > 25$ GeV and a central leading jet ($|\eta| < 1.1$). The $\not\!\!E_T$ may be significantly overestimated if the wrong interaction vertex is used;[e] to reduce this effect, the tracks in the leading jet are required to point back to the primary vertex. The $\not\!\!E_T$ is required to be uncorrelated in ϕ with any jet. A cut on the scalar sum of the E_T of the non–leading jets, called H_T, effectively reduces events from vector boson backgrounds. The leading jet is also required to have $E_T > 115$ GeV because the only available unbiased sample to study the QCD multijet background had this requirement. These cuts are summarized in Table 4. Vector boson backgrounds are estimated using `VECBOS`,[70] while the $t\bar{t}$ background uses `HERWIG`[71] normalized to the DØ measured $t\bar{t}$ cross section. The detector simulation is based on the `GEANT`[72] program. Two techniques were used to calculate the QCD multijet background. One compares the opening angle between the two leading jets and the $\not\!\!E_T$ in the signal sample to the distribution in a generic multi–jet sample. The other selects events from a single jet trigger which pass all the selection criteria except for the $\not\!\!E_T$ requirement. The $\not\!\!E_T$ distribution is fit in the low $\not\!\!E_T$ region, and extrapolated into the signal region. The complete set of background estimates can be found in Table 5.

The DØ data have been analyzed in the context of a minimal SUGRA model. For fixed $\tan\beta$, A_0, and sign of μ, exclusion curves are plotted in the $m_0 - m_{1/2}$ plane, Fig. 6 (left). The limits are from the 3–jet, 79.2pb^{-1}, analysis only. Efficiencies are calculated using `ISAJET`[51] for production of gluinos and five flavors of squarks without stop squark production. For each point in the limit plane, the $\not\!\!E_T$ and H_T cuts are reoptimized based on the predicted background and SUSY signal. Figure 5 shows the $\not\!\!E_T$ as a function of m_0 and $m_{1/2}$ for $\tan\beta$=2, A_0=0, $\mu < 0$. When $m_0 \gg m_{1/2}$, the $\not\!\!E_T$ signature is degraded, because $m_{\widetilde{Q}} \gg M_{\tilde{g}}$ and thus higher multiplicity $\tilde{g}\tilde{g}$ events dominate. Since higher multiplicity also means higher H_T, varying the cuts can maintain sensitivity. These results are robust within the SUGRA framework.[69]

The CDF analysis of the Run Ib data set is not yet complete, but the Run Ia result based on 19 pb^{-1} has been published.[68] The basic requirements are 3 or 4 jets and 60 GeV of $\not\!\!E_T$. The full set of cuts is listed in Table 4. As in the DØ search, the direction of the $\not\!\!E_T$ is not allowed to coincide with that of a jet, and events with leptons are rejected to reduce the background from W and top events. The variable S, which indicates the significance of the $\not\!\!E_T$, is used to reduce fake $\not\!\!E_T$ measurements; S is calculated by dividing the $\not\!\!E_T$ by the square root of the scalar sum of the E_T in the calorimeters. The

---

[e] The calculation of $\not\!\!E_T$ uses the event vertex to calculate E_T for all objects.

Table 4: Selection criteria for Tevatron squark and gluino searches in the 3 or 4 jets+$\not\!\!E_T$ channels. Cuts specific to the DØ 4–jet analysis are in parentheses.

Quantity	Experiment	
	DØ	CDF
Trigger	$\not\!\!E_T > 40$ GeV	$\not\!\!E_T > 35$ GeV 1 jet with $E_T^j > 50$ GeV
$\not\!\!E_T$	$> 75 - 100, (65)$ GeV	> 60 GeV with $S > 2.2$ GeV$^{1/2}$
E_T^j	$> 25, (20)$ GeV	> 15 GeV, $\vert\eta\vert < 2.4$
leading E_T^j	> 115 GeV $\vert\eta\vert < 1.1, (N.A.)$ $H_T > 100 - 160, (N.A.)$	> 50 GeV
$\Delta\phi_i$ between $\not\!\!E_T$ and jet i; i=1 is the leading jet	$5.7^\circ < \Delta\phi_i < 174.3^\circ$ $\sqrt{(\Delta\phi_1 - 180^\circ)^2 + \Delta\phi_2^2} > 28.6^\circ$	$\Delta\phi_i > 30^\circ$ $\Delta\phi_1 < 160^\circ$
Leptons	Veto all (N.A.)	Veto all
Vertices	confirmed, (Only one)	Any number

vector boson backgrounds are estimated using `VECBOS`[70] normalized to the CDF Wjj data. Top backgrounds are determined using `ISAJET`[51] normalized to the CDF measured top cross section. The QCD background is estimated using an independent data sample based on a trigger that required one jet with $E_T > 50$ GeV. First all analysis cuts (Table 4) are applied to this sample except for the S cut, the $\not\!\!E_T$ cut, and the 3 or 4 jets cut. Next the $\not\!\!E_T$ distribution is fit and the number of events expected to pass the $\not\!\!E_T$ cut is derived. Finally the efficiency of the last three cuts is applied to arrive at the final background estimate, shown in Table 5.

The limits derived from the CDF analysis are shown in Fig. 6 (right) within the RIPS framework (see Sec. 2.5). In RIPS, a heavy gluino implies a heavy $\widetilde{\chi}_1^0$, so a light squark ($m_{\widetilde{Q}} \approx M_{\widetilde{\chi}_1^0}$) decay will not produce much $\not\!\!E_T$. The consequence is an apparent hole in the CDF limit for small $m_{\widetilde{Q}}$ and large $M_{\tilde{g}}$. However, lighter gluinos always produce a large $\not\!\!E_T$ because of the enforced mass splitting between $M_{\tilde{g}}$ and $M_{\widetilde{\chi}_1^0}$. The results of this analysis do not change substantially as parameters are varied within the RIPS framework.[68]

The results summarized in Fig. 6 are complemented by the dilepton+$\not\!\!E_T$ analysis shown in Figs. 7 and 9. The limits on the gluino and squark masses in each scenario (minimal SUGRA and RIPS) will be discussed below.

Table 5: The number of expected and observed events for Tevatron squark and gluino searches in the jets+$\not\!\!E_T$ channel after performing the cuts in Table 4.

	DØ		CDF	
Analysis	3 jets	4 jets	3 or 4 jets	4 jets
$\int\mathcal{L}dt(\mathrm{pb}^{-1})$	79.2	13.5	19	19
$W^{\pm}$	$1.56 \pm .67 \pm .42$	4.2 ± 1.2	$13.9 \pm 2.1 \pm 6.0$	$2.6 \pm 0.9 \pm 1.7$
$Z \rightarrow \ell\bar{\ell}, \nu\bar{\nu}$	$1.11 \pm .83 \pm .36$	1.0 ± 0.4	$5.0 \pm 0.9 \pm 2.7$	$0.4 \pm 0.2 \pm 0.4$
$t\bar{t}$	$3.11 \pm .17 \pm 1.35$	–	$4.2 \pm 0.3 \pm 0.5$	$2.2 \pm 0.2 \pm 0.4$
QCD multijets	3.54 ± 2.64	1.6 ± 0.9	$10.2 \pm 10.7 \pm 4.2$	$3.2 \pm 3.8 \pm 1.3$
Total Background	$9.3 \pm 0.8 \pm 3.3$	6.8 ± 2.4	$33.5 \pm 11 \pm 16$	$8 \pm 4 \pm 4$
Events Observed	**15**	**5**	**24**	**6**

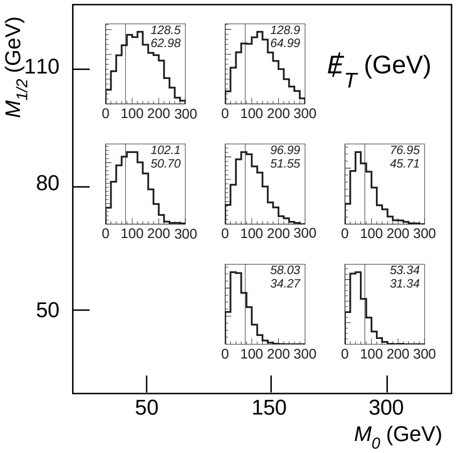

Figure 5: The $\not\!\!E_T$ distribution from simulations of squark/gluino events in the DØ detector based on `ISAJET`[51] and `GEANT`.[72] The simulation used SUGRA mass relations assuming $\tan\beta$=2, A_0=0, and $\mu < 0$ and seven values of m_0 and $m_{1/2}$. The numbers in the upper right-hand corner of each plot are the mean and RMS of the distribution. The normalization is arbitrary.

Dileptons+$\not\!\!E_T$

If, in the cascade decay chain of the $\widetilde{Q}$'s and $\tilde{g}$'s, two charginos decay $\widetilde{\chi}_1^{\pm} \rightarrow \ell\nu\widetilde{\chi}_1^0$, or one neutralino decays $\widetilde{\chi}_2^0 \rightarrow \ell^+\ell^-\widetilde{\chi}_1^0$, the final state can contain 2 leptons, jets, and $\not\!\!E_T$.[55] This channel has the advantage of being relatively clean experimentally. The requirement of two leptons significantly reduces jet backgrounds and removes most of the W backgrounds. Requiring that the mass of

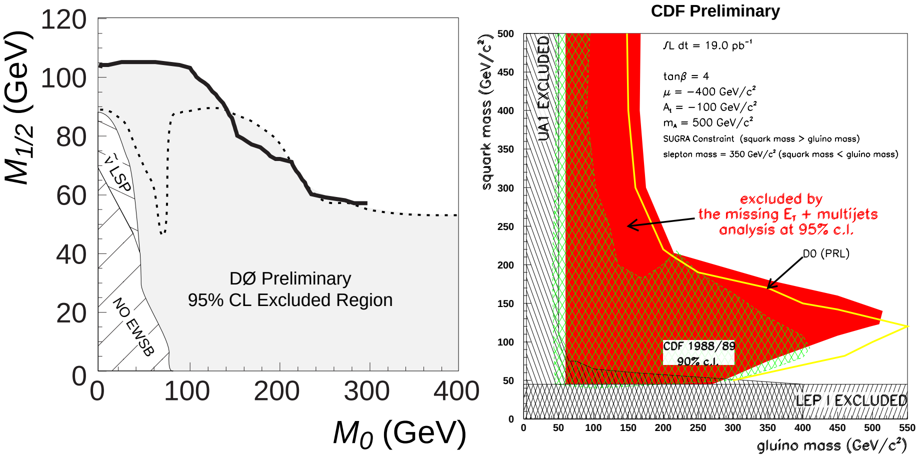

Figure 6: (Left) The DØ Excluded region in the $m_0 - m_{1/2}$ plane with fixed parameters $\tan\beta = 2$, $A_0 = 0$, and $\mu < 0$. The heavy solid line is the limit contour of the DØ jets and missing transverse energy analysis. The dashed line is the limit contour of the DØ dielectron analysis. The lower hashed area is a region where mSUGRA does not predict EWSB correctly. The hashed region above is where the sneutrino is the LSP. (Right) The CDF mass limits on squarks and gluinos from the search in jets and $\not\!\!E_T$[68] using 19 pb^{-1} of data and the ISAJET 7.06 Run I Parameter Set (RIPS) with the indicated values (solid area). For $m_{\widetilde{Q}} < M_{\tilde{g}}$, the cross section used is leading order, and three or more jets are required. For $M_{\tilde{g}} < m_{\widetilde{Q}}$, the cross section is NLO,[65] and four jets are required. The line labelled "DØ PRL" is the DØ result from Run Ia using 13.5 pb^{-1} of data.[67]

the two leptons be inconsistent with the Z mass removes most of the rest of the vector boson backgrounds. If the leptons are required to have p_T>20 GeV, the major background from physics processes is $t\bar{t} \rightarrow bW^+\bar{b}W^- \rightarrow b\bar{b}\ell^+\ell^-\not\!\!E_T$. As the cut on lepton p_T is lowered, $Z \rightarrow \tau^+\tau^-$, where the τ's decay semileptonically, also becomes an important background. The instrumental backgrounds are small. The spectacular signature of *like–sign*, isolated dileptons, which is difficult to produce in the SM, can occur whenever a gluino is produced directly or in a cascade decay, since the gluino is a Majorana particle. This property is exploited in the CDF dilepton searches.

Figures 7 and 8 show the DØ[73] and CDF[75,74] results from Run Ib, once again compared to SUGRA and RIPS, respectively. The CDF limit is based on NLO cross sections,[65] and the DØ limit on LO cross sections. The DØ limits on m_0 and $m_{1/2}$ are calculated including contributions from the production of all sparticles (for instance, associated production of neutralinos or charginos with squarks or gluinos), while the CDF result only considers $\widetilde{Q}$ and $\tilde{g}$ production.

Table 6: Selection criteria for Tevatron searches for squarks or gluinos in the dileptons, 2 jets and $\not\!\!E_T$ channel.

Quantity	Experiment	
	DØ	CDF
$\int \mathcal{L}dt$ (pb^{-1})	92.9	81
$E_T^{e_1}, E_T^{e_2}$	$> 15, 15$ GeV	$> 11, 5$ GeV
$p_T^{\mu_1}, p_T^{\mu_2}$	N.A.	$> 11, 5$ GeV
$E_T^{j_1, j_2}$	> 20 GeV	> 15 GeV
Mass window cut	$M_Z \pm 12$ GeV	N.A.
ΔR between leptons and jets	N.A.	$> .7$
$\not\!\!E_T$	> 25 GeV	> 25 GeV
like sign dileptons	no	yes

Table 6 gives the selection criteria for the two analyses. The experimental cuts are chosen to identify two high–p_T leptons, which come predominantly from $\widetilde{Q}$ and $\tilde{g}$ decays into charginos or neutralinos which in turn decay into real or virtual W or Z bosons.

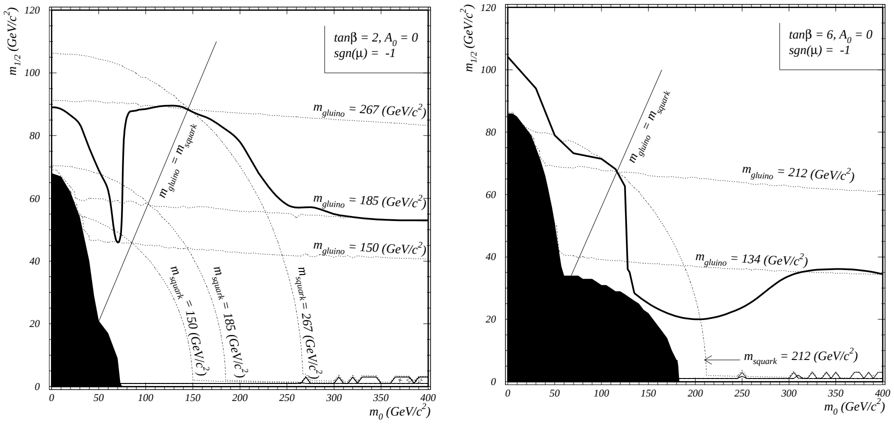

Figure 7: (Left) The DØ limits on the SUGRA parameters m_0 and $m_{1/2}$ from the 2 leptons, 2 jets, and $\not\!\!E_T$ search[73] for $\tan\beta$=2, A_0=0, and $\mu < 0$. (Right) The same plot for $\tan\beta$=6, A_0=0, and $\mu < 0$. In both plots, the dark shaded area is the region in which SUGRA does not produce electroweak symmetry breaking. Selected contours of squark and gluino mass are also shown.

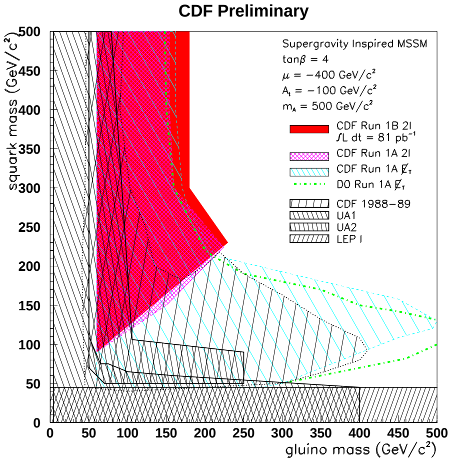

Figure 8: CDF limits on the squark and gluino masses from the 2 like sign leptons, 2 jets, and $\not{E}_T$ search in 81 pb^{-1}. The limits were set using the ISAJET 7.06 Run I Parameter Set (RIPS) with the indicated values.

DØ has also presented an experimental limit in the $M_{\tilde{g}} - m_{\widetilde{Q}}$ plane Fig. 9, which allows a comparison with the CDF limit Fig. 8. For $m_{\widetilde{Q}} \gg M_{\tilde{g}}$ or, equivalently, for $m_0 \gg m_{1/2}$, $\tilde{g}\tilde{g}$ pair production is the dominant SUSY process. As $m_0(m_{\widetilde{Q}})$ is varied with the other parameters fixed, the branching ratios for the 3–body gluino decays to charginos or neutralinos and jets become fairly constant, so the production rate of leptonic final states becomes constant; the experimental limit approaches a constant value asymptotically, as can be seen in both the DØ and CDF plots shown in Figs. 8 and 9, respectively. Observe that, for large enough values of the gluino mass, the leptons easily pass the experimental cuts, so the experimental efficiency also becomes constant.

The relation $m_{\widetilde{Q}} \ll M_{\tilde{g}}$ is not possible in SUGRA, and is treated in an *ad hoc* manner in RIPS. There is no limit in this region for either opposite– or like–sign dilepton pairs because the large, fixed slepton masses limit the branching ratios to leptonic final states. The possibility of like–sign dilepton pairs is further reduced because both the $\tilde{g}\tilde{g}$ and $\tilde{g}\widetilde{Q}$ cross sections (which produce like–sign leptons because the gluino is a Majorana particle) and the $\widetilde{Q}\widetilde{Q}$ cross section (which produces like–sign leptons because the squarks have the same charge) are small in this region. It is very difficult for $\widetilde{Q}\widetilde{Q}^*$ production to yield like–sign leptons in general.

When $m_{\widetilde{Q}} \simeq M_{\tilde{g}}$, the $\tilde{g}\tilde{g}$ cross section is supplemented by the $\tilde{g}\widetilde{Q}$ cross section. Just above the diagonal line at $M_{\tilde{g}} = m_{\widetilde{Q}}$ (*i.e.* $m_{\widetilde{Q}}$ just larger than $M_{\tilde{g}}$) in Figs. 8 and 9, there are "noses" in the limit plots, with the limit becoming stronger close to the diagonal.

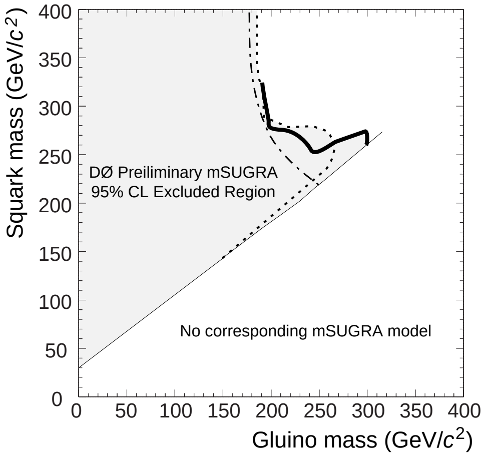

Figure 9: Excluded region from various DØ analyses in the $m_{\widetilde{Q}} - M_{\tilde{g}}$ plane with fixed mSUGRA parameters $\tan\beta = 2$, A_0=0, and $\mu < 0$. Note that there are no mSUGRA models in the region to the right of the diagonal thin line. The heavy solid line is the limit contour of the DØ Run Ib 3 jets and missing transverse energy analysis. The dashed line is the limit contour of the DØ Run Ib dielectron analysis. The dot–dashed line is the limit contour of the DØ Run Ia 3 and 4 jets and missing transverse energy analysis shown only in the region with valid mSUGRA models.

The limits in Figs. 8 and 9 are for a specific choice of parameters within the RIPS or SUGRA framework. If μ, A_t and $\tan\beta$ are varied, the branching ratios into charginos or neutralinos can vary strongly. The sensitive dependence on the parameters can be seen within minimal SUGRA models from the DØ limits in Fig. 7. The dip in the $\tan\beta$=2 limit (left), around m_0= 70 GeV, is a point where $m_{\tilde{\ell}} > M_{\widetilde{\chi}^0_2} > m_{\tilde{\nu}}$ and $\mathrm{BR}(\widetilde{\chi}^0_2 \to \nu\bar{\nu}\widetilde{\chi}^0_1) \simeq 1$, so the detection efficiency is very sensitive to the choice of high energy parameters m_0 and $m_{1/2}$. In Fig. 7 (right), with $\tan\beta$=6, the limits are severely reduced compared to Fig. 7 (left), with $\tan\beta$=2, in the region where the squark mass is large compared to the gluino mass. For large $\tan\beta$, the mass splitting $M_{\widetilde{\chi}_1^\pm,\widetilde{\chi}_2^0} - M_{\widetilde{\chi}_1^0}$ is reduced, so that the leptons from the $\widetilde{\chi}_1^\pm$ and $\widetilde{\chi}_2^0$ decays are softer. The non–trivial shape of the limit curves results from an interplay between the cross section being larger when m_0 and $m_{1/2}$ are smaller (sparticle masses are smaller) and the mass splittings being smaller. Consequently, although the dileptons+jets+$\not\!\!E_T$ signature is an excellent discovery channel with little SM background, it is hard to set significant parameter limits even using SUGRA models.

From the present analyses in the $\not\!\!E_T$+jets and dileptons+$\not\!\!E_T$ channels, some preliminary conclusions can be drawn on the squark and gluino masses. These depend, however, on the assumed SUSY parameters. The DØ limit on the gluino mass effectively develops a plateau for large m_0 at 185 GeV for $\tan\beta = 2$, and at 134 GeV for $\tan\beta = 6$. The CDF limit on the gluino mass is 180 GeV for $\tan\beta = 4$ for large $m_{\widetilde{Q}}$. Instead, for equal squark and gluino masses, the DØ mass limit for $\tan\beta = 2$ is 267 GeV, using all SUSY production and decay modes in the model. From the CDF analyses and $m_{\widetilde{Q}} \simeq M_{\tilde{g}}$, the limit is about 220 GeV for $\tan\beta = 4$. A direct comparison of all the above results is rather difficult since DØ and CDF have done analyses assuming different sets of MSSM parameters (see Figs. 6–9). Moreover, CDF considers only squark and gluino production, while DØ considers all possible sparticle production, and the associated production of neutralinos or charginos with squarks or gluinos can have an impact on the experimental limits.

It would be very useful for purposes of comparing and combining the two experimental limits to have both collaborations use at least one common model (such as SUGRA), and agree on several values of the parameters to do the searches. For example, the two collaborations could present their limits in the $m_{1/2} - \tan\beta$ plane (for large m_0). Secondly, they could move (partially) towards more experimentally–based quantities by plotting contours of cross section limit and also contours of acceptance × efficiency in the m_0–$m_{1/2}$ plane. This would eliminate the strong model dependence on the branching ratios. The experimental acceptance for the signature of two leptons+jets is much less model–dependent, since it simply reflects the hard kinematics from the decays of two heavy objects. A presentation of cross section × branching ratio limits, in addition to the mass limits, would be of more general use to model–builders.

4.3 Top Squarks

The top squark (stop) is a special case worth a separate discussion.[76,77] The mass degeneracy in the stop sector is expected to be strongly broken, and, for sufficiently large mixing, the lightest stop can be expected to be rather light, possibly lighter than the lightest chargino. The lightest stop has about a tenth the production cross section of a top quark of the same mass, because the threshold behavior is β^3 (compared to β for fermion pairs) and only half the scalar partners are being considered. At leading order, the cross section is independent of the gluino mass and depends only on the stop mass.[f] Due to the large left–right mixing, the NLO SUSY QCD corrections must deal with different left– and right–handed couplings of the quarks to squarks and gluinos. The results for the stop–pair production cross section as a function of the stop mass are plotted in Fig. 10.[78]

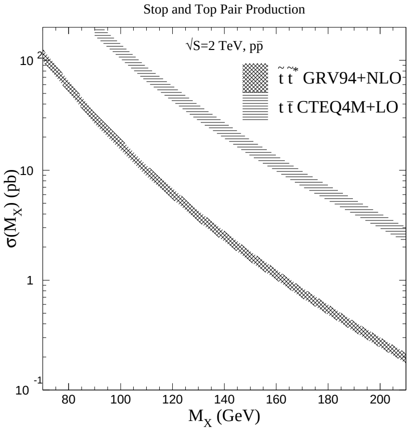

Figure 10: The cross section for pair production of one stop quark versus the stop mass at the Tevatron, calculated to NLO. The band represents the variation of the scale from 1/2 to 2 times the stop mass. The top pair production cross section versus the top mass is shown for reference, calculated only at LO. The band represents the variation of the scale from 1/2 to 2 times the transverse mass $p_T \oplus m_t$, where p_T is the transverse momentum of the top quark.

The stop can be produced directly as $\tilde{t}\tilde{t}^*$ pairs or, depending on the stop mass, indirectly[76] in decays of the top $t \to \tilde{t}\widetilde{\chi}_1^0$, or sparticles, such as $\widetilde{\chi}_i^{\pm} \to b\tilde{t}$. Also depending on the stop mass, one of three decay modes is expected to dominate. If (a) $m_{\tilde{t}_1} > m_{\widetilde{\chi}_1^{\pm}} + m_b$, then $\tilde{t}_1$ can decay into $b\widetilde{\chi}_1^{+}$, followed by the decay of the chargino. This can look similar to the top decay $t \to bW$, but with different kinematics and branching ratios for the final state. Instead, if the stop is the lightest charged SUSY particle, it is expected to decay exclusively through a chargino–bottom loop as (b) $\tilde{t}_1 \to c\widetilde{\chi}_1^0$, which looks quite different from SM top decays. Finally, the stop can decay (c) $\tilde{t} \to bW\widetilde{\chi}_1^0$ or if the stop is quite heavy into $\tilde{t} \to t\widetilde{\chi}_1^0$

---

[f] Since the incoming partons are not tops, then if flavor changing neutral currents are suppressed by a Supersymmetric GIM mechanism, stop production via gluino interchange is not allowed. After including the NLO SUSY QCD corrections the dependence on $m_{\tilde{g}}$ and stop mixing becomes explicit but, in practice, numerical results are insensitive to the exact gluino mass and the mixing.

The possible signals from $\tilde{t}\tilde{t}^*$ production, with decay (a) and depending on the chargino decay modes, are: (i) $b\bar{b}\ell^+\ell^-\not{E}_T$, ($ii$) $b\bar{b}\ell^\pm jj\not{E}_T$, or ($iii$) $b\bar{b}jjjj\not{E}_T$. These are similar to $t\bar{t}$ final states, except (iii) has real $\not{E}_T$. If decay (b) dominates, this yields a signature of 2 acollinear charm jets and $\not{E}_T$. Finally, if decay (c) occurs, the events are similar to $t\bar{t}$ events, except that the kinematics of the individual t and $\bar{t}$ are altered and there can be much more $\not{E}_T$.

If the stop is in the range $100 - 150$ GeV, $\tilde{t}\tilde{t}^*$ production may be too small to observe and it might be easier to observe a light stop in top quark decays $t \to \tilde{t}\widetilde{\chi}_1^0$. If $\widetilde{\chi}_1^0$ is Higgsino–like, then the $\mathrm{BR}(t \to \tilde{t}\widetilde{\chi}_1^0)$ can be 50%. If decay (a) occurs, then top quark events have the same signatures as in the SM but they have more $\not{E}_T$ and softer jets and leptons. In case (b), fewer leptons and jets are produced and the $\not{E}_T$ distribution is affected. If there is one SM top decay and one SUSY top decay, the final state can be $b\ell^\pm c\not{E}_T$, which would appear at a small rate in the Wjj sample, but not in the SM $t\bar{t}$ event sample.

An indirect limit can also be set on the decay (b). Such decays would not fall in the SM $t\bar{t}$ dilepton or lepton+jets samples, but instead would deplete them. Given a theoretical prediction for the $t\bar{t}$ production cross section, the branching ratio for decays which deplete the SM $t\bar{t}$ samples can be bounded in a straightforward manner. If decay (a) occurs, the analysis is more involved, since the kinematic acceptance for the stop decays must be calculated for many different choices of MSSM parameters. Also in case (a), some $\tilde{t}\tilde{t}^*$ events will feed into the top quark event samples.

Direct Top Squark Pair Production

DØ has searched for $\tilde{t}\tilde{t}^*$ production[77] with $\tilde{t} \to c\widetilde{\chi}_1^0$ using 7.4 pb^{-1} of Run Ia data.[79] The signature is two acollinear jets and $\not{E}_T$, satisfying the selection criteria in Table 7. The dijet cross section at the Tevatron is large, and thus this signature has large instrumental backgrounds. It also has backgrounds from vector boson production. The QCD and vector boson backgrounds would, naively, be a factor of $1/\alpha_s$ larger than for the hadronic squark/gluino search, as this search requires only 2 jets while the latter searches require at least 3 or 4 jets. This is not the case since the multijet backgrounds can be controlled by requiring $\Delta\phi > 45^\circ$ between the $\not{E}_T$ and each jet, and that the jets not be back–to–back. The vector boson backgrounds are controlled by requiring that

Table 7: Selection criteria for the DØ 2 jet+$\not\!\!E_T$ hadronic direct stop pair production search. j_1 and j_2 are the leading and sub–leading jets ranked by E_T.

Quantity	DØ
$E_T^{j_1}, E_T^{j_2}$	> 30 GeV
$\Delta\phi$ j_1–j_2	$90^\circ < \Delta\phi < 165^\circ$
$\Delta\phi$ j_1–$\not\!\!E_T$	$10^\circ < \Delta\phi < 125^\circ$
$\Delta\phi$ j_2–$\not\!\!E_T$	$10^\circ < \Delta\phi$
Lepton veto	e and μ
$\not\!\!E_T$	> 40 GeV

the two leading jets are separated by at least $\Delta\phi > 90^\circ$. After these cuts, the dominant backgrounds are from W and Z boson production and decay, with the largest being $W \to \tau\nu$. If the τ decays hadronically, only 1 additional jet is necessary to fake the signature. Top quark production is not as important a background for the light stop search as for the conventional hadronic squark search because of the lower jet multiplicity requirement. As with the hadronic squark/gluino searches, the cuts are not very efficient for signal events. The efficiency is largest when the stop is heavy compared to the $\widetilde{\chi}_1^0$ (near the kinematic boundary for the decay $\tilde{t}_1 \to t\widetilde{\chi}_1^0$), reaching a maximum value of only 4%. The mass difference $m_{\tilde{t}} - M_{\widetilde{\chi}_1^0}$ determines the E_T of the charm jet and rapidly limits this search mode as the charm jets become too soft (see Fig. 11).

With the assumption that BR($\tilde{t}_1 \to c\widetilde{\chi}_1^0$)=1, the predicted SUSY final state depends only on $M_{\widetilde{\chi}_1^0}$ and $m_{\tilde{t}_1}$. The result of this search is a 95% C.L. exclusion limit on a region in the $M_{\widetilde{\chi}_1^0} - m_{\tilde{t}_1}$ plane, shown in Fig. 11. The production rate has been calculated using only LO production cross sections evaluated at the scale $Q^2 = 2stu/(s^2+t^2+u^2)$ from `ISAJET`,[51] so the limit will change somewhat if re–evaluated with NLO production cross sections.

CDF and DØ have also presented results from a search for $\tilde{t}_1\tilde{t}_1^*$ production, with $\tilde{t}_1 \to b\widetilde{\chi}_1^\pm$.[77] The CDF search is in the lepton+jets channel, and uses a shape analysis of the transverse mass[g] of the lepton and $\not\!\!E_T$.[80] The selection criteria are given in Table 8. For both searches, the detection efficiency is smaller than for $t\bar{t}$ production with a top quark of the same mass because of the softer leptons from the 3–body decay $\widetilde{\chi}_1^\pm \to \ell\nu\widetilde{\chi}_1^0$. The mass splitting

---

[g] Transverse mass squared is $M_T^2 = (|\vec{p}_T^{\,\ell}| + |\vec{\not\!\!E}_T|)^2 - (\vec{p}_T^{\,\ell} + \vec{\not\!\!E}_T)^2$, and is a useful experimental quantity when information about the longitudinal component of momentum is missing.

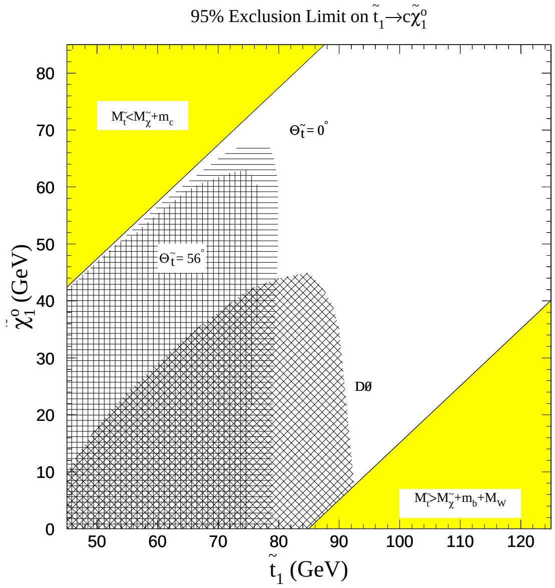

Figure 11: Mass limits from the DØ search for $\tilde{t}\tilde{t}^*$ production with the decay $\tilde{t} \rightarrow c\widetilde{\chi}^0_1$ at the Tevatron.[79] The decay is kinematically forbidden in the two solid grey regions. The hashed regions marked $\Theta_{\tilde{t}}$ show the LEP excluded regions as a function of the stop mixing angle, which determines the strength of the stop coupling to the Z boson. The mixing does not affect the tree level process at hadron colliders.

Table 8: Selection criteria for the CDF lepton+jets+b–tag direct stop pair production search. $\ell = e$ or μ.

Quantity	CDF cuts
E_T^ℓ	> 20 GeV
$\not\!\!E_T$	> 20 GeV
$E_T^{j_1}$, η range	> 15 GeV, $\lvert\eta\rvert < 2.0$
$E_T^{j_2}$, η range	> 8 GeV, $\lvert\eta\rvert < 2.4$
Jets	≤ 4, $E_T^j > 8$ GeV
SVX b–tag	1, $E_T^j > 8$ GeV

$M_{\tilde{t}} - M_{\widetilde{\chi}^\pm_1}$ sets the efficiency for detecting the jets. The results of the CDF search are shown in Fig. 12 (left). The decay $\widetilde{\chi}^\pm_1 \rightarrow W^*\widetilde{\chi}^0_1$ is assumed using the masses (i) $M_{\widetilde{\chi}^\pm_1} = 80$ GeV and $M_{\widetilde{\chi}^0_1} = 30$ GeV and (ii) $M_{\widetilde{\chi}^\pm_1} = 70$ GeV

Table 9: Selection criteria for the DØ dielectron+jets+$\not\!\!E_T$direct stop pair production search.

Quantity	DØ cuts
$E_T^{e_1}, E_T^{e_2}$	$> 16, 8$ GeV
E_T^j	> 30 GeV
$E_T^{e_1} + E_T^{e_2} + \lvert\not\!\!E_T\rvert$	< 90 GeV
M_{ee}	< 60 GeV
$\not\!\!E_T$	> 22 GeV

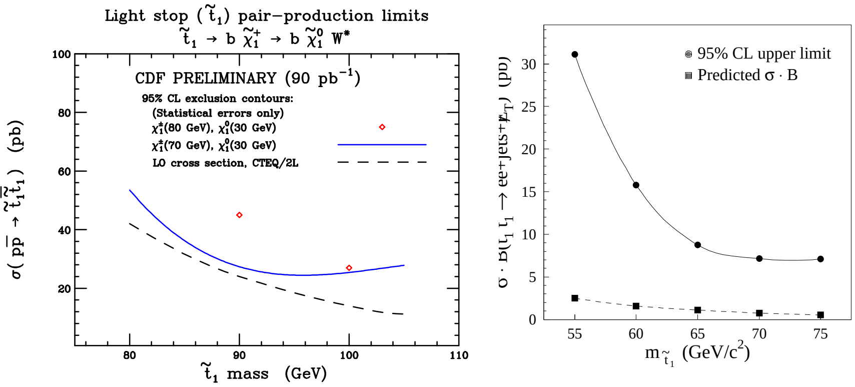

Figure 12: (Left) The CDF cross section limit on direct production of the top squark using 90 pb^{-1} of data. The decay mode is $\tilde{t} \to b\widetilde{\chi}_1^+(\to W^*\widetilde{\chi}_1^0)$. One W must decay semi–leptonically giving a signature of a lepton, $\not\!\!E_T$, and jets. The theoretical cross section is from ISAJET 7.06. (Right) The DØ 95% confidence level cross section limit on the cross section for stop production times the branching ratio to a final state containing 2 electrons as a function of the mass of the $\tilde{t}$ is shown as a solid line.[81] The mass of the lightest chargino is assumed to be 47 GeV. The predicted cross section times branching ratio from `ISAJET`[51] is also shown as a dashed line.

and $M_{\widetilde{\chi}_1^0} = 30$ GeV. Given these mass choices, there is little other parameter dependence. Presently, the cross section limits are above the predicted cross sections due to the high E_T cuts.

DØ searches in the dilepton channel[81] using the cuts listed in Table 9. The signature is similar to the squark and top dilepton searches. The results are shown in Fig. 12 (right), assuming $M_{\widetilde{\chi}_1^\pm} = 47$ GeV and $M_{\widetilde{\chi}_1^0} = 28.5$ GeV. A substantial background comes from $Z \to \tau^+\tau^-$, again requiring a high threshold for the E_T cuts, and no limit can be set.

The above analyses were done in regions of SUSY parameters that have been excluded by LEP. They show, however, the procedures to be followed in redoing these studies for other regions of the MSSM parameter space.

Top Squark Production From Top Decays

CDF has presented another analysis using the SVX–tagged lepton+jets sample to search for the decay $t \to \tilde{t}_1 \widetilde{\chi}_1^0$, with $\tilde{t}_1 \to b\widetilde{\chi}_1^\pm$.[82] If one of the top quarks in a $t\bar{t}$ event decays $t \to bW(\to \ell\nu)$ and the other $t \to \tilde{t}_1 \widetilde{\chi}_1^0$ followed by $\tilde{t}_1 \to b\widetilde{\chi}_1^\pm(\to jj\widetilde{\chi}_1^0)$ or $t \to bW(\to jj)$ and $t \to \tilde{t}_1 \widetilde{\chi}_1^0$ followed by $\tilde{t}_1 \to b\widetilde{\chi}_1^\pm(\to \ell\nu\widetilde{\chi}_1^0)$, the signature is $b\bar{b}\ell\nu jj + \not\!\!E_T$, the same as in the SM, but where the $\not\!\!E_T$ includes the momentum of the $\widetilde{\chi}_1^0$. The lepton+jets channel has a large number of events, so a kinematic analysis can be performed on the event sample. Due to the mass of the $\widetilde{\chi}_1^0$ and the intermediate sparticles in the decay chain, the jets from the SUSY decay are significantly softer. This difference is exploited as the basis of the search.

Table 10: Selection criteria for the CDF search for top decaying into stop in the signature of 1 lepton (ℓ), $\not\!\!E_T$, and 3 jets including at least one b tag, where $\ell = e$ or μ. The quantity $|\cos\theta^*|$ is the polar angle of a jet in the rest frame of the ℓ, $\not\!\!E_T$ and jets. ΔR_i is the distance between a jet i and the next nearest jet in $\eta - \phi$ space. The jets are ordered in E_T, so $E_T^1 > E_T^2 > E_T^3$.

Quantity	CDF cuts
$\int \mathcal{L} dt$	110 pb^{-1}
E_T^ℓ	> 20 GeV
$\not\!\!E_T$	> 45 GeV
$M_T(\ell \not\!\!E_T)$	> 40 GeV
$p_T(\ell \not\!\!E_T)$	> 50 GeV
$E_T^{1,2}$	> 20 GeV, $\lvert\eta\rvert < 2.0$
E_T^3	> 15 GeV, $\lvert\eta\rvert < 2.0$
$\lvert\cos\theta^*\rvert_{1,2,3}$	$< 0.9, 0.8, 0.7$
$\Delta R_{1,2,3}$	≥ 0.9
Number of SVX b–tags	≥ 1 for E_T^j >15 GeV

The cuts listed in Table 10 are optimized for acceptance of the SUSY decay and rejection of W+jets background. A likelihood function is computed for each event reflecting the probability that the jets with the 2nd and 3rd highest E_T in the event are consistent with the stiffer SM distribution (as compared to the SUSY distribution). The distribution of this likelihood function shows a significant separation of these two hypotheses. After applying the cuts listed in Table 10, nine events remain, all of which fall outside of the SUSY signal region. For stop masses between 80 and 150 GeV and chargino masses between 50 and 135 GeV, a BR($t \to \tilde{t}_1 \widetilde{\chi}_1^0$)=50% is excluded at the 95% C.L., provided that $M_{\widetilde{\chi}_1^0} = 20$ GeV. Because $M_{\widetilde{\chi}_1^0}$ is fixed in this manner, it is not related to $M_{\widetilde{\chi}_1^\pm}$ as in SUGRA. At present, only this one example is available (for $M_{\widetilde{\chi}_1^0}$ already excluded by LEP); more statistics will significantly improve it.

4.4 Sleptons

At hadron colliders, sleptons can only be pair produced through their electroweak couplings to the γ, Z and W bosons. Figure 13 shows the cross sections as a function of the corresponding slepton mass compared to the differential Drell–Yan pair production cross section, $d\sigma_{\mathrm{D-Y}}/dQ$, where $Q = 2M_X$. The rate for slepton pair production is at most a few tens or hundreds of fb at the Tevatron, and so far neither collaboration has presented results on searches for sleptons in the SUGRA or RIPS framework (we describe limits in gauge mediated models later).

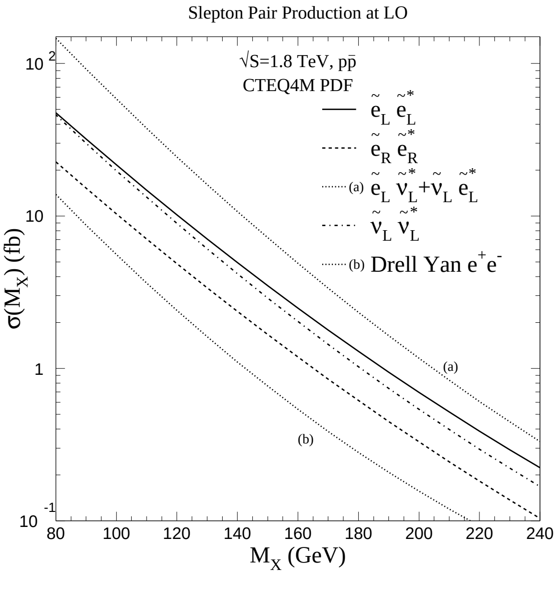

Figure 13: Production cross sections for sleptons versus slepton mass at the Tevatron. The Drell–Yan cross section for producing e^+e^- (curve b) is plotted as a function of $M_{e^+e^-} = 2M_X$. On this scale, the Drell–Yan peak ($Z \to e^+e^-$) would appear at $M_X = 45$ GeV.

A (stable) charged slepton is not a viable LSP candidate, so the decays $\tilde{\ell}^{\pm}_{L,R} \rightarrow \ell^{\pm}\tilde{\chi}^0_i$ or $\tilde{\ell}^{\pm}_L \rightarrow \nu\tilde{\chi}^{\pm}_i$ are expected. The sneutrino, instead, can be the LSP, or it can decay invisibly $\tilde{\nu} \rightarrow \nu\tilde{\chi}^0_1$, or visibly $\tilde{\nu} \rightarrow \tilde{\chi}^{\pm}_i\ell^{\mp}$. If $m_{\tilde{\nu}} < m_{\tilde{\ell}} < M_{\tilde{\chi}^0_1}$, then the decay $\tilde{\ell} \rightarrow \ell'\nu'\tilde{\nu}$ (or $\tilde{\ell} \rightarrow q\bar{q}\tilde{\nu}$) is possible. Promising signatures are (*i*) $e^+e^-, \mu^+\mu^-, \tau^+\tau^-$ plus $\not{E}_T$,[83] (*ii*) $e\mu, e\tau, \mu\tau$ plus $\not{E}_T$, and (*iii*) e, μ or τ+jets plus $\not{E}_T$ (or jets plus $\not{E}_T$). Although charged slepton production can lead to charged leptons in the final state, there is no guarantee.

The major background to same–flavor lepton pairs is Drell–Yan pair production, with fake $\not{E}_T$ from mismeasurement of the lepton or jets in the event. Most of this background can be removed by vetoing on a dilepton mass window around the Z mass, by requiring significant $\not{E}_T(\geq 25$ GeV$)$, and by vetoing events with the $\not{E}_T$ pointing in ϕ along one of the leptons or a jet. Top quark production is also a major background to a slepton heavier than the lighter gaugino, as it produces dilepton events that have real $\not{E}_T$.[83] Untangling a few heavy slepton events from top events would be difficult at the present low level of statistics.

Inclusive searches have the advantage of a larger acceptance than searches in exclusive channels. A unique signature of slepton production directly or in cascade decays would be the apparent violation of lepton universality. If the sleptons are not degenerate, both the production and decays of the sleptons will favor one or two leptons over the others, resulting in an imbalance in the detected $e/\mu/\tau$ ratios in SUSY–enhanced channels. The dominant backgrounds to inclusive leptons come from heavy flavor production (*e.g.* b–quarks), and (single) W and Z boson production.[84] Because sparticles are produced in pairs, it may be possible to discriminate against SM backgrounds by requiring the identification of a part of the decay of the second sparticle. Examples of channels that may have enhanced SUSY contributions over SM backgrounds (and hence possibly apparent lepton universality violation) are those that have, in addition to the lepton, a γ, W, Z, additional lepton, or a third–generation particle.

4.5 Charged Higgs Bosons

Even though Higgs bosons are not sparticles, the discovery of one or more would be considered *indirect* evidence for SUSY.[h] If it is light enough, the charged Higgs boson $H^{\pm}$ can be produced in the decay of the top quark $t \rightarrow bH^+$.[85] The branching fraction for this decay depends on the charged

---

[h] If $M_{H^{\pm}} \lesssim 300$ GeV, then there must exist extra light–matter fields beyond the SM to partially cancel the $H^{\pm}$ contribution to BR$(b \rightarrow s\gamma)$.

Higgs boson mass and $\tan\beta$. When kinematically allowed, this branching ratio is larger than 50% for $\tan\beta$ less than approximately 0.7 or greater than approximately 50, and completely dominates for very small or very large values of $\tan\beta$. However, as discussed in section 2.1, values of $\tan\beta \leq 0.6 - 0.7$ or above 60 would be associated with large top or bottom Yukawa couplings, which will become infinite at scales not far above the TeV scale. In general, at reasonably small values of $\tan\beta$, the charged Higgs boson decays $H^+ \to c\bar{s}$; at large $\tan\beta$ it instead decays $H^+ \to \tau^+\nu_\tau$.

CDF has searched for the decay $t \to bH^+$ using both direct[86,87] and indirect[61] methods. Direct searches look for an excess over SM expectations of events with τ leptons from the charged Higgs boson decay $H^+ \to \tau^+\nu_\tau$ (dominant for large $\tan\beta$). On the other hand, indirect searches are "disappearance" experiments, relying on the fact that decays into the charged Higgs boson mode will deplete the SM decays $t \to bW$, decreasing the number of events in the dilepton and lepton+jets channels.

The CDF direct search at large $\tan\beta$ uses two sets of cuts, listed in Table 11, to search for an excess of τ's in $t\bar{t}$ events. The first set selects a sample containing a τ that decays hadronically, an SVX b–tagged jet, $\not\!\!E_T$ and objects indicating activity from the second top decay: a second jet and a third jet or lepton. As $M_{H^\pm}$ approaches m_t, the b produced in the top decay $t \to bH$ becomes less energetic, causing a reduced efficiency for the jet and b–tagging requirements. To maintain efficiency in this region, a second set of cuts accepts events that have two high–E_T τ's and $\not\!\!E_T$.

The signature for hadronically decaying τ's is a narrow jet associated with one or three tracks with no other tracks nearby. Typically the τ tracks are required to be within a cone of 10° with no other tracks within a cone of 30°. Fake rates, measured as the probability that a generic jet is identified as a τ, are approximately 1% or less. These fake rates are too high to identify τ's in a sample dominated by QCD. However, if another selection criterion is added that further purifies the sample, τ's can be identified with a good signal–to–background ratio. For example, hadronic decays of the τ are observed in (*i*) monojet ($W \to \tau\nu$), (*ii*) lepton, $\not\!\!E_T$ and jet ($Z \to \tau\tau$) and (*iii*) the lepton+jets top quark samples.[88,89]

The CDF direct search for $t\bar{t}$ events with one or two charged Higgs bosons decaying to τ leptons sets limits by two methods. In the first method, a $t\bar{t}$ production cross section and a SUSY model ($M_{H^\pm}$ and $\tan\beta$) is assumed and the number of expected τ events is computed. If the number expected is too large to be consistent with the observed number at the 95% C.L., the SUSY model is excluded for that $t\bar{t}$ cross section. This method excludes a charged Higgs with mass less than 155 GeV (100 GeV) if $\tan\beta$ is greater than approximately 100 (50) and the top cross section[i] is 7.5 pb, as shown in Fig. 14 (left).

The second method combines the observation of $t \to bW$ decays into leptons (e or μ) and jets with the number of τ decays from the direct search. This has the advantage that a top production cross section does not need to be assumed. The lepton+jets sample defines a top production cross section which, in turn, through the SUSY model, predicts the number of τ events expected. If the number is too large to be consistent with the observation, the model is excluded. The limits set by this method are presented in detail elsewhere.[87] Qualitatively, the limits are similar to those set by the indirect method (discussed below).

Table 11: Selection criteria for the CDF direct search for $t \to bH^{\pm}(\to \tau\nu)$ in 100 pb^{-1} of data. The τ's are identified in their hadronic decay modes as one or three isolated, high–p_T tracks. Events are accepted if they pass the cuts in either analysis path.

Quantity	CDF
Analysis path 1:	
E_T^{τ}	> 20 GeV
$\not\!\!E_T$	> 30 GeV
$E_T^{j_1}$, SVX tagged	> 15 GeV
$E_T^{j_2}$	> 10 GeV
Additional object	e, μ, τ or 3$^{\text{rd}}$ jet with $E_T > 10$ GeV
Analysis path 2:	
$E_T^{\tau_1}, E_T^{\tau_2}$	> 30 GeV
$\Delta\phi(\tau_1, \tau_2)$	$< 160°$
$\not\!\!E_T$	> 30 GeV

At small $\tan\beta$ a direct search is difficult since the charged Higgs decays into two jets. Instead only the indirect method is applied.

The indirect method can be applied to both small and large $\tan\beta$ searches. The observed numbers of dilepton and lepton+jets events are consistent (at the 95% C.L.) with a minimum production and decay rate in the SM. For an assumed $t\bar{t}$ cross section (and a charged Higgs boson mass and $\tan\beta$), a simulation of the expected mixture of SM and charged Higgs boson decays predicts a number of events in the SM channels. At points in the parameter space where the decays to charged Higgs bosons are more pronounced, the SM contributions are diminished. If the number expected in a SM channel is not consistent with the rate defined by the data, the assumed values are excluded. This method provides the limit displayed in Fig. 14 (left). The cross section of 5 pb is the expected cross section for a top mass of 175 GeV; the curves using 7.5 pb show the sensitivity of the limit to the assumed top cross section. Also shown in the figure is how the limit in the region of large $\tan\beta$ can be extended using the assumptions of the indirect method. In this region the possibility that a τ decay produces a high–p_T lepton is included.

---

[i] The reader should be aware that there are subtleties in analyses that assume cross sections. The CDF experiment normalizes all cross sections to its measured proton–antiproton cross sections, rather than to a hard process such as W production. The CDF total cross section, in the judgement of one of the authors (HF), is most likely 10% too high, and thus all cross sections (in particular the top cross section) are too high. For analysis which compare different channels internally this has no effect, but for analyses which compare to theoretical predictions the reader should be careful. The D0 experiment normalizes to a weighted mean of the CDF and E710 values for the total cross section which is 2.4% lower than the CDF value.

The area in Fig. 14 (left) labeled "ratio method" is the exclusion region for an indirect search that does not make an assumption for the $t\bar{t}$ cross section. If charged Higgs boson decays were competing with SM decays, the ratio of dilepton events to lepton+jets events would decrease, regardless of the $t\bar{t}$ cross section. This occurs because the lepton+jets yield is proportional to the SM branching ratio while the dilepton yield is proportional to the SM branching ratio squared. For each SUSY parameter point, the lepton+jets sample can be used to infer a top cross section which, in turn, predicts a number of dilepton events. The point is excluded if the prediction is inconsistent with the dilepton data. Although this method excludes less parameter space, it is important since the $t\bar{t}$ cross section may be enhanced by SUSY mechanisms[118] such as $\tilde{g} \to t\tilde{t}$. At present, this method only excludes values of $\tan\beta \lesssim 0.7$, which are not of much interest according to present theoretical bias.

DØ has also searched for a charged Higgs boson lighter than the top quark using the indirect method.[90] The analysis compares the number of events observed in the lepton+jets channel to the number predicted assuming a theoretical $t\bar{t}$ production cross section. The limits depend on the mass of the charged Higgs, $\tan\beta$, and the top quark mass m_t. Table 12 shows the selection criteria used in the search. Fig. 14 (right) shows the excluded region.

Recent studies have shown that quantum SUSY effects (SUSY QCD and electroweak radiative corrections) to the decay mode $t \to bH^+$ (with subsequent decays into τ's) may be important and should be considered in future analyses.[91]

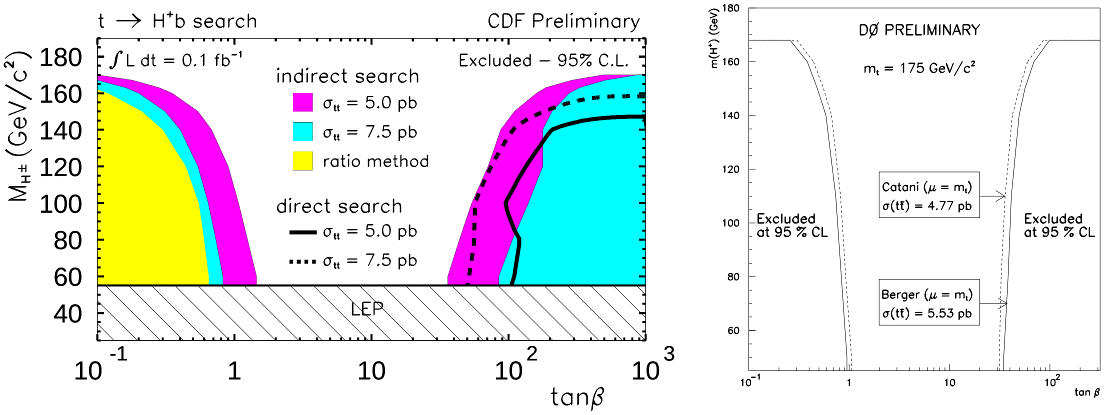

Figure 14: (Left) Exclusion space for the CDF searches for charged Higgs boson decays of the top quark in $t\bar{t}$ events. The shaded regions are from the indirect searches. For the regions labeled $\sigma_{t\bar{t}} = 5.0$ and 7.5 pb a top production cross section is assumed and points are excluded if the predicted SUSY decays have depleted the SM channels to an extent that they are inconsistent with the data. The "ratio method" is an indirect method comparing the number of lepton+jets events to the number of dilepton events and no top cross section is assumed. The region excluded with solid lines at high $\tan\beta$ is from a direct search for events where one or both top quarks in a $t\bar{t}$ event decay to $bH^+(\to \tau^+\nu)$ and information from the SM channels is ignored. (Right) The results of a DØ indirect search for a charged Higgs boson assuming $m_t = 175$ GeV and a $t\bar{t}$ production cross section of 5.53 pb and 4.77 pb. This limit is based on the full Run I DØ data sample.

4.6 Neutral Higgs Bosons

Within the MSSM, the main production channels for the lightest CP–even Higgs boson h at the Tevatron are the same as for a SM Higgs boson, Wh or Zh production.[92] The cross sections behave in such a way that these channels are relevant for large values of the CP–odd mass M_A (the SM limit) or for small M_A and small $\tan\beta$. The heavy CP–even Higgs boson H could become marginally relevant for searches at an upgraded Tevatron through ZH, WH production, in some restricted region of parameter space, complementary to the one relevant for the light CP–even Higgs boson searches. In addition, the enhancement of the bottom Yukawa coupling in the large $\tan\beta$ regime can render the production processes $hb\bar{b}$, $Ab\bar{b}$, and $Hb\bar{b}$ useful to perform searches in a large region of parameter space.[93]

Both collaborations have searched for a neutral Higgs boson in the mode $q\bar{q}' \to W^* \to W(\to e\nu, \mu\nu)h(\to b\bar{b})$. DØ has searched in 100 pb^{-1} of data

Table 12: Selection criteria of the DØ search for a charged Higgs boson produced in top quark decays. In addition, events are vetoed if the $\not{E}_T$ is aligned in ϕ within 25° of a muon, or if the muons in a μ event with a μ–tagged jet have a good fit to the decay $Z \rightarrow \mu\mu$.

Quantity	DØ topological	DØ tagged
E_T threshold on leptons	20 GeV	20 GeV
Max η for leptons	2 (e) 1.7 (μ)	2 (e) 1.7 (μ)
Number of jets	4	3
jet E_T threshold	15 GeV	20 GeV
$\not{E}_T$	25 GeV (e) 20 (μ)	20 GeV
H_T	180 GeV	110 GeV
Sum of lepton E_T and $\not{E}_T$	60 GeV	N.A.
Aplanarity	0.065	0.04
$\lvert\eta_W\rvert$	2.0	N.A.
μ–tagged jets	veto	require

using a data sample containing a lepton, $\not{E}_T$ and two jets.[94] One of the jets must have a muon associated with it for b–tagging. The cuts are listed in Table 13. Twenty–seven events pass the selection criteria; 25.5 ± 3 events are expected from Wjj and $t\bar{t}$. The limits shown in Fig. 15 are set by a simple event–counting method and by fitting the $b\bar{b}$ dijet mass spectrum.

CDF has recently completed a similar search for the same decay mode using 109 pb^{-1} of data.[95] All events must have one SVX b–tag. These events are split into single–tagged (one SVX tag) and double–tagged samples (two SVX tags or one SVX and one lepton (e or μ) tag). The 36 (6) single–tagged (double–tagged) events are consistent with the 30 ± 5 (3.0 ± 0.6) expected from SM W+jets and $t\bar{t}$. Both the single– and double–tagged dijet mass distributions are fit simultaneously to set the limits shown in Fig. 15.

The process $q\bar{q} \rightarrow Z^* \rightarrow Zh$ occurs at a comparable rate to the W^* process. CDF has searched for both associated production processes assuming $W/Z \rightarrow jj$.[96] The event selection criteria are listed in Table 13. In 91 pb^{-1} of data, 589 events remain, consistent with the expectation from QCD heavy–flavor production and fake tags. To set limits, the $b\bar{b}$ dijet mass spectrum is fit. Also shown in Fig. 15 is the SM production cross section for Wh and Zh as a function of the Higgs boson mass. The present experimental limits are roughly two orders of magnitude away from the predicted cross section. However, Run II will provide at least 20 times the data. This plus the possibilities of looking at other decay modes (*i.e.* $Zh \rightarrow \nu\nu b\bar{b}$) holds promise for Higgs physics at the Tevatron.[13]

Table 13: Selection criteria of Tevatron searches for the associated production of a neutral Higgs boson and a W or Z, and the Higgs boson decays to $b\bar{b}$.

Quantity	CDF	DØ
	$WH \to \ell\nu b\bar{b}$	
$E_T^e(E_T^\mu)$	$> 25(20)$ GeV	$> 20(20)$ GeV
$\not{E}_T e\ (\mu)$	$> 25(20)$ GeV	$> 20(20)$ GeV
$E_T^{j_1}, E_T^{j_2}$	> 15 GeV	> 15 GeV
b–tagging	one SVX tag	one μ tag

	$(W,Z)H \to jjbb$
Quantity	CDF
$E_T^{j_{1-4}}$	> 15 GeV
b–tagging	2 SVX tags
$P_T(b\bar{b})$	> 50 GeV

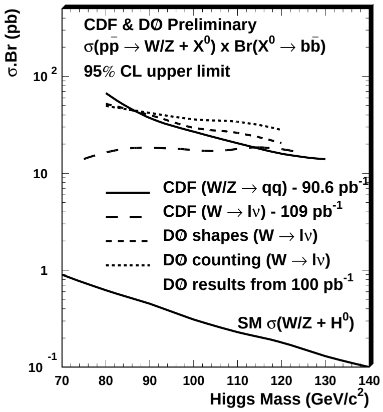

Figure 15: Limits from CDF and DØ for the associated production of a neutral Higgs boson and a W or Z boson. The CDF limits are shown for the final states of $\ell\nu b\bar{b}$ and $jjb\bar{b}$, and the DØ limit is for the final state $\ell\nu b\bar{b}$. The limit is set using a simple counting method and by fitting the $b\bar{b}$ spectrum ("shapes").

DØ has also searched for a fermio–phobic Higgs, *i.e.* one with suppressed couplings to fermions.[97] For a light neutral Higgs boson, the decay through a virtual W loop to a $\gamma\gamma$ final state can be dominant.[98] Events are selected containing two photons with $E_T > 20$ and 15 GeV, and two jets with $E_T > 20$ and 15 GeV. No evidence of a resonance is seen in the mass distribution of the 2 photons, and DØ excludes, at a 95% C.L., such a Higgs with masses less than 81 GeV. The branching fraction for $h \to \gamma\gamma$ is taken from Ref. [98].

Table 14: Selection criteria for the D0 search for a Higgs boson produced in association with a hadronically-decaying W and which decays to two photons.

Quantity	DØ
E_T threshold on photons	1 above 20 GeV, 1 above 15
$\lvert\eta\rvert$ on photons	<1.1 or 1.5< $\lvert\eta\rvert$ <2.25
E_T threshold jets	1 above 20 GeV, 1 above 15
$\lvert\eta\rvert$ on jets	< 2
vector sum of photon E_T	< 10 GeV
vector sum of jet E_T	< 10 GeV

4.7 R–Parity Violation and a Short–Lived LSP

Allowing for R–parity violation in the MSSM opens a host of possibilities at the Tevatron. Both baryon–number–violating operators (UDD) and lepton–number–violating ones (LLE and LQD) are possible. There are many resonant and non–resonant particle production mechanisms and subsequent decay processes which have been analyzed in the literature.[103] In this section, we restrict ourselves to the experimental analyses performed so far.

The possible excess of HERA events at large Q^2 has triggered interest in studying the consequences of the interaction of a light squark (preferably a top or charm squark) with an electron and a d quark.[105] If the gluino were heavier than this squark, then gluino pair production at the Tevatron and the decay $\tilde{g} \to \bar{c}\tilde{c}_L$ through R–conserving couplings, followed by the RPV decay $\tilde{c}_L \to e^+ d$, would yield the signature of two electrons and 4 jets. If the RPV decay $\tilde{c}_L \to e^+ d$ is allowed through the coupling λ'_{121}, then from the structure of the R–parity violating Lagrangian (Eq. (24)) it follows that $\tilde{s}_L \to \nu_e d$, $\tilde{d}_R \to e^- c$, and $\tilde{d}_R \to \nu_e s$ are also allowed. If $m_{\tilde{c}_L} \simeq m_{\tilde{s}_L}$ (which is guaranteed) $\simeq m_{\tilde{d}_R}$ (which is probable), then the gluino decays equally to $\tilde{c}_L\bar{c}$, $\tilde{s}_L\bar{s}$, and $\tilde{d}_R\bar{d}$ (+ h.c.) final states. Assuming that only RPV decays occur, then 1/2 of gluino decays produce a charged lepton. Therefore, $\tilde{g}\tilde{g}$ production produces like–sign dileptons 1/8 of the time. The requirement of only RPV decays demands $M_{\tilde{\chi}_1^0} > m_{\tilde{Q}}$.

CDF has performed a search[104] considering the RPV squark decays with the signature of two like–sign electrons and two jets. In 105 pb^{-1} of Run Ia and Ib data, no events remain after all cuts are applied (see Table 15). Varying

Quantity	CDF
$E_T^{e_1}, E_T^{e_2}$	> 15 GeV, $\lvert\eta\rvert <1.1$
$Q_{e_1} + Q_{e_2}$	± 2
$E_T^{j_1}, E_T^{j_2}$	> 15 GeV, $\lvert\eta\rvert <2.4$
$S = \not{E}_T/\sqrt{\Sigma E_t}$	< 5 GeV$^{1/2}$

Table 15: Selection criteria of the CDF search for R–parity violating processes using 105 pb^{-1} of data.

the masses of the SUSY particles does not alter the acceptance significantly since they are heavy enough for the decay products to easily pass the E_T thresholds. Because of this, the limit on the cross section times branching ratio is approximately constant at 0.19 pb. For $m_{\tilde{c}_L} = 200$ GeV, this excludes $M_{\tilde{g}} < 230$ GeV, assuming BR($\tilde{g}\tilde{g} \rightarrow e^{\pm}e^{\pm}X) = 1/8$.

Allowing for possible R–parity conserving squark decays, the decay $\widetilde{Q} \rightarrow q\widetilde{\chi}_1^0$ is possible, where $\widetilde{\chi}_1^0$ is the LSP. Since the LSP has no R–parity conserving decays kinematically accessible, the R–parity violating decay $\widetilde{\chi}_1^0 \rightarrow c\bar{d}e^-$ or $\bar{c}de^+$ occurs through a virtual charm or down squark, while $\widetilde{\chi}_1^0 \rightarrow d\bar{s}\nu$ or $\bar{d}s\bar{\nu}$ occurs through a virtual strange or down squark. The exact branching ratio for $\widetilde{\chi}_1^0 \rightarrow e^{\pm} + X$ depends on sparticle masses and the mixing of the neutralinos. For the analysis, five squark masses are assumed to be degenerate and any squark pair can lead to like–sign dielectron events, since $\widetilde{\chi}_1^0$ is a Majorana particle. Squark masses less than 210 GeV are excluded if the mass of the $\widetilde{\chi}_1^0$ is more than half of the squark mass and the gluino is heavy. For lighter $\widetilde{\chi}_1^0$, the 3–body decay of the $\widetilde{\chi}_1^0$ can produce electrons that are too soft to satisfy selection criteria.

4.8 R–Parity Violation and Long–Lived Heavy Charged Sparticles

If R–parity is violated, and the LSP is charged, it can manifest itself as a long–lived charged particle (see Sec. 2.4) in a collider detector. The particle can be identified by measuring the dE/dx energy loss as it passes through the CDF SVX and CTC detectors. For a given momentum, a heavy particle has a slower velocity and hence a greater energy loss than a relativistic particle ($\beta \simeq 1$). If the particle is weakly interacting or massive enough to kinematically suppress showering, it will penetrate the detectors and be triggered on and reconstructed as a muon with too much energy loss. A result using part of the Run I data has been presented by CDF [102] and is updated with the full data set here. In 90 pb^{-1} of inclusive muon triggers ($p_T >$30 GeV), CDF searches for particles with ionization consistent with $\beta\gamma < 0.6$ and finds 12 events depositing more than twice the energy expected from a minimum ionizing muon. This is consistent with the number of events expected from muons which overlap with other tracks to fake a large dE/dx signal.

The CDF result can be used to exclude some SUSY scenarios with R–parity violation (RPV). For example, the lightest tau slepton could be the LSP. Its production rate through R–parity–conserving couplings can be determined from Fig. 13. If λ_{333} is the only large RPV coupling, the decay $\tilde{\tau} \to \tau\nu_\tau$ can occur with a lifetime fixed by λ_{333} and $m_{\tilde{\tau}}$ (see Sec. 2.4). For small enough λ_{333}, this decay can occur outside the tracker, leading to the desired signal if the $\tilde{\tau}$ is travelling slowly enough.

4.9 Photon and $\not\!\!E_T$ Signatures

An Unexpected Turn: the CDF $ee\gamma\gamma\not\!\!E_T$ Event

Supersymmetry has so many parameters that the full range of its allowed signatures may be hard to predict. In April 1995, the CDF experiment recorded an event with a very unusual topology[106] which may have SUSY interpretations. It has four electromagnetic clusters, which pass the typical cuts for two electrons and two photons, and $\not\!\!E_T$. A display of the event is shown in Fig. 16.

The electron in the central region of the detector is well–isolated and is associated with a track that has a p_T in good agreement with the e^- hypothesis. The two photons are also well–isolated and have no associated tracks. The "electron" at large η is more difficult to identify positively. The associated track should only cross a part of the inner CTC where the occupancy is too high to find the track. Hence, its charge cannot be determined. The VTX, a wire chamber surrounding the SVX but inside the CTC, measuring in the $r - z$ view, has a track at the correct η for the electron hypothesis. The path through the cluster and the event vertex can be searched for tracks in the SVX, and this analysis is underway. The probability that the event could be produced in the SM, including the probability that one or more of the objects is fake, is being estimated. The preliminary results indicate that the number of expected $\ell\ell\gamma\gamma\not\!\!E_T$ events is many orders of magnitude less than one. However, the data set was derived from over three trillion collisions, and the probability of *all* signatures which would be considered "rare" must be estimated (an impossible task) to determine the significance of one event.

There have been two main proposals for a possible SUSY explanation of the event: the Gravitino LSP and the Higgsino LSP model (for non–SUSY explanations, see Refs. [107], for example). Both proposals also suggest other signatures that should be expected within these models and which are presented in the following. The Tevatron collaborations have completed some of

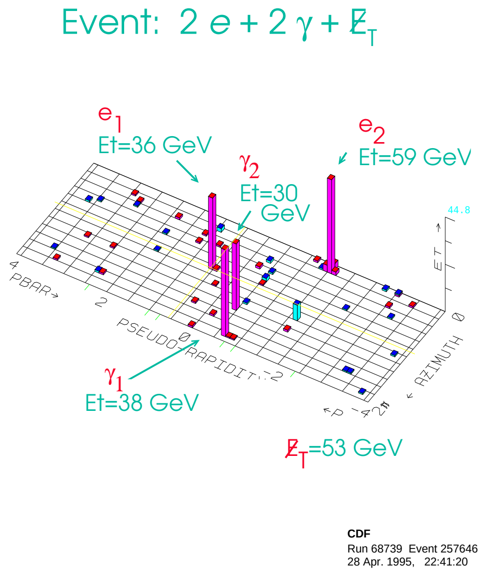

Figure 16: The very unusual CDF event containing two 'electrons', two 'photons' and missing $\not{E}_T$. The display is the calorimeter cylinder unrolled into a plane. The towers represent energy deposition, with the height of the tower proportional to E_T.

these searches, which are also discussed below.

Gauge–Mediated Low Energy SUSY–Breaking: Gravitino LSP

The CDF analysis of the above one event reminded theorists of low-energy SUSY breaking models,[108,109,110,113] which had long ago lost favor to SUGRA models. In these models the (usually ignored) gravitino ($\widetilde{G}$) is very light and becomes the LSP. The lightest SM superpartner becomes the next–to–lightest supersymmetric particle (NLSP), which is unstable and decays into its SM partner plus the Goldstino component of the gravitino.[114] In the simplest gauge–mediated models, the squarks are heavy and the gauginos obey the unification relationship in Eq. (11). Generically the NLSP can be a neutralino or a slepton (most plausibly a right–handed slepton and, due to the larger

Yukawa coupling, a $\tilde{\tau}$). If the scale of SUSY breaking is not far above the electroweak scale ($\leq$ a few 1000 TeV), the NLSP will decay within the detector, leading to distinctive signatures as displaced vertices or heavy charged sleptons decaying into leptons, possibly with a kink to a minimum ionizing track.[108,110,111]

If a gaugino–like neutralino is the NLSP, the only modification to SUGRA phenomenology, where all sparticles decay down to $\tilde{\chi}_1^0$, is that $\tilde{\chi}_1^0$ then decays to a photon and $\not\!\!E_T$. The production of $\tilde{\chi}_2^0\tilde{\chi}_1^\pm$, $\tilde{\chi}_1^+\tilde{\chi}_1^-$ and $\tilde{\ell}_R^+\tilde{\ell}_R^-$ pairs, followed by cascade decays, leads to the final states $WZ\gamma\gamma+\not\!\!E_T$, $W\ell^+\ell^-\gamma\gamma+\not\!\!E_T$, $WW\gamma\gamma+\not\!\!E_T$ and $\ell^+\ell^-\gamma\gamma+\not\!\!E_T$, all with comparable rates.[110] A logical starting place for searches is in the inclusive two photon and $\not\!\!E_T$ channel.[115] In particular, the CDF event can be interpreted as either $\tilde{e}\tilde{e}^*$ production,[108,113] followed by $\tilde{e} \to e\widetilde{\chi}_1^0$ or $\widetilde{\chi}_1^+\widetilde{\chi}_1^-$ production,[113] followed by $\widetilde{\chi}_1^- \to e^-\bar{\nu}_e\widetilde{\chi}_1^0$. If the coupling between the gravitino and matter is large enough, then the lightest neutralino can decay $\widetilde{\chi}_1^0 \to \gamma\widetilde{G}$ inside a collider detector, yielding the desired signature of $e^+e^-\gamma\gamma\not\!\!E_T$. However, it follows that if one adjusts the parameters of the model to explain the multilepton plus photons CDF event, then a very large rate of multijet plus multileptons plus photon(s) events is to be expected.[115,116] The fact than none of these other signatures has been detected makes the above LSP $\widetilde{G}$ explanation of the CDF $ee\gamma\gamma\not\!\!E_T$ event unlikely. Other possible explanations may, however, remain open.

Signatures of photons+$\not\!\!E_T$ can point towards models of low–energy SUSY breaking, but there are other possible signatures in these models.[111,112] If the NLSP is a neutralino which is mainly Higgsino–like, then $\tilde{\chi}_1^0$ decays to the lightest Higgs boson (or the heavy CP–even or the CP–odd neutral Higgs bosons if they are sufficiently light) plus a gravitino. The Higgs boson will subsequently decay into $b\bar{b}$. Hence, the signature of 4 b–jets, which reconstruct the lightest Higgs boson mass in pairs, plus $\not\!\!E_T$ is possible. If the NLSP is a right–handed slepton, then the decay $\tilde{\ell} \to \ell\widetilde{G}$ occurs, yielding lepton pairs and $\not\!\!E_T$ as final signature of slepton pair production. The dilepton signature will suffer from large irreducible backgrounds, but the production and decay of heavier sparticles can give spectacular signals. For example, the pair production of a left–handed slepton which cascade decays into a right–handed slepton and a neutralino can yield six leptons+$\not\!\!E_T$ in the final state. Also, since the NLSP slepton can be $\tilde{\tau}_R$, signatures with many τ leptons are possible.

If any of the above signatures were observed experimentally, a measurement of the decay length of the NLSP would provide information about the scale of supersymmetry breaking. However, the scale of SUSY breaking might be sufficiently large that an NLSP slepton would decay outside the detector. In this case, heavy charged particle pair production without missing energy could be a manifestation of gauge–mediated low–energy SUSY–breaking models.

Higgsino LSP

The Higgsino LSP model[109] involves a region of MSSM parameter space in which the $\widetilde{\chi}_2^0$ is photino–like and the $\widetilde{\chi}_1^0$ is Higgsino–like, so the radiative decay $\widetilde{\chi}_2^0 \to \gamma\widetilde{\chi}_1^0$ dominates over other $\widetilde{\chi}_2^0$ decay modes (see, for example, Eq. (5)).[117] The event can be again interpreted as (i) $\tilde{e}\tilde{e}^*$ production, but with $\tilde{e} \to e\widetilde{\chi}_2^0$, or (ii) $\widetilde{\chi}_1^+\widetilde{\chi}_1^-$ production, with $\widetilde{\chi}_1^- \to e^-\bar{\nu}\widetilde{\chi}_2^0$, and the subsequent radiative decay of the $\widetilde{\chi}_2^0$ yielding the observed signature.

In these models, photons only arise from the decay of $\widetilde{\chi}_2^0$. Other signatures involving two photons might come from the process $\tilde{\nu}\tilde{\nu}^* \to \nu\bar{\nu}\widetilde{\chi}_2^0\widetilde{\chi}_2^0$, but there is no guarantee that the $\tilde{\nu}$ is light enough to produce a substantial signal. Because the $\widetilde{\chi}_2^0$ is photino–like, direct $\widetilde{\chi}_2^0\widetilde{\chi}_2^0$ production is not large. In this model, the dominant neutralino and chargino production processes are $\widetilde{\chi}_1^+\widetilde{\chi}_1^-$, $\widetilde{\chi}_1^0\widetilde{\chi}_3^0$, and $\widetilde{\chi}_1^\pm\widetilde{\chi}_1^0, \widetilde{\chi}_1^\pm\widetilde{\chi}_3^0$. None of these involve the direct production of $\widetilde{\chi}_2^0$. Typically, the decay $\widetilde{\chi}_3^0 \to Z^*\widetilde{\chi}_1^0$ occurs, yielding no photon. One of the next largest processes is $\widetilde{\chi}_1^\pm\widetilde{\chi}_2^0$, which would produce a trilepton signature in SUGRA models, but can produce $\ell\gamma\not{E}_T$ or $jj\gamma\not{E}_T$ signatures in the Higgsino LSP model.

If the stop is light, this discussion changes, because the $\widetilde{\chi}_1^\pm$ can decay $\widetilde{\chi}_1^\pm \to b\tilde{t}_1$, followed by $\tilde{t}_1 \to c\widetilde{\chi}_1^0$. The signature is then a rather distinct $\gamma bc\not{E}_T$. However, such a light stop would appear in top decays, depleting the observed SM decays to an unacceptable level. This is only true, though, if there are no other sources of top quark production from SUSY, which there obviously can be. Surprisingly, such models can be constructed that are in accord with the present SUSY limits.[118] If the gluinos are heavy enough so that $\tilde{g} \to t\tilde{t}_1^*$, or $\to \bar{t}\tilde{t}_1$, and gluino production is further fed by squark decay $\widetilde{Q} \to q\tilde{g}$, then one can compensate for the lost top quarks in SUSY decay modes. This leads to more sources of $\gamma bc\not{E}_T$ events than just $\widetilde{\chi}_1^\pm\widetilde{\chi}_2^0$ events, as well as other signatures.

Inclusive Two Photons and $\not{E}_T$ Signatures

The generic $\gamma\gamma\not{E}_T + X$ signature has no significant background from real photons. The main backgrounds are caused by jets and electrons faking photons. The SM production of $W(\to e\nu)\gamma$ plus jets can fake some of the signatures if the electron is misidentified as a photon. These events have a $\not{E}_T$ spectrum typical of W events, peaked at about $M_W/2 \simeq 40$ GeV, with a long tail to high $\not{E}_T$. The dominant instrumental background, however, is from di–jet and γ+jet production, where the large production cross section overcomes the small probability ($\simeq 10^{-4} - 10^{-3}$) that a jet fakes a photon.

Figure 17 shows the $\not\!\!E_T$ distributions from DØ (left) and CDF (right) diphoton events [119,120] after imposing the selection criteria given in Table 16. For the DØ analysis, the shape of the $\not\!\!E_T$ spectra agrees well with backgrounds containing two electromagnetic–like clusters, where at least one of the two clusters fails the photon selection criteria. Two events satisfy all selection criteria, with a predicted background, dominated by jets faking photons, of 2.3 ±0.9 events. For the CDF analysis, the shape of the $\not\!\!E_T$ distribution is in good agreement with the resolution of the $Z \to e^+e^-$ control sample. The event on the tail in $\not\!\!E_T$ is the "$ee\gamma\gamma\not\!\!E_T$" event. If the source of this event is an anomalously large $WW\gamma\gamma$ production cross section that yields one event in $\ell\ell\gamma\gamma\not\!\!E_T$, CDF would expect dozens of events with two photons and four jets. However, the jet multiplicity spectrum in diphoton events is well–modeled by an exponential, and there are no diphoton events with 3 or 4 jets. As mentioned before, events with diphotons, jets and $\not\!\!E_T$ can be signatures of gauge–mediated low–energy supersymmetry–breaking models.

Table 16: Selection criteria for $\gamma\gamma$+$\not\!\!E_T$+X searches

Quantity	DØ	CDF
$E_T^{\gamma_1}, E_T^{\gamma_2}$	$> 20, 12$ GeV	$> 25, 25$ GeV
$\lvert\eta^\gamma\rvert$	< 1.2 or between 1.5 and 2.0	< 1.1
$\not\!\!E_T$	> 25 GeV	> 35 GeV
$\Delta\phi$ between $\not\!\!E_T$ and nearest jet	N.A.	$> 10°$

DØ presents limits[120] in the framework of the Gravitino LSP scenario by considering neutralino and chargino pair production. Assuming $M_2 \simeq 2M_1$ and large values of $m_{\widetilde{Q}}$, the signatures are a function of only M_2, μ, and $\tan\beta$. Event rates are predicted using `PYTHIA`.[52] Figure 18 shows the limit on the cross section for $\widetilde{\chi}_1^\pm\widetilde{\chi}_1^\pm$ and $\widetilde{\chi}_1^\pm\widetilde{\chi}_2^0$ production as a function of the $\widetilde{\chi}_1^\pm$ mass when $|\mu|$ is large and thus the $\widetilde{\chi}_1^\pm$ mass is approximately twice the $\widetilde{\chi}_1^0$ mass. The figure also shows, more generally, the excluded region in the M_2–μ plane ($\mu < 0$ gives larger $\widetilde{\chi}_1^\pm, \widetilde{\chi}_2^0 - \widetilde{\chi}_1^0$ mass splittings, small $|\mu|$ means $\widetilde{\chi}_1^\pm, \widetilde{\chi}_1^0$, and $\widetilde{\chi}_2^0$ are more Higgsino–like), along with a prediction for the region that might explain the CDF $ee\gamma\gamma\not\!\!E_T$ event as chargino pair production. The latter explanation requires 100 GeV $< M_{\widetilde{\chi}_1^\pm} <$ 150 GeV with $M_{\widetilde{\chi}_1^0} < 0.6 M_{\widetilde{\chi}_1^\pm}$ to produce one event with a reasonable probability.[113]

As can be seen from Fig. 18, the cross section limit is typically 0.24 pb for either $\widetilde{\chi}_1^+\widetilde{\chi}_1^-$ or $\widetilde{\chi}_1^\pm\widetilde{\chi}_2^0$ production. By combining all chargino and neutralino pair production processes, a $\widetilde{\chi}_1^\pm$ with mass below 150 GeV is excluded. Hence,

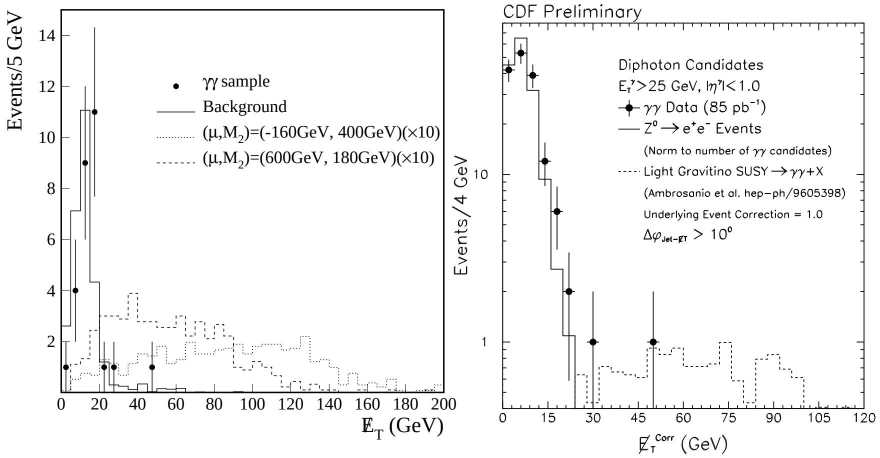

Figure 17: (Left) The $\not\!\!E_T$ spectra in the DØ search for events with 2 photons, one with $E_T >$ 25 GeV, the other with $E_T >$ 12 GeV.[120] The points are the data, the solid line is the estimated background from di–jet events and direct photon events. The dotted lines are for gaugino production within gauge–mediated models using the parameters listed and $M_1 \simeq 2M_2$. (Right) The CDF $\not\!\!E_T$ spectrum for events with two central photons with $E_T >$ 25 GeV. Events which have any jet with $E_T >$ 10 GeV pointing within 10 degrees in azimuth of the $\not\!\!E_T$ are removed. The solid histogram shows the resolution from the $Z \to e^+e^-$ control sample. The dashed line shows the expected distribution from all SUSY production in a model [115] with $M_2 = 225$ GeV, $\mu = 300$ GeV, $\tan\beta = 1.5$, and $M_{\widetilde{Q}} = 300$ GeV.

to keep the chargino interpretation of the $ee\gamma\gamma\not\!\!E_T$ event, it is necessary to expand on the analysis of Ref. [113]. The chargino mass limit is much higher than in SUGRA models, because of the 100% branching fraction for the decay $\widetilde{\chi}_1^0 \to \gamma\widetilde{G}$ and the high detectability of the photon and $\not\!\!E_T$. The result eliminates the possibility of observing signatures of this particular model at LEP200. The $\not\!\!E_T$ cut needed to control QCD backgrounds makes the analysis sensitive to the mass splittings between $\widetilde{\chi}_1^0$ and $\widetilde{\chi}_1^\pm$ or $\widetilde{\chi}_2^0$. However, the simplest models predict unification mass relations between the gauginos, which thus gives acceptable mass splittings.

DØ also has a limit on the cross section for $\tilde{e}\tilde{e}^* \to e^-e^+\widetilde{\chi}_2^0\widetilde{\chi}_2^0$, $\tilde{\nu}\tilde{\nu}^* \to \nu\bar{\nu}\widetilde{\chi}_2^0\widetilde{\chi}_2^0$, and $\widetilde{\chi}_2^0\widetilde{\chi}_2^0 \to \gamma\gamma\widetilde{\chi}_1^0\widetilde{\chi}_1^0$ using the same analysis as for the Gravitino LSP search. Such signatures might also be expected in Higgsino LSP models. The limit on the cross section for such processes is about 0.35 pb for $M_{\widetilde{\chi}_2^0} - M_{\widetilde{\chi}_1^0} >$ 30 GeV, which is close to the maximum cross section predicted in these models.

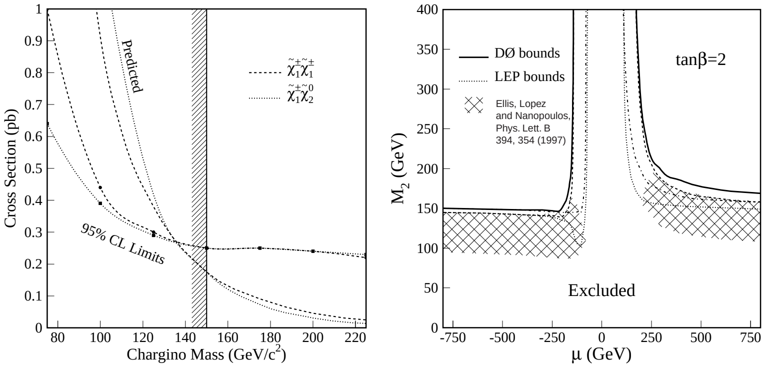

Figure 18: (Left) The DØ cross section limit on $\widetilde{\chi}_1^\pm\widetilde{\chi}_1^\pm$ and $\widetilde{\chi}_1^\pm\widetilde{\chi}_2^0$ production, assuming $M_{\widetilde{\chi}_1^\pm} \approx 2M_{\widetilde{\chi}_1^0}$ and BR($\widetilde{\chi}_1^0 \to \gamma\widetilde{G}$) = 100%. The top dotted (dashed) curve is the cross section from `PYTHIA` for $\widetilde{\chi}_1^\pm\widetilde{\chi}_2^0$ ($\widetilde{\chi}_1^+\widetilde{\chi}_1^-$) production. The bottom dotted (dashed) curve is the cross section limit from the DØ collaboration[120] on $\widetilde{\chi}_1^\pm\widetilde{\chi}_2^0$ ($\widetilde{\chi}_1^+\widetilde{\chi}_1^-$) production. The vertical, hatched line marks the 95% C.L. lower limit on the lightest chargino mass from considering all chargino and neutralino pair production processes and all values of μ. (Right) The limits on the parameters M_2 and μ in gauge–mediated models based on `PYTHIA` for $\tan\beta$=2 and $M_{\widetilde{Q}}$=800 GeV.[120] The hatched area is the region proposed[113] to explain the CDF ee$\gamma\gamma\not\!\!E_T$ event. The solid line shows the DØ bounds. The long–dashed line shows a contour with $M_{\widetilde{\chi}_1^\pm} = 150$ GeV and the dash–dotted line shows a contour with $M_{\widetilde{\chi}_1^0} = 75$ GeV. The dotted lines show an interpretation of preliminary LEP results at an energy of 161 GeV.

Single Photon, Heavy Flavor, and $\not\!\!E_T$

CDF has searched for the signature $\gamma bc\not\!\!E_T$, as predicted in Higgsino LSP models with a light stop.[118] The data sample of 85 pb^{-1} contains events with an isolated photon with $E_T^\gamma > 25$ GeV and a jet with an SVX b–tag. The $\not\!\!E_T$ spectrum of these events can be seen in Fig. 19. After requiring $\not\!\!E_T$>20 GeV, 98 events remain.[119]

The estimated background to the 98 events is $77 \pm 23 \pm 20$ events. The shape is consistent with background. About 60% of the background is due to jets faking photons, 13% to real photons and fake b–tags, and the remainder to SM $\gamma b\bar{b}$ and $\gamma c\bar{c}$ production; all of these sources require fake $\not\!\!E_T$. When the $\not\!\!E_T$ cut is increased to 40 GeV, 2 events remain. More than 6.43 events of anomalous production in this topology is excluded.

The efficiency used in the limits is derived from a "baseline" model with $M_{\widetilde{\chi}_1^0} = 40$ GeV, $M_{\widetilde{\chi}_2^0} = 70$ GeV, $m_{\tilde{t}_1} = 60$ GeV, $m_{\widetilde{Q}} = 250$ GeV, and $M_{\tilde{g}} =$

Table 17: Summary of the 85 pb^{-1} data sample for the CDF $\gamma b \not\!\!E_T$ search. Limits are set using all cuts which results in two events.

Quantity	Cut	Cumulative Number of Events
E_T^{γ}, ID cuts	> 25 GeV	511335
SVX b–tag	≥ 1	1487
E_T^b, $\lvert\eta\rvert < 2.0$	> 30 GeV	1175
$\not\!\!E_T$	> 20 GeV	98
$\not\!\!E_T$, $\Delta\phi(\gamma - \not\!\!E_T) < 2.93$	> 40 GeV	2

225 GeV.[a] The distribution of the number of jets in the data is shown in Fig. 19 compared to that expected from backgrounds and the SUSY model (scaled ×10). There are more jets expected in the SUSY model than the data indicates because of the hard kinematics of squark and gluino decays. The baseline model predicts 6.65 events, so this model is excluded (at the 95% C.L.). This result does not rule out the Higgsino LSP model in general, only one version with a fairly light mass spectrum. A more general limit can be set by holding the lighter sparticle masses constant and varying the squark and gluino masses. In this case squarks and gluinos less than 200 GeV and 225 GeV, respectively, are excluded.

4.10 Other Anomalies

There are other anomalies in the current data beyond the "$ee\gamma\gamma\not\!\!E_T$" event. These are, so far, either single, rare events or discrepancies on the tails of distributions where statistics are low and backgrounds difficult to calculate. In addition, there is the problem of calculating probabilities for "anomalies" *a posteriori*. The expected number of events in any one channel from SUSY is usually small with the present integrated luminosity. New physics will most likely show up as a few events on the tails of SM distributions. Since there are many potential SUSY signatures, one can only follow a strategy of systematically analyzing *all* high–mass channels and looking for discrepancies on the tails of distributions. The single events such as the "$ee\gamma\gamma\not\!\!E_T$" event have been useful as "guideposts" indicating promising new channels, such as the $\gamma bj\not\!\!E_T$ channel described above. It is still possible that a sensible picture of these events will emerge from the Run I data when a complete survey of all channels is completed using both detectors. At the very least, this is an important exercise for preparing the Run II analyses.

---

[a] This analysis predates LEP results which exclude this example.

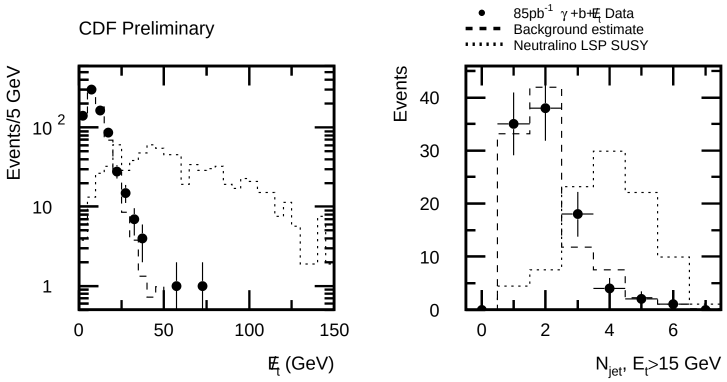

Figure 19: CDF results for the $\not\!\!E_T$ (left) and the jet multiplicity with $E_T > 15$ GeV (right) in events with a photon and a SVX b–tag. The search is for the signature $b\gamma\not\!\!E_T$ in a scenario where $\widetilde{\chi}^0_2 \rightarrow \gamma\widetilde{\chi}^0_1$ and the stop is light. The jet multiplicity histogram is made by requiring $\not\!\!E_T$>20 GeV. The SUSY model is normalized to the area of the data histogram – this is scaling by a factor of 100 for the $\not\!\!E_T$ histogram and a factor of 10 for the $n_{\rm jet}$ histogram. The SUSY model has a Higgsino LSP [118] generated with `PYTHIA` 6.1.

Top Dilepton Events

As discussed earlier, the signature of dileptons+2 jets+$\not\!\!E_T$ is a promising SUSY search channel (see Sec. 32). However, such events would also be a background to the SM top quark search using dileptons. The consistency of this dilepton sample with that expected from $t\bar{t}$ production has been the subject of intense investigation.[121] There are a number of peculiarities, none by themselves statistically significant at a level required to claim new physics. However, there are several events that have low probabilities of being from top decay or any other SM process.[122] Such events should be taken seriously as potential SUSY candidates.

The most interesting of the anomalous CDF events[106,88] is Event 129896 of Run 67581, which has *three*, clean, isolated, high–p_T leptons, large $\not\!\!E_T$, and a high–E_T jet. In addition, the most energetic of the leptons is a positron with $E_T \simeq 200$ GeV, significantly larger than is typical for top events (0.06 ± 0.02 events are expected). The corrected $\not\!\!E_T$ is over 100 GeV, also large for top decay (0.6 ± 0.1 events are expected). The event contains a jet with $E_T \simeq$ 100 GeV; the total transverse energy plus $\not\!\!E_T$ is about 450 GeV. The other two leptons are an electron with $E_T = 27$ GeV and a muon (μ^-) with $p_T = 27$

GeV/c. The invariant mass of the e^+e^- pair is 130 GeV, well away from M_Z; the pair has very high p_T. In the SM top quark analysis, the event is classified as a dilepton+2 jet event, because the lower E_T electron fails the fiducial cut by 4 mm and is thus defined to be a jet; however, the electron passes all other standard electron criteria and is a "golden" electron in all other ways.[a] The kinematics of the event are unusual: the invariant mass $M_{e\mu j}$ is on the order of m_t, while the other hemisphere contains only the high–E_T positron. The three isolated leptons and the kinematics make the event unlikely to come from SM top production and decay. The event is a high–mass trilepton $+\not{E}_T$ event, and is consequently a good SUSY candidate.[122]

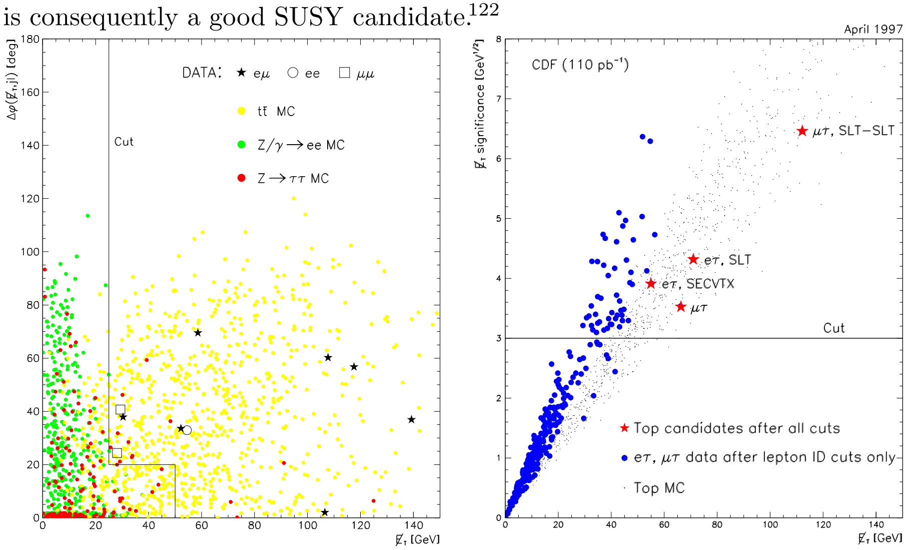

Figure 20: (Left) Scatterplot of the angle $\Delta\phi(\not{E}_T,\ell j)$ between the corrected $\not{E}_T$ and the closest lepton or jet versus corrected $\not{E}_T$ for the ee, $\mu\mu$, and $e\mu$ candidate events, compared with the expected distributions for $t\bar{t}$ and background. Background and top contributions are *not* normalized to the expected number of events. (Right) The distribution of $\not{E}_T$ significance versus $\not{E}_T$ for events with a primary lepton and a tau candidate (the slope of the data and background is different, because the background is dominated by QCD) in the CDF data compared with the $t\bar{t}$ Monte Carlo. Three of the four final candidate events (stars) have b–tagged jets.

Other discrepancies in the top dilepton sample involve the kinematics. Some of the anomalous behavior in the kinematics can be seen in Fig. 20 (left), which shows $\not{E}_T$ versus $\Delta\phi$ between the $\not{E}_T$ and the nearest jet or lepton.[88,123] Also shown is the distribution expected from Monte Carlo $t\bar{t}$ events, but corresponding to 100 times the luminosity. There are several events out in regions less populated by top quark events (one is the trilepton event). Figure 20 (right) shows the distribution in $\not{E}_T$ significance[88] vs $\not{E}_T$ for the CDF tau–lepton top sample. None of these latter discrepancies is at a statistical level that is significant; these will be channels of great interest in Run II.

---

[a] In the top quark analysis the fiducial volume was conservatively chosen to be the same as for the precision electroweak measurement of the ratio of W to Z cross sections. The 4 mm miss does not affect the electron identification.

5 Conclusions

As can be seen from Table 1, there has been a large effort in SUSY searches at the Tevatron. However, given the wide range of possible experimental signatures in the minimal Supersymmetric extension of the Standard Model, there is still work in progress and much to be done. Many Run I analyses are under way.

Our quantitative conclusions on Run I are reflected in the Figures and Tables of this review; here we will add a few more general qualitative observations:

1. A systematic exploration of signatures and channels is just starting. In addition, the detectors have not yet been exploited fully; for example, better c–tagging and dijet resolution to investigate final states with reconstructed W and Z bosons may be possible. These tools will allow the study of new channels.

2. There are some events involving leptons and/or photons that are provocative, and can be "guideposts" for Run II and further Run I analyses.

3. There is a substantial need for theorists and experimentalists to work together to understand better how to derive and present limits from the Tevatron. We should move on parallel paths toward more "model–independent" predictions and limits (*e.g.* presenting plots of cross section versus experimentally measured quantities like thresholds), and confront specific models in ways that allow the two experiments to compare their results.

4. The analyses so far are luminosity limited: the reach of the searches is just entering the interesting regions.

In Run II, two upgraded detectors at the Tevatron will collect more data at a higher energy of 2 TeV. The nominal integrated luminosity is 2 fb^{-1}, with a possible extension to 10 or even 30 fb^{-1}. The production cross sections for heavy sparticles will increase significantly with the higher energy. Chargino and neutralino searches, as well as squark and gluino searches, will cover a wide range of SUSY parameter space in Run II. Most importantly, by extending

Run II up to an integrated luminosity of about 20 fb^{-1} and combining search channels, the Tevatron can perform a crucial test of the MSSM Higgs boson sector.

The experience gained from Run I analyses will greatly increase the quality of the Run II searches.[124,125] New triggering capabilities will open up previously inaccessible channels, particularly those involving τ's and heavy flavor. Increased b–tagging efficiency and $\not\!\!E_T$ resolution will enhance many analyses. A factor of 20 or more data combined with improved detector capabilities makes the next Run at the Tevatron an exciting prospect.

Acknowledgments

The authors would like to thank the following people for useful discussions and comments:

Howard Baer, Andy Beretvas, Jeff Berryhill, Brendan Bevensee, Sue Blessing, Amber Boehnlein, Dhiman Chakraborty, Piotr Chankowski, Max Chertok, Dan Claes, Regina Demina, James Done, Eric Flattum, Carla Grosso–Pilcher, John Hobbs, Marcus Hohlmann, Teruki Kamon, Stefan Lammel, Adam Lyon, Doug Norman, Marc Paterno, Stefan Pokorski, Jianming Qian, Aurore Savoy-Navarro, H.C. Shankar, Michael Spira, David Stuart, Benn Tannenbaum, Xerxes Tata, Dave Toback, Carlos Wagner, Noah Whiteman, Peter Wilson and Peter Zerwas.

Part of this manuscript was completed at the Aspen Center for Physics.

References

1. S. Glashow, Nucl. Phys. **20**, 579 (1961); A. Salam, *Elementary Particle Theory*, ed. N. Svartholm, 367 (1968); S. Weinberg, Phys. Rev. Lett. **19**, 1264 (1967).
2. F. Abe, *et al.*, (CDF), Phys. Rev. **D50**, 2966 (1994) and Phys. Rev. Lett. **74**, 2626 (1995); S. Abachi, *et al.*, (DØ), Phys. Rev. Lett. **74**, 2632 (1995).
3. P.W. Higgs, Phys. Rev. Lett. **12**, 132 (1964) and Phys. Rev. **145**, 1156 (1966); F. Englert and R. Brout, Phys. Rev. Lett. **13**, 321 (1964); G.S. Guralnik, C.R. Hagen and T.W. Kibble, Phys. Rev. Lett. **13**, 585 (1964).
4. K. Wilson, as quoted by L. Susskind, Phys. Rev. **D20**, 2619 (1979); G. 't Hooft, in *Recent Developments in Gauge Theories*, eds. G. 't Hooft, *et al.*, (Plenum Press, New York, 1980); L. Maiani, in *Proceedings of the Gif-sur-Yvette Summer School*, edited by R. Barloutand, J.F. Cavaignac,

and D. Nanopoulos (Natl. Inst. Nucl. Phys., Paris, 1980); M. Veltman, Acta Phys. Polon. **12B**, 473 (1981).

5. Y. Gol'fand and E. Likhtam, JETP Lett. **13**, 323 (1971); P. Ramond, Phys. Rev. **D3**, 2415 (1971); A. Neveu and J.H. Schwarz, Nucl. Phys. **B31**, 86 (1971); J.L. Gervais and B. Sakita, Nucl. Phys. **B34**, 632 (1971); D. Volkov and V. Akulov, Phys. Lett. **B46**, 109 (1973); J. Wess and B. Zumino, Nucl. Phys. **B78**, 39 (1974).
6. J. Wess and J. Bagger, *Supersymmetry and Supergravity* (Princeton University Press, Princeton, N.J., 1983); H.–P. Nilles, Phys. Rep. **110**, 1 (1984); H. E. Haber and G. L. Kane, Phys. Rep. **117**, 75 (1985); R. Barbieri, Riv. Nuovo Cim. **11**, 1 (1988); R. Arnowitt, A Chamseddine and P. Nath, *Applied N=1 Supergravity* (World Scientific, Singapore, 1984); P. West, *Introduction to Supersymmetry and Supergravity* (World Scientific, Singapore, 1986); R. Mohapatra, *Unification and Supersymmetry* (Springer–Verlag, Berlin, 1986).
7. For those experimentalists just beginning on SUSY, we recommend: S. Dawson, *SUSY and Such*, lectures given at the NATO Advanced Study Institute on Techniques and Concepts of High Energy Physics, July 11–22, 1996, St. Croix, Virgin Islands, hep–ph/9612229; X. Tata, *QCD and Beyond*, ed. D.E. Soper, 163 (World Scientific, Singapore, 1996), hep–ph/9510287, and Ref. 3 therein; X. Tata, *What is Supersymmetry and How Do We Find It?*, lectures given at the 9th Jorge Andre Swieca Summer School, Feb. 16–28, 1997, Sao Paulo, Brazil, hep–ph/9706307.
   Intended for theorists: M. Dine, *Supersymmetry Phenomenology (with a Broad Brush)* , lectures given at TASI '96, hep–ph/9612389; J. Lykken, *Introduction to SUSY*, lectures given at TASI '96, hep–ph/9612114; J. Bagger, *QCD and Beyond*, ed. D.E. Soper, 109 (World Scientific, Singapore, 1996), hep–ph/9604232.
8. J. Wess and B. Zumino, Phys. Lett. **49B**, 52 (1974); J. Iliopoulos and B. Zumino, Nucl. Phys. **B76**, 310 (1974); S. Ferrara, J. Iliopoulos and B. Zumino, Nucl. Phys. **B77**, 413 (1974); E. Witten, Nucl. Phys **B188** 513 (1981).
9. J. Ellis, E. Enqvist, D.V. Nanopoulos and F. Zwirner, Mod. Phys. Lett. **A1**, 57 (1986); R. Barbieri and G.F. Giudice, Nucl. Phys. **B306**, 63 (1988); G. Anderson, D. Castaño and A. Riotto, Phys. Rev. **D55**, 2950 (1997).
10. S. Dawson, E. Eichten and C. Quigg, Phys. Rev **D31**, 1581 (1985), and references on particular signatures given afterwards in this chapter.
11. M. Carena, J.R. Espinosa, M. Quirós and C.E.M. Wagner, Phys. Lett. **B335**, 209 (1995); M. Carena, M. Quirós and C.E.M. Wagner, Nucl.

Phys. **B461**, 407 (1996); H. Haber, R. Hempfling and H. Hoang, Z. Phys. **75**, 539 (1997); M. Carena, P. Zerwas and the Higgs Physics Working Group, *Physics at LEP2*, Vol. 1, eds. G. Altarelli, T. Sjöstrand and F. Zwirner, CERN Report No. 96–01.

12. A. Stange, W. Marciano and S. Willenbrook, Phys. Rev. **D49**, 1354 (1994) and Phys. Rev. **D50**, 4491 (1994); J. Dai J. Gunion and R, Vega, Phys. Rev. Lett **71**, 2699 (1993); Report of the TeV 2000 Study Group: Light Higgs Physics, FERMILAB–PUB–96/046; W.M. Yao, FERMILAB–CONF–96–383–E, 1996 Snowmass proceedings; S. Kim, S. Kuhlmann and W.M. Yao, 1996 Snowmass proceedings.
13. S. Mrenna and G.L. Kane, hep–ph/9406337; S. Mrenna, in *Perspectives on Higgs Physics*, edited by G.L. Kane (World Scientific, Singapore, 1997).
14. John Peoples, letter of January, 1996.
15. S. Dimopoulos and H. Georgi, Nucl. Phys. **B193**, 150 (1981); S. Dimopoulos, S. Raby and F. Wilczek, Phys. Rev. **D24**, 1681 (1981); L. Ibañez and G.G. Ross, Phys. Lett. **B105**, 439 (1981).
16. J. Ellis, S. Kelley and D.V. Nanopoulos, Phys. Lett. **B260**, 131 (1991); P. Langacker and M.X. Luo, Phys. Rev. **D44**, 817 (1991); U. Amaldi, W. de Boer and H. Fürstenau, Phys. Lett. **B260**, 447 (1991); F. Anselmo, L. Cifarelli, A. Peterman and A. Zichichi, Nuovo Cim. **104A**, 1817 (1991); P. Langacker and N. Polonsky, Phys. Rev. **D47**, 4028 (1993); A. Faraggi and B. Grinstein, Nucl. Phys. **B422**, 3 (1994); J. Bagger, K. Matchev and D. Pierce, Phys. Lett. **B348**, 443 (1995); R. Barbieri, M. Ciafaloni and A. Strumia, Nucl. Phys. **B442**, 461 (1995); M. Bastero–Gil and J. Perez Mercader, Nucl. Phys. **B450**, 21 (1995); P. Chankowski, Z. Pluciennik and S. Pokorski, Nucl. Phys. **B439**, 23 (1995); P. Chankowski, Z. Pluciennik, S. Pokorski, and C. Vayonakis, Phys. Lett. **B358**, 264 (1995); P. Langacker and N. Polonsky, Phys. Rev. **D52**, 3082 (1995).
17. M. Carena, S. Pokorski and C.E.M. Wagner, Nucl. Phys. **B406** 59 (1993).
18. P. Fayet, Nucl. Phys. **B90**, 104 (1975).
19. See J.F. Gunion, H.E. Haber, G.L. Kane and S. Dawson, *The Higgs Hunter's Guide* (Addison–Wesley, Reading, MA, 1990).
20. Y. Okada, M. Yamaguchi and T. Yanagida, Prog. Theor. Phys **85**, 1 (1991); H. Haber and R. Hempfling, Phys. Rev. Lett. **66**, 1815 (1991); J. Ellis, G. Ridolfi and F. Zwirner, Phys. Lett. **B257**, 83 (1991) and Phys. Lett. **B262**, 477 (1991); R. Barbieri, M. Frigeni and F. Caravaglios, Phys. Lett. **B258**, 167 (1991); Y. Okada, M. Yamaguchi and T. Yanagida, Phys. Lett. **B262**, 54 (1991); A. Brignole, J. Ellis,

G. Ridolfi and F. Zwirner, Phys. Lett. **B271**, 123 (1991); M. Dress and M. Noijiri, Phys. Rev. **D45**, 2482 (1992); R. Hempfling and A. Hoang, Phys. Lett. **B331**, 99 (1994); J. Kodaira, Y. Yasui and K. Sasaki, Phys. Rev. **D50**, 7035 (1994); J.A. Casas, J.R. Espinosa, M. Quirós and A. Riotto, Nucl. Phys., **B436**, 3 (1995).

21. G. Farrar and P. Fayet, Phys. Lett **B 76**, 575 (1978).
22. L. Alvarez-Guamé, J. Polchinski and M.B. Wise, Nucl. Phys. **B221**, 495 (1983); J. Bagger, S. Dimopoulos and E. Masso, Phys. Rev. Lett. **55**, 920 (1985).
23. W.A. Bardeen, M. Carena, T. Clark, K. Sasaki and C.E.M. Wagner, Nucl. Phys. **B396**, 33 (1992).
24. V. Barger, M.S. Berger and P. Ohmann, Phys. Rev. **D 47**, 1093 (1993); P. Langacker and N. Polonsky, Phys. Rev. **D49**, 1454 (1994); W.A. Bardeen, M. Carena, S. Pokorski and C.E.M. Wagner, Phys. Lett. **320B**, 110 (1994).
25. L. Hall, R. Rattazzi and U. Sarid, Phys. Rev. **D50**, 7048 (1994).
    R. Hempfling, Phys. Rev. **D49**, 6168 (1994).
26. M. Carena, M. Olechowski, S. Pokorski and C.E.M. Wagner, Nucl. Phys. **B426**, 269 (1994).
27. C.T. Hill, Phys. Rev. **D24**, 691 (1981); C.T. Hill, C. Leung and S. Rao, Nucl. Phys. **B262**, 517 (1985).
28. M. Carena, M. Olechowski, S. Pokorski and C.E.M. Wagner, Nucl. Phys. **B419**, 213 (1994); M. Carena, P. Chankowski, M. Olechowski, S. Pokorski and C.E.M. Wagner, Nucl. Phys. **B491**, 103 (1997).
29. M. Carena and C.E.M. Wagner, Proceedings of the 2nd IFT Workshop on Yukawa Couplings and the Origins of Mass, Gainesville, 1994, hep–ph/9407208; Nucl. Phys. **B452**, 45 (1995).
30. M. Drees and S. P. Martin, Report of Subgroup 2 of the DPF Working Group on Electroweak Symmetry Breaking and Beyond the Standard Model, hep–ph/9504324.
31. A. Pomarol and N. Polonsky, Phys. Rev. Lett. **73**, 2292 (1994); M. Olechowski and S. Pokorski, Phys. Lett. **B344**, 201 (1995); D. Matalliotakis and H.P. Nilles, Nucl. Phys. **B435**, 115 (1995); M. Carena and C.E.M. Wagner, Proceedings of the 2nd IFT Workshop on Yukawa Couplings and the Origins of Mass, Gainesville 1994, hep–ph/9407209.
32. R. Barbieri and L. Maiani, Nucl. Phys. **B243**, 129 (1989).
    R. Barbieri, N. Cabbibo, L. Maiani and S. Petrarca, Phys. Lett. **B127**, 458 (1983).
33. G.R. Farrar and A. Masiero, hep–ph/9410401.
    G.R. Farrar, hep–ph/9508291.

34. G.R. Farrar, hep–ph/9710277, and references therein.
ALEPH Collaboration note, CERN–PPE/97–002.
35. See, for example, C. Kolda, in *Proceedings of the 5th International Conference on SuperSymmetries in Physics*, to be published in Nucl. Phys. **B**, hep–ph/9707450.
36. M. Dine, A.E. Nelson and Y. Shirman, Phys. Rev. **D51**, 1362 (1995) and Phys. Rev. **D53**, 2658 (1995).
37. S. Raby, Phys. Rev. **D56**, 2852 (1997).
38. M. Diaz, talk presented at the International Europhysics Conference on High-Energy Physics (HEP 97), Jerusalem, Israel, hep–ph/9712213; talk given at International Workshop on Quantum Effects in the Minimal Supersymmetric Standard Model, Barcelona, Spain, hep–ph/9711435 and references therein; M. Carena, S. Pokorski and C.E.M. Wagner, in preparation.
39. H. Dreiner, An introduction to Explicit R–parity Violation, to be published in *Perspectives on Supersymmetry*, ed. G.L. Kane, (World Scientific, Singapore, 1997), hep–ph 9707435 and references therein; G. Bhattacharyya, A Brief Review on R–Parity–Violating couplings, invited talk at Beyond the Desert, Castle Ringberg, Tengernsee, Germany, June 1997, hep–ph/9709395.
40. G.R. Farrar and P. Fayet, Phys. Lett. **B76**, 575 (1978).
G.R. Farrar, Phys. Rev. Lett. **53**, 1029 (1984).
41. F. Abe, *et al.*, (CDF), Nucl. Instrum. Meth. **A271**, 387 (1988).
42. S. Abachi, *et al.*, (DØ), Nucl. Instrum. Meth. **A338**, 185 (1994), and references therein.
43. D. Amidei, *et al.*, (CDF), Nucl. Instrum. Meth. **A350**, 73 (1994).
44. B. Flaugher and K. Meier, Proceedings of the 1990 Summer Study on High Energy Physics, ed. E.L. Berger, 129 (World Scientific, Singapore, 1990).
45. F. Abe, *et al.*, (CDF), Phys. Rev. Lett. **75**, 11 (1994).
46. F. Abe, *et al.*, (CDF), Phys. Rev. **D45**, 1448 (1992).
47. F. Abe, *et al.*, (CDF), Phys. Rev. **D50**, 2996 (1994).
48. Q. Zhu, Ph. D. thesis, New York University, 1994.
49. S. Abachi, *et al.*, (DØ), Phys. Lett. **B357**, 500 (1995).
50. S. Abachi, *et al.*, (DØ), Phys. Rev. **D52**, 4877 (1995).
51. F. Paige and S.D. Protopopescu, *Supercollider Physics*, ed. D. Soper, 41 (World Scientific, 1986); H. Baer, F. Paige, S. Protopopescu and X. Tata, in *Proceedings of the Workshop on Physics at Current Accelerators* and Brookhaven National Laboratory report No. 38304, 1986 (unpublished).
52. T. Sjöstrand, Comput. Phys. Commun. **82**, 74 (1994).

S. Mrenna, Comput. Phys. Commun. **101**, 232 (1997).
53. H. Baer, X. Tata and J. Woodside, Phys. Rev. **D44**, 207 (1991), Phys. Rev. **D41**,906 (1990), and Phys. Rev. Lett. **63**, 352 (1989).
54. H. Baer, K. Hagiwara and X. Tata, Phys. Rev. **D35**, 1598 (1987).
P. Nath and R. Arnowitt, Mod. Phys Lett **A2**, 331 (1987).
55. V. Barger, Y. Keung and R. J. Phillips, Phys. Rev. Lett. **55**, 166 (1985).
R. M. Barnett, J. Gunion and H. Haber, Phys. Lett. **B 315**, 349 (1993).
H. Baer, C. Kao and X. Tata, Phys. Rev. **D48**, 2978 (1993).
56. R. Barbieri, F. Caravaglios, M. Frigeni and M. Mangano, Nucl. Phys. **B367**, 28 (1991); J. Lopez, D. Nanopoulos, X. Wang and A. Zichichi, Phys. Rev. **D48**, 2062 (1993) and Phys. Rev. **D52**, 142 (1995); J. Lopez, D. Nanopoulos, G. Park, X. Wang and A. Zichichi, Phys. Rev. **D50**, 2164 (1994); T. Kamon, J. Lopez, P. McIntyre and J. T. White, Phys. Rev. **D50**, 5676 (1994); E. Diehl, C. Kolda, G. L. Kane and J. D. Wells, Phys. Rev. **D52**, 4223 (1995); H. Baer, C. Kao and X. Tata, Phys. Rev. **D48**, 5175 (1993).
57. H. Baer and X. Tata, Phys. Rev. **D47**, 2739 (1993).
58. H. Baer, C. Chen, C. Kao and X. Tata Phys. Rev. **D52**, 1565 (1995).
H. Baer, C. Chen, F. Paige and X. Tata, Phys. Rev. **D54**, 5866 (1996).
59. H. Baer, *et al.*, Phys. Rev. Lett. **79**, 986 (1997).
60. F. Abe, *et al.*, (CDF), Phys. Rev. Lett. **76**, 4307 (1996).
61. B. Bevensee, (CDF), *Proceedings of The International Workshop on Quantum Effects in the MSSM*, (Barcelona, Spain, 1997), FERMILAB–CONF–97/405–E.
62. S. Abachi, *et al.*, (DØ), Phys. Rev. Lett. **76**, 2228 (1996).
63. B. Abbott, *et al.*, (DØ), submitted to Phys. Rev. Lett., FERMILAB PUB–97/201–E, hep–ex/9705015.
64. S. Mrenna, G.L. Kane, G.D. Kribs and J.D. Wells, Phys. Rev. **D53**, 1168 (1996).
65. W. Beenakker, R. Hopker, M. Spira and P.M. Zerwas, Z. Phys. **C69**, 163 (1995), Phys. Rev. Lett. **74** 2905 (1995), and Nucl. Phys. **B492**, 51 (1997); W. Beenaker, R. Hopker, and M. Spira, hep–ph/9611232.
66. M. Misiak, S. Pokorski, J. Rosiek, hep–ph/9703442, to appear in the Review Volume *Heavy Flavors II*, eds. A.J. Buras and M. Lindner, (Advanced Series on Directions in High-Energy Physics, World Scientific, Singapore).
67. S. Abachi, *et al.*, (DØ), Phys. Rev. Lett. **75**, 618 (1995).
68. F. Abe, *et al.*, (CDF), Phys. Rev. **D56**, 1357 (1997).
69. S. Abachi *et al.*, (DØ), FERMILAB–CONF–97/357–E.
70. F.A. Berends, H. Kuijf, B. Tausk and W.T. Giele, Nucl. Phys. **B357**,

32 (1991).
71. G. Marchesini and B. R. Webber, Nucl. Phys. **B238**, 1 (1984) and Nucl. Phys. **B310**, 461 (1988).
72. R. Brun and F. Carminati, CERN Program Library Long Writeup W5013, 1993 (unpublished).
73. S. Abachi, *et al.*, (DØ), *Proceedings of the* 28th *International Conference on High Energy Physics*, eds. Z. Ajduk and A. K. Wroblewski (World Scientific, Singapore, 1997), FERMILAB–CONF–96/427–E.
74. F. Abe, *et al.*, (CDF), Phys. Rev. Lett. **76**, 2006 (1996).
75. J. Done, (CDF), *Proceedings of 1996 Divisional Meeting of the Division of Particles and Fields*, (DPF '96 Minneapolis, MN, 1996), FERMILAB–CONF–96/371–E.
76. H. Baer, M. Drees, R. Godbole, J. Gunion and X. Tata, Phys. Rev. **D44**, 725 (1991).
77. H. Baer, J. Sender and X. Tata, Phys. Rev. **D50**, 4517 (1994).
78. W. Beenakker, M. Kramer, T. Plehn, M. Spira and P.M. Zerwas, DESY–97–214, CERN–TH/97–177, RAL–TR–97-056, hep–ph/9710451.
79. S. Abachi, *et al.*, (DØ), Phys. Rev. Lett. **76**, 2222 (1996).
80. P. Azzi, (CDF), *Proceedings of XXXII Rencontres de Moriond, QCD and High Energy Hadronic Interactions*, Les Arcs, France, 1997, FERMILAB–CONF–97/148–E (to be published).
81. S. Abachi, *et al.*, (DØ), FERMILAB–PUB–96/449–E, hep–ex/9612009.
82. P.J. Wilson, (CDF), *Proceedings of Les Rencontres de Physique de La Vallee D'Aosta,* La Thuile, Italy, 1997, FERMILAB–CONF–97–241–E (to be published).
83. H. Baer, C. Chen, F. Paige and X. Tata, Phys. Rev. **D49**, 3283 (1994).
84. F. Abe, *et al.*, (CDF), Phys. Rev. **D52**, 2624 (1995).
85. R.M. Godbole and D.P. Roy, Phys. Rev. **D43**, 3640 (1991).
    M. Guchait and D.P. Roy, Phys. Rev. **D55**, 7263 (1997).
86. F. Abe, *et al.*, (CDF), Phys. Rev. Lett. **72**, 1977 (1994); see also C. Jessop, Ph.D thesis, Harvard University, 1994. This analysis uses 4.2 pb^{-1} from the 1989 run and a signature of a hadronically–decaying $\tau + \geq 1$ jet $+\not{E}_T$.
87. F. Abe, *et al.*, (CDF), Phys. Rev. **D54**, 357 (1997).
88. M. Hohlmann, Ph.D. Thesis, Univ. of Chicago, 1997.
89. M. Gallinaro, Ph.D. Thesis, University of Rome, 1996.
90. S. Abachi, *et al.*, (DØ), FERMILAB–CONF–97/386–E.
91. J. Gausch, R. Jimenez and J. Sola, Phys. Lett. **B360**, 47 (1995); J. Coarasa, D. Garcia, J. Guasch, R. Jimenez, J. Sola, to appear in Z. Phys. **C**; J. Guasch and J. Sola, to appear in Phys. Lett. **B**, hep–ph/9707535;

J. Sola, hep–ph/9708494.

92. A. Stange, W. Marciano and S. Willenbrock, Phys. Rev. **D50**, 4491 (1994).
93. J. Dai, J. F. Gunion and R. Vega, Phys. Lett. **B387** 801 (1996).
94. S. Abachi, *et al.*, (DØ), *Proceedings of the* 28^{th} *International Conference on High Energy Physics*, eds. Z. Ajduk and A. K. Wroblewski (World Scientific, Singapore, 1997), FERMILAB–CONF–96/427–E.
95. F. Abe, *et al.*, (CDF), submitted to Phys. Rev. Lett., FERMILAB–PUB–97–247–E.
96. J. A. Valls, (CDF), *Proceedings 32nd Rencontres de Moriond*, Les Arcs, France, March, 1997, FERMILAB–CONF–97/135–E.
97. S. Abachi, *et al.*, (DØ), FERMILAB–CONF–97/325–E.
98. A. Stange, W. Marciano and S. Willenbrock, Phys. Rev. **D49**, 2 (1994).
99. F. Abe, *et al.*, (CDF), Phys. Rev. **D54**, 735 (1996). This analysis uses 18.7 pb^{-1} from Run Ia and a signature of a hadronically–decaying $\tau + \geq 1$ jet $+\not\!\!E_T$.
100. F. Abe, *et al.*, (CDF), Phys. Rev. Lett. **73**, 2667 (1994); J. Wang, Ph.D thesis, University of Chicago, 1994. This analysis uses 19.3 $\mathrm{pb}^{-1}$from Run Ia and a signature of two leptons + $\not\!\!E_T$.
101. S. Abachi, *et al.*, (DØ), FERMILAB–CONF–97/325–E.
102. K. Maeshima, (CDF), *Proceedings of the 28th International Conference on High Energy Physics*, eds. Z. Ajduk and A. K. Wroblewski (World Scientific, Singapore, 1997), FERMILAB–CONF–96–412–E.
103. S. Dimopoulos, R. Esmailzadeh, L.J. Hall and G.D. Starkman, Phys. Rev. **D41**, 2099 (1990); H. Dreiner and G. Ross, Nucl. Phys. **B365**, 597 (1991); D. P. Roy, Phys. Lett. **B283**, 270 (1992); V. Barger, M. Berger and P. Ohmann, Phys. Rev. **D50**, 4299 (1994); H. Baer, C. Kao and X. Tata, Phys. Rev. **D51**, 2180 (1995); M. Guchait and D.P. Roy, Phys. Rev. **D54**, 3276 (1996); J. Kalinowski, R. Ruckl, H. Spiesberger and P.M. Zerwas, hep–ph/9708272.
104. X. Wu, (CDF), talk at International Europhysics Conference on High Energy Physics, Jerusalem, Israel, 1997.
105. D. Choudhury and S. Raychaudhuri, Phys. Rev. **D56**, 1778 (1997).
106. S. Park, (CDF), *Proceedings of the 10th Topical Workshop on Proton–Antiproton Collider Physics*, eds. R. Raja and J. Yoh, (AIP Press, Woodbury, NY, 1996).
107. G. Bhattacharyya and R.N. Mohapatra, Phys. Rev. **D54**, 4204 (1996). J. L. Rosner, Phys. Rev. **D55**, 3143 (1997).
108. S. Dimopoulos, M. Dine, S. Raby and S. Thomas, Phys. Rev. Lett. **76**, 3494 (1996) and Phys. Rev. **D55**, 1372 (1997).

109. S. Ambrosanio, G.L. Kane, G.D. Kribs, S.P. Martin and S. Mrenna, Phys. Rev. Lett. **76**, 3498 (1996).
110. S. Dimopoulos, S. Thomas and J. Wells, Phys. Rev. **D54**, 3283 (1996) and Nucl. Phys. **B488**, 39 (1997).
111. S. Dimopoulos, M. Dine, S. Raby, S. Thomas and J. Wells, Nucl. Phys. Proc. Suppl. **A52**, 38 (1997).
112. D. Dicus, B. Dutta and S. Nandi, Phys. Rev. Lett. **78**, 3055 (1997) and Phys. Rev. **D56**, 5748 (1997).
113. J. Ellis, J.L. Lopez and D.V. Nanopoulos, Phys. Lett. **B394**, 354 (1997).
114. P. Fayet, Phys. Lett. **B70**, 461 (1977); P. Fayet, Phys. Lett. **B84**, 416 (1979); R. Casalbuoni, S. de Curtis, D. Dominici, F. Feruglio and R. Gatto, Phys. Lett. **B215**, 313 (1988).
115. S. Ambrosanio, G.L. Kane, G.D. Kribs, S.P. Martin and S. Mrenna, Phys. Rev. **D54**, 5395 (1996).
116. H. Baer, M. Brhlik, C–H. Chen and X. Tata, Phys. Rev. **D55**, 4463 (1997).
117. H.E. Haber, G.L. Kane and M. Quiros, Phys. Lett. **B160**, 297 (1985) and Nucl. Phys. **B273**, 333 (1986).
118. S. Mrenna and G.L. Kane, Phys. Rev. Lett. **77**, 3502 (1996).
119. R.L. Culbertson, (CDF and DØ), to be published in Nucl. Phys. **B**, *Proceedings of the 5th International Conference on Supersymmetries in Physics* (SUSY '97), Philadelphia, PA, 1997, FERMILAB–CONF–97–277–E.
120. S. Abachi, *et al.*, (DØ), submitted to Phys. Rev. Lett., FERMILAB–PUB–97/273–E.
121. The CDF Collaboration, private communication.
122. This is well–documented inside CDF. Also see R.M. Barnett and L.J. Hall, Phys. Rev. Lett. **77**, 3506 (1996).
123. F. Abe, *et al.*, (CDF), to be published in Phys. Rev. Lett., FERMILAB–PUB–97/096–E, hep-ex/9704007.
124. D. Amidei, *et al.*, *Future Electroweak Physics at the Fermilab Tevatron: Report of the TeV-2000 Study Group*, FERMILAB–PUB–96–082.
125. J. Amundson, *et al.*, *Report of the Supersymmetry Theory Subgroup* in *New Directions for High-Energy Physics*, eds. D. Cassel, L. Gennari and R. Siemann, 644 (SLAC, Stanford, 1997).

A Appendix A

A.1 Typical Decay Modes of Supersymmetric Particles.

Table 18: Typical final states from sparticle decay, assuming $\widetilde{\chi}^0, \widetilde{\chi}^\pm, \tilde{\ell}, \tilde{\nu} < \widetilde{Q}(\neq \tilde{t}, \tilde{b}), \tilde{g}$. HLSP denotes models with a Higgsino LSP and GLSP denotes models with a Gravitino LSP. Event signatures from sparticle pair production can be constructed by combining two decays.

Particle	Intermediate State	Final State	Comment
$\widetilde{\chi}_i^0$		$\rightarrow \not{E}_T$	
		$\rightarrow \ell\bar{\ell}\ \not{E}_T$	
		$\rightarrow jj\ \not{E}_T$	
		$\rightarrow \gamma\ \not{E}_T$	HLSP, GLSP
	$\rightarrow t\tilde{t}^*$	$\rightarrow bW\bar{c}\ \not{E}_T$	$m_{\tilde{t}} < m_b + M_{\widetilde{\chi}_1^\pm}$
	$\cdots$	$\rightarrow bW\bar{b}\ell\ \not{E}_T$	
	$\cdots$	$\rightarrow bW\bar{b}jj\ \not{E}_T$	
	$\rightarrow b\tilde{b}^*$	$\rightarrow b\bar{b}\ \not{E}_T$	
$\widetilde{\chi}_i^\pm$		$\rightarrow \ell\ \not{E}_T$	
		$\rightarrow jj\ \not{E}_T$	
		$\rightarrow \ell\gamma\ \not{E}_T$	HLSP, GLSP
		$\rightarrow jj\gamma\ \not{E}_T$	HLSP, GLSP
	$\rightarrow b\tilde{t}^*$	$\rightarrow b\bar{c}\ \not{E}_T$	$m_{\tilde{t}} < m_b + M_{\widetilde{\chi}_1^\pm}$
	$\cdots$	$\rightarrow b\bar{b}\ell\ \not{E}_T$	
	$\cdots$	$\rightarrow b\bar{b}jj\ \not{E}_T$	
	$\rightarrow t\tilde{b}^*$	$\rightarrow bW\bar{b}\ \not{E}_T$	
$\tilde{\ell}$	$\rightarrow \ell\widetilde{\chi}_1^0$	$\rightarrow \ell\ \not{E}_T$	
	$\rightarrow \ell\widetilde{\chi}_2^0$	$\rightarrow \ell\ \not{E}_T$	
	$\cdots$	$\rightarrow \ell\ell'\bar{\ell}'\ \not{E}_T$	
	$\cdots$	$\rightarrow \ell jj\ \not{E}_T$	
		$\rightarrow \ell\gamma\ \not{E}_T$	HLSP, GLSP
	$\rightarrow \nu\widetilde{\chi}_1^\pm$	$\rightarrow \ell\ \not{E}_T$	
	$\cdots$	$\rightarrow jj\ \not{E}_T$	
	$\cdots$	$\rightarrow b\bar{c}\ \not{E}_T$	$m_{\tilde{t}} < m_b + M_{\widetilde{\chi}_1^\pm}$

A.2 Typical Decay Modes of Supersymmetric Particles (continued,1).

Table 19: Typical final states from sparticle decays (continued,1).

Particle	Intermediate State	Final State	Comment
$\tilde{\nu}$	$\to \nu\widetilde{\chi}_1^0$	$\to \not\!\!E_T$	
	$\to \nu\widetilde{\chi}_2^0$	$\to \not\!\!E_T$	
	$\cdots$	$\to \ell^{'}\bar{\ell}^{'}\ \not\!\!E_T$	
	$\cdots$	$\to jj\ \not\!\!E_T$	
		$\to \gamma\ \not\!\!E_T$	HLSP, GLSP
	$\to \ell\widetilde{\chi}_1^{\pm}$	$\to \ell\bar{\ell}^{'}\ \not\!\!E_T$	
	$\cdots$	$\to \ell jj\ \not\!\!E_T$	
	$\cdots$	$\to \ell b\bar{c}\ \not\!\!E_T$	$m_{\tilde{t}} < m_b + M_{\widetilde{\chi}_1^{\pm}}$
$\tilde{t}$	$\to c\widetilde{\chi}_1^0$	$\to c\ \not\!\!E_T$	$m_{\tilde{t}} < m_b + M_{\widetilde{\chi}_1^{\pm}}$
	$\to b\widetilde{\chi}_1^{\pm}$	$\to b\ell\ \not\!\!E_T$	
	$\cdots$	$\to bjj\ \not\!\!E_T$	
	$\to t\widetilde{\chi}_1^0$	$\to bW\ \not\!\!E_T$	$M_{\tilde{t}} > m_t + M_{\widetilde{\chi}_1^0}$
	$\to \tilde{b}W$	$\to bW\ \not\!\!E_T$	
$\tilde{b}$	$\to b\widetilde{\chi}_1^0$	$\to b\ \not\!\!E_T$	
	$\to b\widetilde{\chi}_2^0$	$\to b\ \not\!\!E_T$	
	$\cdots$	$\to b\ell\bar{\ell}\ \not\!\!E_T$	
	$\cdots$	$\to bjj\ \not\!\!E_T$	
	$\to t\widetilde{\chi}_1^{\pm}$	$\to bW\ell\ \not\!\!E_T$	
	$\cdots$	$\to bWjj\ \not\!\!E_T$	
	$\cdots$	$\to bW\bar{b}c\ \not\!\!E_T$	$m_{\tilde{t}} < m_b + M_{\widetilde{\chi}_1^{\pm}}$
	$\to \tilde{t}W$	$\to cW\ \not\!\!E_T$	$m_{\tilde{t}} < m_b + M_{\widetilde{\chi}_1^{\pm}}$
	$\cdots$	$\to b\ell W\ \not\!\!E_T$	
	$\cdots$	$\to bjjW\ \not\!\!E_T$	

Table 20: Typical final states from sparticle decays (continued,2).

Particle	Intermediate State	Final State	Comment
$\widetilde{Q}$	$\to j\widetilde{\chi}_1^0$	$\to j \not\!\!E_T$	
	$\to j\widetilde{\chi}_2^0$	$\to j \not\!\!E_T$	
	$\cdots$	$\to j\ell\bar{\ell} \not\!\!E_T$	
	$\cdots$	$\to jjj \not\!\!E_T$	
	$\to j\widetilde{\chi}_1^\pm$	$\to j\ell \not\!\!E_T$	
	$\cdots$	$\to jjj \not\!\!E_T$	
	$\cdots$	$\to jb\bar{c} \not\!\!E_T$	$m_{\tilde{t}} < m_b + M_{\widetilde{\chi}_1^\pm}$
	$\to j\tilde{g}$	$\to jjj \not\!\!E_T$	
		$\to j\gamma \not\!\!E_T$	HLSP, GLSP
$\tilde{g}$	$\to j\widetilde{Q}$	$\to jj \not\!\!E_T$	
	$\to t\tilde{t}^*$	$\to bW\bar{c} \not\!\!E_T$	$m_{\tilde{t}} < m_b + M_{\widetilde{\chi}_1^\pm}$
	$\to b\tilde{b}^*$	$\to b\bar{b} \not\!\!E_T$	
	$\to jj\widetilde{\chi}_1^0$	$\to jj \not\!\!E_T$	
	$\to jj\widetilde{\chi}_2^0$	$\to jj \not\!\!E_T$	
	$\cdots$	$\to jj\ell\bar{\ell} \not\!\!E_T$	
	$\cdots$	$\to jjjj \not\!\!E_T$	
	$\to jj\widetilde{\chi}_1^\pm$	$\to jj\ell \not\!\!E_T$	
	$\cdots$	$\to jjjj \not\!\!E_T$	
	$\cdots$	$\to jjb\bar{c} \not\!\!E_T$	
	$\to t\bar{t}\widetilde{\chi}_1^0$	$\to bW\bar{b}W \not\!\!E_T$	
	$\to t\bar{b}\widetilde{\chi}_1^\pm$	$\to bW\bar{b}\ell \not\!\!E_T$	
	$\cdots$	$\to bW\bar{b}jj \not\!\!E_T$	

B Appendix B

B.1 Examples of Multijet Signatures for SUSY.

Table 21: Examples of R–Parity Conserving SUSY signatures at the Tevatron: Jets+$\not\!\!E_T$. Not all signatures are listed – we have (somewhat arbitrarily) restricted the list. We assume that the LSP is the $\widetilde{\chi}_1^0$. Note that $\widetilde{Q}$ decays give one or 3 jets, $\tilde{g}$ decays give 2,4, or 6 jets, and the $\widetilde{\chi}_i^\pm$, $\widetilde{\chi}_i^0$, $\tilde{\ell}$, and $\tilde{\nu}$ decays give an even number of jets.

R–Parity Conserving Signatures: Jets +$\not\!\!E_T$		
Signature	Production	Decay
$j\not\!\!E_T$	$\widetilde{Q}\widetilde{\chi}_1^0$	$\widetilde{Q} \rightarrow q\widetilde{\chi}_1^0$
$jj\not\!\!E_T$	$\widetilde{Q}\widetilde{Q}^*$	$\widetilde{Q} \rightarrow q\widetilde{\chi}_1^0$; $\widetilde{Q}^* \rightarrow \bar{q}\widetilde{\chi}_1^0$
	$\widetilde{\chi}_1^\pm\widetilde{\chi}_1^0$	$\widetilde{\chi}_1^\pm \rightarrow q\bar{q}\widetilde{\chi}_1^0$
	$\tilde{t}\tilde{t}^*$	$\tilde{t} \rightarrow c\widetilde{\chi}_1^0$
$jjj\not\!\!E_T$	$\widetilde{Q}\widetilde{\chi}_1^0$	$\widetilde{Q} \rightarrow q\widetilde{\chi}_1^\pm, \widetilde{\chi}_1^\pm \rightarrow q\bar{q}\widetilde{\chi}_1^0$
	$\widetilde{Q}\tilde{g}$	$\widetilde{Q} \rightarrow q\widetilde{\chi}_1^0; \tilde{g} \rightarrow q\bar{q}\widetilde{\chi}_1^0$
$jjjj\not\!\!E_T$	$\widetilde{Q}\widetilde{Q}^*$	$\widetilde{Q} \rightarrow q\widetilde{\chi}_1^0$; $\widetilde{Q}^* \rightarrow q\widetilde{\chi}_1^\pm \rightarrow q(q\bar{q}\widetilde{\chi}_1^0)$
	$\tilde{g}\tilde{g}$	$\tilde{g} \rightarrow q\bar{q}\widetilde{\chi}_1^0$
$5j\not\!\!E_T$	$\widetilde{Q}\tilde{g}$	$\widetilde{Q} \rightarrow q\widetilde{\chi}_1^\pm \rightarrow q(q\bar{q}\widetilde{\chi}_1^0)$; $\tilde{g} \rightarrow q\bar{q}\widetilde{\chi}_1^0$
$6j\not\!\!E_T$	$\widetilde{Q}\widetilde{Q}^*$	$\widetilde{Q} \rightarrow q\widetilde{\chi}_1^\pm \rightarrow q(q\bar{q}\widetilde{\chi}_1^0)$
	$\tilde{g}\tilde{g}$	$\tilde{g} \rightarrow q\bar{q}\widetilde{\chi}_1^0$; $\tilde{g} \rightarrow q\widetilde{Q} \rightarrow q(q\widetilde{\chi}_1^\pm \rightarrow q(q\bar{q}\widetilde{\chi}_1^0))$
$> 6j\not\!\!E_T$	$\widetilde{Q}\tilde{g}$	$\widetilde{Q} \rightarrow q\widetilde{\chi}_1^\pm \rightarrow q(q\bar{q}\widetilde{\chi}_1^0)$; $\tilde{g} \rightarrow q\widetilde{Q} \rightarrow q(q\widetilde{\chi}_1^\pm \rightarrow q(q\bar{q}\widetilde{\chi}_1^0))$
	$\tilde{g}\tilde{g}$	$\tilde{g} \rightarrow t\tilde{t} \rightarrow (Wb)(\widetilde{\chi}_1^\pm b) \rightarrow (jjb)(jjb\widetilde{\chi}_1^0)$; $\tilde{g} \rightarrow q\bar{q}\widetilde{\chi}_1^0$

Table 22: Examples of R–Parity Conserving SUSY signatures at the Tevatron: b–tags + jets $+\not{E}_T$. We have shown only a few modes. The signatures change depending on the relative masses of the $\tilde{b}, \tilde{t}$, $\widetilde{\chi}_1^{\pm}$ and $\widetilde{\chi}_1^0$.

R-Parity Conserving Signatures: b quarks		
Signature	Production	Decay
$b\not{E}_T$	$\tilde{b}\widetilde{\chi}_1^0$	$\tilde{b} \to b\widetilde{\chi}_1^0$
$bj\not{E}_T$	$\tilde{b}\tilde{t}$	$\tilde{b} \to b\widetilde{\chi}_1^0; \tilde{t} \to c\widetilde{\chi}_1^0$
$bjj\not{E}_T$	$\tilde{b}\tilde{g}$	$\tilde{b} \to b\widetilde{\chi}_1^0; \tilde{g} \to q\bar{q}\widetilde{\chi}_1^0$
	$\tilde{t}\widetilde{\chi}_1^0$	$\tilde{t} \to b\widetilde{\chi}_1^{\pm}$
$bjjj\not{E}_T$	$\tilde{b}\tilde{b}$	$\tilde{b} \to b\widetilde{\chi}_1^0;\ \tilde{b} \to \tilde{t}W, \tilde{t} \to c\widetilde{\chi}_1^0$
	$\tilde{b}\tilde{t}$	$\tilde{b} \to b\tilde{g}, \tilde{g} \to q\bar{q}\widetilde{\chi}_1^0;\ \tilde{t} \to c\widetilde{\chi}_1^0$
$bjjj\ldots\not{E}_T$	$\tilde{b}\tilde{b}$	$\tilde{b} \to b\tilde{g}\tilde{g} \to q\bar{q}\widetilde{\chi}_1^0;\ \tilde{b} \to \tilde{t}W\tilde{t} \to c\widetilde{\chi}_1^0$
$bbj\ldots\not{E}_T$	$\tilde{b}\tilde{b}$	$\tilde{b} \to b\widetilde{\chi}_1^0$
	$\tilde{t}\tilde{t}^*$	$\tilde{t} \to b\widetilde{\chi}_1^{\pm}, \widetilde{\chi}_1^{\pm} \to qq'\widetilde{\chi}_1^0$
$bbbj\ldots\not{E}_T$	$\tilde{g}\tilde{b}$	$\tilde{g} \to b\bar{b}\widetilde{\chi}_1^0;\ \tilde{b} \to b\widetilde{\chi}_1^0$
	$\tilde{g}\tilde{t}$	$\tilde{g} \to b\bar{b}\widetilde{\chi}_1^0;\ \tilde{t} \to b\widetilde{\chi}_1^{\pm}, \widetilde{\chi}_1^{\pm} \to qq'\widetilde{\chi}_1^0$
$bbbbj\ldots\not{E}_T$	$\tilde{g}\tilde{g}$	$\tilde{g} \to b\bar{b}\widetilde{\chi}_1^0$
$bb\ell jj\not{E}_T$	$\tilde{t}\tilde{t}$	$\tilde{t} \to b\widetilde{\chi}_1^{\pm}, \widetilde{\chi}_1^{\pm} \to e\nu\widetilde{\chi}_1^0, \widetilde{\chi}_1^{\pm} \to qq'\widetilde{\chi}_1^0$
$bb\ell\ell\not{E}_T$	$\tilde{t}\tilde{t}$	$\tilde{t} \to b\widetilde{\chi}_1^{\pm}, \widetilde{\chi}_1^{\pm} \to e\nu\widetilde{\chi}_1^0$

B.3 Examples of SUSY Signatures that Include Leptons.

Table 23: Examples of R–Parity Conserving SUSY signatures at the Tevatron: Leptons. We have shown only a few modes. Note that (for example) $\tilde{e}$ decays can give 0, 1, or 3 (charged) leptons, and $\tilde{\nu}$ decays can give 1 or 2 leptons. The signatures will change depending on the relative masses of the sneutrinos and sleptons in the different generations. We have not shown explicitly the differences in the "left" and "right" slepton decays. The decays that single out the τ (for example, from the H^+) are omitted here. Decay modes involving neutralinos and charginos can be created by feed–down from squark and gluino decays. Gluino decays can lead to leptons with uncorrelated charges.

R–Parity Conserving Signatures – "Generic" Leptons		
Signature	Production	Decay
$\ell \not{E}_T$	$\tilde{e}\tilde{\nu}$	$\tilde{e} \to e\widetilde{\chi}_1^0;\ \tilde{\nu} \to \nu\widetilde{\chi}_1^0$
	$\widetilde{\chi}_1^{\pm}\widetilde{\chi}_2^0$	$\widetilde{\chi}_1^{\pm} \to e\nu\widetilde{\chi}_1^0;\ \widetilde{\chi}_2^0 \to \nu\nu\widetilde{\chi}_1^0$
$\ell\ell \not{E}_T$	$\widetilde{\chi}_1^{\pm}\widetilde{\chi}_1^{\pm}$	$\widetilde{\chi}_1^{\pm} \to e\nu\widetilde{\chi}_1^0$
	$\widetilde{\chi}_2^0\widetilde{\chi}_2^0$	$\widetilde{\chi}_2^0 \to ee\widetilde{\chi}_1^0;\ \widetilde{\chi}_2^0 \to \nu\nu\widetilde{\chi}_1^0$
	$\tilde{e}\tilde{e}$	$\tilde{e} \to e\widetilde{\chi}_1^0$
$\ell\ell\ell \ldots \not{E}_T$	$\widetilde{\chi}_1^{\pm}\widetilde{\chi}_2^0$	$\widetilde{\chi}_1^{\pm} \to e\nu\widetilde{\chi}_1^0;\ \widetilde{\chi}_2^0 \to ee\widetilde{\chi}_1^0$
	$\widetilde{\chi}_2^0\widetilde{\chi}_2^0$	$\widetilde{\chi}_2^0 \to ee\widetilde{\chi}_1^0;\ \widetilde{\chi}_2^0 \to ee\widetilde{\chi}_1^0$
	$\tilde{e}\tilde{e}$	$\tilde{e} \to e\widetilde{\chi}_2^0, \widetilde{\chi}_2^0 \to ee\widetilde{\chi}_1^0$
	$\tilde{e}\tilde{\nu}$	$\tilde{e} \to e\widetilde{\chi}_2^0, \widetilde{\chi}_2^0 \to ee\widetilde{\chi}_1^0;\ \tilde{\nu} \to e\widetilde{\chi}_1^{\pm}$
$\ell j \ldots \not{E}_T$	$\widetilde{\chi}_1^{\pm}\widetilde{\chi}_2^0$	$\widetilde{\chi}_1^{\pm} \to e\nu\widetilde{\chi}_1^0;\ \widetilde{\chi}_2^0 \to q\bar{q}\widetilde{\chi}_1^0$
	$\tilde{g}\tilde{g}$	$\tilde{g} \to qq'\widetilde{\chi}_1^{\pm};\ \tilde{g} \to q\bar{q}\widetilde{\chi}_1^0$
$\ell\ell j \ldots \not{E}_T$	$\tilde{e}\tilde{e}$	$\tilde{e} \to e\widetilde{\chi}_1^0;\ \tilde{e} \to \nu\widetilde{\chi}_1^{\pm}(\to e\nu\widetilde{\chi}_1^0)$
	$\widetilde{\chi}_1^{\pm}\widetilde{\chi}_2^0$	$\widetilde{\chi}_1^{\pm} \to qq'\widetilde{\chi}_1^0;\ \widetilde{\chi}_2^0 \to ee\widetilde{\chi}_1^0$
	$\tilde{g}\tilde{g}$	$\tilde{g} \to qq'\widetilde{\chi}_1^{\pm}, \widetilde{\chi}_1^{\pm} \to e\nu\widetilde{\chi}_1^0$
	$\tilde{t}\tilde{t}^*$	$\tilde{t} \to b\widetilde{\chi}_1^{\pm}, \widetilde{\chi}_1^{\pm} \to e\nu\widetilde{\chi}_1^0$
$\ell\ell\ell \ldots j \ldots \not{E}_T$	$\widetilde{\chi}_1^{\pm}\widetilde{\chi}_3^0$	$\widetilde{\chi}_1^{\pm} \to e\nu\widetilde{\chi}_1^0;\ \widetilde{\chi}_3^0 \to q\bar{q}\widetilde{\chi}_2^0(\to ee\widetilde{\chi}_1^0)$
	$\tilde{g}\tilde{g}$	$\tilde{g} \to qq'\widetilde{\chi}_1^{\pm};\ \tilde{g} \to q\bar{q}\widetilde{\chi}_2^0$

B.4 Examples of SUSY Signatures that Include Photons.

Table 24: Examples of R–Parity Conserving SUSY signatures at the Tevatron: γ's+$\not\!\!E_T$. In the light Gravitino scenario (GLSP) $\widetilde{\chi}_1^0 \to \gamma\widetilde{G}$ always occurs. If the decay has a long lifetime, one of the two $\widetilde{\chi}_1^0$ may decay outside the detector (LLG). In the Higgsino LSP scenario (HLSP), $\widetilde{\chi}_2^0 \to \gamma\widetilde{\chi}_1^0$ often occurs.

R-Parity Conserving Signatures: Photons			
Signature	Production	Decay	Comment
$\gamma\not\!\!E_T$	$\widetilde{\chi}_1^0\widetilde{\chi}_1^0$	$\widetilde{\chi}_1^0 \to \gamma\widetilde{G}, \widetilde{\chi}_1^0 \to \gamma\widetilde{G}$	LLG
$\gamma j\not\!\!E_T$	$\widetilde{Q}\widetilde{\chi}_1^0$	$\widetilde{Q} \to q\widetilde{\chi}_1^0, \widetilde{\chi}_1^0 \to \gamma\widetilde{G}$	LLG
$\gamma jj\not\!\!E_T$	$\widetilde{\chi}_1^\pm\widetilde{\chi}_1^0$	$\widetilde{\chi}_1^\pm \to W\widetilde{\chi}_1^0, \widetilde{\chi}_1^0 \to \gamma\widetilde{G}$	LLG
	$\widetilde{\chi}_1^\pm\widetilde{\chi}_2^0$	$\widetilde{\chi}_1^\pm \to qq'\widetilde{\chi}_1^0, \widetilde{\chi}_2^0 \to \gamma\widetilde{\chi}_1^0$	HLSP
$\gamma jjj\ldots\not\!\!E_T$	$\tilde{g}\tilde{g}$	$\tilde{g} \to q\widetilde{Q} \to q(q\widetilde{\chi}_1^\pm \to q(q\bar{q}\widetilde{\chi}_1^0))$	LLG
	$\widetilde{Q}\tilde{g}$	$\widetilde{Q} \to q\widetilde{\chi}_1^0;\ \tilde{g} \to q\bar{q}\widetilde{\chi}_2^0, \widetilde{\chi}_2^0 \to \gamma\widetilde{\chi}_1^0$	HLSP
$\gamma b\not\!\!E_T$	$\widetilde{\chi}_1^\pm\widetilde{\chi}_2^0$	$\widetilde{\chi}_1^\pm \to \tilde{t}b, \tilde{t} \to c\widetilde{\chi}_1^0;\ \widetilde{\chi}_2^0 \to \gamma\widetilde{\chi}_1^0$	HLSP
$\gamma\ell\not\!\!E_T$	$\widetilde{\chi}_1^\pm\widetilde{\chi}_1^0$	$\widetilde{\chi}_1^\pm \to e\nu\widetilde{\chi}_1^0, \widetilde{\chi}_1^0 \to \gamma\widetilde{G}$	LLG
	$\widetilde{\chi}_1^\pm\widetilde{\chi}_2^0$	$\widetilde{\chi}_1^\pm \to e\nu\widetilde{\chi}_1^0;\ \widetilde{\chi}_2^0 \to \gamma\widetilde{\chi}_1^0$	HLSP
	$\tilde{e}\tilde{\nu}$	$\tilde{e} \to e\widetilde{\chi}_2^0, \widetilde{\chi}_2^0 \to \gamma\widetilde{\chi}_1^0;\ \tilde{\nu} \to \nu\widetilde{\chi}_1^0$	HLSP
$\gamma\ell jj\ldots\not\!\!E_T$	$\tilde{g}\tilde{g}$	$\tilde{g} \to qq'\widetilde{\chi}_1^\pm(\to e\nu\widetilde{\chi}_1^0);\ \tilde{g} \to q\bar{q}\widetilde{\chi}_2^0, \widetilde{\chi}_2^0 \to \gamma\widetilde{\chi}_1^0$	HLSP
$\gamma\ell\ell\not\!\!E_T$	$\widetilde{\chi}_2^0\widetilde{\chi}_2^0$	$\widetilde{\chi}_2^0 \to ee\widetilde{\chi}_1^0;\ \widetilde{\chi}_2^0 \to \gamma\widetilde{\chi}_1^0$	HLSP
$\gamma\ell\ell jj\ldots\not\!\!E_T$	$\tilde{g}\tilde{g}$	$\tilde{g} \to q\bar{q}\widetilde{\chi}_2^0, \widetilde{\chi}_2^0 \to ee\widetilde{\chi}_1^0, \widetilde{\chi}_2^0 \to \gamma\widetilde{\chi}_1^0$	HLSP
$\gamma\gamma jj\ldots\not\!\!E_T$	$\widetilde{\chi}_1^\pm\widetilde{\chi}_2^0$	$\widetilde{\chi}_1^\pm \to qq'\widetilde{\chi}_1^0;\ \widetilde{\chi}_2^0 \to q\bar{q}\widetilde{\chi}_1^0, \widetilde{\chi}_1^0 \to \gamma\widetilde{G}$	GLSP
$\gamma\gamma\ell jj\ldots\not\!\!E_T$	$\widetilde{\chi}_1^\pm\widetilde{\chi}_2^0$	$\widetilde{\chi}_1^\pm \to e\nu\widetilde{\chi}_1^0;\ \widetilde{\chi}_2^0 \to q\bar{q}\widetilde{\chi}_1^0, \widetilde{\chi}_1^0 \to \gamma\widetilde{G}$	GLSP
$\gamma\gamma\ell\ell jj\ldots\not\!\!E_T$	$\tilde{e}\tilde{e}$	$\tilde{e} \to e\widetilde{\chi}_1^0, \widetilde{\chi}_1^0 \to \gamma\widetilde{G}$	GLSP
	$\widetilde{\chi}_1^\pm\widetilde{\chi}_1^\mp$	$\widetilde{\chi}_1^\pm \to e\nu\widetilde{\chi}_2^0, \widetilde{\chi}_2^0 \to \gamma\widetilde{\chi}_1^0$	HLSP